Targeting the PPARγ and ER pathways *via* modulation of inflammation in the tumor microenvironment: a novel lung cancer prevention strategy

A DISSERTATION

SUBMITTED TO THE FACULTY OF THE GRADUATE SCHOOL

OF THE UNIVERSITY OF MINNESOTA

BY

Erika L. Louiselle

IN PARTIAL FULFILLMENT OF THE REQUIREMENTS

FOR THE DEGREE OF

DOCTOR OF PHILOSOPHY

Advisor: Jill M. Siegfried PhD

May 2019

Acknowledgements

My heart lies within the advancement of science that directly impacts medicine, and I am grateful to have worked in a laboratory in which life-changing biomedical discovery with the capacity to directly affect patient care is flourishing. The support I have received while conducting my research for this body of work has been unwavering, patient, and crucial to my success. I owe a large debt of gratitude to my laboratory manager Dr. Mariya Farooqui for her kindness, resourcefulness, and patience in assisting my growth as a scientist. I would also like to acknowledge the diligent, hard-work of students who contributed to the data in this project and lab members for their support: Huiyu Li, Zhijie Li, MiKayla Boeder, MiKinzie Boeder, Oshin Miranda, and Abdulaziz Almotlak. Additionally, I would like to thank my committee members. Your support and guidance throughout this project was crucial to my success.

To my advisor Dr. Jill Siegfried, who never let me dwell on failure, pushed me through the dark moments, and challenged my mind to expand beyond what I knew possible, you are a role-model of what it looks like to become a resilient, brilliant, and successful female scientist, and I am eternally grateful for your willingness to shape and strengthen me over the past five years.

I would lastly like to gratefully acknowledge my funding and support from the PharmacoNeuroImmunology T32 training grant, from which I was able to fund my research as a graduate student, explore fields of study outside my own,

travel to support the university, and build a network of collaborative support through fellow colleagues and mentors.

I lovingly dedicate this body of work to God, my husband Matthew, and my parents Kelly Reith and Theresa Pirozzoli. To my parents, who never let me go a day without believing I am strong, intelligent, and capable, thank you for the gift of life and every ounce of love and support through the years. To my husband, my constant source of faith and the keeper of my heart, thank you for the sacrifice it took to walk alongside me in this journey and for witnessing my every failure and victory; I love you. And to God, I walk this earth to share the gifts You have bestowed upon me. Thank You for the boundless lessons, strength, and growth the past five years have brought.

Abstract

Lung cancer exceeds all other diagnosed cancers in annual mortality, surpassing the top two annually diagnosed cancers breast and prostate, combined. The vast majority of diagnosed lung cancer cases are in current or former smokers, accounting for 85% of all cases. The number of diagnosed lung cancer cases continues to rise, addressing the need for novel intervention strategies. Despite current advances in chemoprevention for other less-fatal types of cancer, the only currently recognized chemopreventive strategy for lung cancer is smoking cessation. However, former smokers retain a 2.5-fold increased risk of developing lung cancer compared with never smokers, despite cessation efforts. About 40% of all newly diagnosed lung cancers occur in former smokers. As such, chemoprevention strategies for lung cancer are direly needed for the large and ever-growing high-risk population.

Preclinical evaluation of existing therapies with established safety and efficacy profiles represents a fruitful opportunity to advance the field. Identification of ERβ expression has been found to be a lucrative method to identify lung cancers that confer poor survival and presents as a potential target for chemopreventive efforts. Preclinical evaluation of anti-estrogens in cell lines and mouse models of lung cancer shows great promise in advancing this class of drugs towards future clinical use in lung cancer prevention. Furthermore, anti-estrogens such as fulvestrant, a complete ER antagonist, have shown anti-tumorigenic activity in lung cancer and others such as tamoxifen have already

been successfully implemented in both primary and secondary breast cancer prevention modalities. Preclinical and clinical evidence underpinning the importance of managing ER signaling to control lung cancer initiation and progression, although efficacious, alludes to the potential for increased efficacy when used in combination with other agents. Pioglitazone, a synthetic peroxisome proliferator-activated receptor gamma (PPARγ) agonist belonging to the thiazolidinediones (TZDs) drug class has also been used in preclinical studies to mitigate lung tumorigenesis, progression, and metastasis after a retrospective analysis found that diabetics using TZDs experienced a 33% reduction in lung cancer incidence. PPARγ has also been implicated as a protective pathway in lung cancer initiation and progression in early phase clinical testing. Patients with improved histology scores demonstrated a link between an increased ER gene signature and positive-response to PPARγ activation, which conferred a chemopreventive effect in dysplasias with a persistent and progressive phenotype. This link presents a unique opportunity to utilize two known mechanisms that are efficacious in protecting against carcinogen-induced lung cancer initiation and progression. Cross-talk between PPARγ signaling and estrogen receptor (ER) signaling has also been previously reported in other cancer models.

NNK is a principal carcinogen in cigarette smoke, and along with its ability to induce mutations in oncogenes, NNK can act as an inflammatory mediator of the tumor microenvironment (TME) by promoting macrophage infiltration into the

lungs. Furthermore, in previously reported NNK-models of lung cancer, immune cells thought to be macrophages that were positive for both aromatase and estradiol were localized to preneoplastic lesions. Taken together, macrophages are hypothesized to play a key role in regulation of the lung TME both through ER-dependent and independent mechanisms, and both ER and PPARγ pathways are also known to be functional.

To develop a novel approach to prevent lung cancer, preclinical studies were developed to evaluate the therapeutic potential and chemopreventive capabilities of two FDA-approved agents, pioglitazone and fulvestrant, re-purposed in a lung cancer tumor microenvironment (TME) *in vitro* model and an NNK-induced adenocarcinoma chemoprevention *in vivo* model. To test pioglitazone and fulvestrant in a preclinical model simulating the lung TME, we selected a human NSCLC adenocarcinoma cell line with a similar KRAS mutational signature found in smoking-induced lung cancer and a human immortalized macrophage cell line. Additionally, we tested the effects of pioglitazone and fulvestrant in a murine primary cell culture model, utilizing mouse-derived adenocarcinoma cells immortalized from NNK-induced *in vivo* tumors and primary murine bone marrow-derived macrophages (BMDMs).

Major Results

Preliminary results from co-culture simulation of the TME *in vitro* using human macrophages and lung adenocarcinoma cells show pioglitazone and fulvestrant together can significantly suppress inflammatory modulators such as IL-1β, IL-10, Amphiregulin (AREG), and vascular endothelial growth factor (VEGF) compared to single treatments. Single treatments individually did not suppress tumor-promoting pathways IL-1β and AREG in co-culture models of the TME. Similar effects were observed in the murine primary cell model system of the TME. Comparison of resting-state M0 with tumor-associated macrophage (TAM) resembling M2 macrophages revealed that TAM-like macrophages are more sensitive to ER blockade. M2 compared with M0 macrophages displayed more than 2-fold increased expression of the estradiol-synthesizing enzyme aromatase. Furthermore, compensatory increased expression of aromatase seen with ER blockade through fulvestrant treatment was reduced by 50% with the addition of pioglitazone.

In vivo use of combined pioglitazone and fulvestrant in both female pre and post-menopausal NNK-induced adenocarcinoma mouse models of former smoking showed significant treatment benefit. The pre-menopausal model conferred a reduction in lung tumor size by 48% compared with placebo ($p= 0.0265$), compared to 23% for pioglitazone alone ($p=0.5303$) and 5% for fulvestrant alone ($p=0.3591$), and the post-menopausal model conferred a reduction in lung tumor size by 51% compared with placebo ($p= 0.2601$),

compared to 28% for pioglitazone alone (p=0.9867) and 13% for fulvestrant alone (p=0.2402). Inflammatory secreted protein analysis of the bronchio-alveolar lavage fluid (BALF) revealed maximum down-modulation of pro-tumorigenic growth and inflammatory mediators IL-10, IL-1β, EGF, AREG, and CCL2 with combination treatment compared to single treatments after a 3 week treatment duration. Furthermore, tissue analysis of the lungs after a 14 week treatment duration revealed a significant suppression of macrophage density with both single and combination treatments. The greatest suppression of macrophage burden was seen in combination treatment. Despite the robust macrophage chemotaxis suppression, early-stage immunomodulation, and anti-tumor effect of the combination, pioglitazone and fulvestrant combined treatment activated feedback loops by increasing expression of phosphorylated Akt in preneoplastic airways and MMP9-positive tumor-infiltrating immune cells after a 14 week treatment duration.

Conclusion and Significance

Assessment of pioglitazone and fulvestrant in combination reveals a strong anti-tumor effect conferred by a reduction in tumor incidence and size in NNK-exposed pre and post-menopausal mouse models of lung cancer after a 14 week treatment duration. This result is likely to be mediated, in part, by the strong inflammatory regulation of tumor-supporting factors seen at early time points. A significant regulation of pathways known to directly support tumor formation and

progression such as IL-10, IL-1β, AREG, VEGF, EGF, and MMP9 was observed, suggesting downstream crossover of pioglitazone and fulvestrant in hitting on these targets as well as other potential upstream regulators. Additionally, combination effectively suppressed a known monocyte chemotaxis factor CCL2. CCL2 regulation may be partially responsible for the robust decrease in macrophage burden with the combination in a late-stage assessment of the TME. Reduced macrophage density may also be a contributing factor in starving formed tumors of necessary growth factors and cytokines to invigorate further proliferation and survival.

In vitro analysis of inflammatory mediators regulated in the lung TME confirms maximal regulation of the inflammatory landscape within the TME seen with combination. Individual treatments can confer possible activation of pro-inflammatory and pro-proliferative compensatory signaling pathways such as IL-1β and EGFR that are suppressed with combination treatment, again suggesting crossover of PPARγ and ER downstream targets implicated in tumor inflammation and growth signaling. Additionally, combination treatment can most effectively regulate heightened M0 and M2 macrophage aromatase expression and estradiol secretion, suggesting an enhanced effect on ER regulation with the addition of pioglitazone previously described in other models. Taken together, the combination of pioglitazone and fulvestrant are shown to re-educate the lung TME away from tumor-promoting estrogenic activity, primarily modulated by macrophages.

Thus, the strong combination effect of pioglitazone and fulvestrant on lung tumor growth and macrophage function, and the ability of the combination to suppress compensatory signaling pathways, supports the hypothesis of ER/PPARγ cross-talk in lung cancer and provides a rationale for further investigation of chemopreventive effects of this combination.

Table of Contents

List of Tables

Tables in Chapter 3

List of Figures

Figures in Chapter I

Figures in Chapter II

1. Introduction

1.1 Lung Cancer Prevalence and Epidemiology

Lung cancer stands as the leading cause of death in both men and women in the United States with an estimated toll of 154,050 deaths in 2018 making it 25.3% of all cancer-related deaths [1]. Lung cancer has remained the number one cause of cancer-related death in men since the 1950's, and in 1987, it became the number one cancer killer in women, surpassing breast cancer [2]. Despite ongoing research efforts, lung cancer 5-year survival rates remain staggering low at 18.6% assessed by the National Cancer Institute's (NCI) Survival, Epidemiology, and End Results (SEER) data program in 2018. Furthermore, lung cancer accounts for 13.5% of all new cancer cases [2]. Taken together, this data indicates the need for improved treatment and prevention strategies.

According to a statistical report published in 2018, lung cancer rates closely correlate with historical differences in smoking initiation and cessation as well as prevalence of smoking in certain generational cohorts [3]. According to the Surgeon General's report on the consequence of smoking, adult per capita cigarette consumption rose to all-time high between the years of 1940 and 1980 [4]. At its peak, per capita cigarettes smoked annually topped 4,000 which could, in part, account for the plethora of newly diagnosed cases but does not address the aggressiveness of the disease underlying survival rates and the prevalence in non-smoking populations. In 1964, 40% of all Americans were active smokers,

and when assessed by sex, 53% of men and about 33% of women were active smokers [4]. In 2018, it was reported that approximately 20% of lung cancer related-deaths were in never-smoker cohorts totaling roughly 30,000 people [5].

To date, smoking is identified as the number one cause of lung cancer fatality with approximately 80% of all lung cancer deaths attributable to a history of smoking [6]. In addition to the risks associated with traditional cigarette smoke, there is also research in risks associated with other types of tobacco. Cigar and pipe smoke increases cancer risk 5.1 fold compared with nonsmokers [7]. Lung cancer risk is not yet well-defined for inhalant drug use such as marijuana and cocaine; however research has identified similar molecular and histological aberrations indicating premalignancy of the lung tissue [7]. There are also other risk factors that have been attributed to the disease. Such factors include radon exposure, second-hand smoke exposure, carcinogen exposure such as asbestos and diesel gasoline exhaust fumes, prior radiation therapy, air pollution, carcinogenic chemicals such as arsenic in drinking water, and genetic mutations [6].

Although smoking accounts for the largest risk of lung cancer, nonsmoking and never smoking populations also presented with 20% of all lung cancer cases in 2018, suggesting other factors that may increase susceptibility in these populations [5]. Statistics reflect lung cancer deaths in nonsmokers continues to rise in rank and now presents as the 7th most lethal cancer in these individuals

and is thought to be attributable to secondhand smoke, environmental factors, and genetic driver mutations, as well as other factors previously mentioned [8].

1.2 Lung Cancer Histological Classification and Therapeutic Implications

Lung cancer is divided into two broad categories: small cell lung cancer (SCLC) and non-small cell lung cancer (NSCLC). Small cell lung cancer comprises 15% of all diagnosed lung cancer cases while its counterpart non-small cell comprises the other 85% of diagnosed cases [7]. SCLC is considered to be a subtype characteristic of neuroendocrine differentiation, and is thus, classified differently than is NSCLC [9]. NSCLC can be further divided into three subcategories based on pathological differences: adenocarcinoma, squamous cell carcinoma, and large cell carcinoma [10]. Adenocarcinoma and squamous cell carcinoma combined account for over 70% of all cases, making them the two main subtypes [10]. Adenocarcinoma is the most common subtype of lung cancer overall, comprising 40% of all diagnosed cases and 60% of its NSCLC subtype [9]. Adenocarcinoma can present as either noninvasive (in situ) or invasive and is found along the periphery of the lung lobe, often superficially. Adenocarcinoma can be classified based on growth patterns as lepidic, meaning growing along alveolar structures; acinar, meaning growing in glandular patterns; papillary, meaning growing with the presence of “fibrovascular cores”; micropapillary, meaning growing in cellular “tufts” without the presence of a fibrovascular core; or solid, meaning growing in patternless sheets [9].

Squamous cell carcinoma, on the other hand, presents in 20% of cases and is typically seen growing in a solid, nested pattern along major airways in the central portion of the lung lobe [9].

Over the past 20 years, advances have been made to more accurately identify molecular drivers of individual subtypes, allowing treatment plans to be specialized rather than treating subtypes as a singular disease. For example, epidermal growth factor receptor (EGFR) mutations in the tyrosine kinase domain are of the most common driver mutations in NSCLC, occurring in approximately 10% of all North American diagnosed cases [11]. Among the other common mutations are KRAS, occurring in about 15%-20% of NSCLC and 30%-50% of adenocarcinoma cases, receptor tyrosine kinase anaplastic lymphoma kinase (ALK), occurring in 3%-7% of NSCLC cases overall, and human epidermal growth factor receptor 2 (HER2), occurring in 2% of NSCLC cases, the majority of which are reported as adenocarcinoma [11].

1.3 The Role of NNK in Lung Carcinogenesis

Tobacco smoke, already implicated as the leading risk factor in lung cancer incidence, has been thoroughly studied to understand the chemically-driven biological changes underlying tumorigenesis in lung epithelium. The key carcinogen responsible for lung tumorigenesis is nitrosamine 4-(methylnitro-samino)-1-(3-pyridiyl)-1-butanone (NNK), also referred to as nicotine-derived

nitrosamine ketone [12]. The other major class of carcinogens proven to induce tumorigenesis discussed in the literature are polycyclic aromatic hydrocarbons (PAHs). However, nitrosamines have a more potent effect on carcinogenesis, producing a 100% success rate of inducing lung cancer in various rodent models [12, 13]. Studies have shown that NNK is a procarcinogen requiring metabolism through several cytochrome pigment 450 (CYP450) enzymes to convert it to the active forms 4-(methylnitrosamino)-1-(3-pyridyl)-1-butanol (NNAL) and NNAL-Gluc that are able to bind to DNA to form adducts [10]. Three such activation steps are required: 1. carbonyl reduction, 2. Pyridine N-oxidation, and 3. A-hydroxylation [12]. Once active, NNAL and NNAL-Gluc show affinity for DNA, can bind to and form DNA adducts, and induce DNA mutations if repair mechanisms are unsuccessful. This DNA damage ultimately leads to mutations in key oncogenes and tumor suppressor genes resulting in tumor initiation [14]. Several targets that are modulated by NNK to confer oncogenic activity are K-ras, Fas ligand (FasL), mitogen-activated protein kinase/extracellular signal-related kinase 1 (MAPK/ERK1), proto-oncogene c-Myc, and B cell leukemia/lymphoma 2 (Bcl2), Cyclin D1 (CycD1), Nuclear Factor kappa-light-chain-enhancer of activated B cells (NF-κB), and EGFR, among others [12].

In addition to NNK's roles in DNA mutation and alteration of oncotargets, NNK has also been shown to have immunomodulatory effects, altering immune targets such as interleukin-8 (IL-8), interleukin-6 (IL-6), monocyte chemoattractant protein 1 (MCP1), and prostaglandin E_2 (PGE2) [12].

While NNK has been well-studied to have potent effects on lung tumor initiation, there are some published chemopreventive agents that have protective effects against NNK-induced tumorigenesis [12]. Deactivating known NNK-stimulated oncogenes can provide an opportunity to intervene prior to tumorigenesis and progression. EGFR activation is a known effect of NNK exposure, and as such, targeting the pathway can prevent overly active proliferative effects [12]. Additionally, agents that can deactivate NNK-mediated phosphatidylinositol 3-kinase/ Protein Kinase B (PI3K/Akt) activation may also serve as viable chemoprevention strategies. Other targetable strategies include inhibition of CYP-mediated NNK conversion to active metabolites, activation of detoxification pathways, and increasing mechanisms to repair DNA damage from NNAL and NNAL-Gluc adduct formation [12]. For instance, some studies have shown β-estradiol can induce CYP450 enzymes to convert tobacco to active forms, making the estrogen pathway a targetable chemoprevention strategy [16].

1.4 Chemoprevention Status in Lung Cancer

Due to staggeringly high rates of lung cancer diagnoses and lung cancer-related deaths annually, research to identify effective chemoprevention options has likewise, been propelled. Chemoprevention is defined as “the use of dietary or pharmaceutical interventions to slow or reverse the progression of pre-malignancy to invasive cancer” and is becoming a useful strategy in other types of cancer [16]. The hallmarks of a successful chemopreventive agent include

delineating a high-risk population that is in need and identifying compounds that are both efficacious and have a favorable safety profile [16]. Lung cancer high-risk individuals can be pinpointed *via* algorithms that mesh patients' age and cumulative smoking history with known risk prediction models [17]. Despite the ability to ascertain patients at an increased risk of lung cancer, FDA-approved chemopreventive compounds are still lacking, despite a number of compounds that have undergone testing in preclinical and clinical stages [16]. Currently, smoking cessation is the only known factor capable of reducing lung cancer risk, and the risk of lung cancer still remains elevated in a former smoker than an individual with no smoking history with greater than half of diagnoses occurring in former smoker cohorts [16,18].

Chemopreventive intervention can be divided into 3 classes: primary, secondary, and tertiary [19]. Primary chemoprevention targets at-risk individuals who do not have a history of cancer diagnosis, whereas secondary can target individuals already exhibiting dysplastic lesions but that have not yet advanced into malignancy. Tertiary chemoprevention involves preventing neogenesis of a primary lesion in individuals who have a previously diagnosed pulmonary cancer [19].

A number of agents have progressed through preclinical testing into early phase clinical trials for lung cancer chemoprevention, but only 7 have entered phase III, and all without success [19]. Prior to entering phase III, phase II trial outcomes outline intermediate endpoints, that is, endpoints meant to predict the

overall objectives of a phase III trial which definitively measure reduced cancer incidence and morbidity [19]. Intermediate endpoints, for example, can include biomarkers effective of predicting response to a chemoprevention compound that results in a decrease in lung cancer incidence. However, to-date, no such biomarkers have been validated as accepted intermediate endpoints in lung cancer prevention [19]. Several suggested lung cancer chemoprevention agents that have undergone clinical trials address comorbid disease in high risk patients which could be advantageous to patients at high-risk of cancer. These patients often have other coinciding conditions to be managed like chronic obstructive pulmonary disease (COPD), pulmonary arterial hypertension (PAH), and diabetes mellitus (DM). Such chemoprevention agents have the potential to address premalignant risk as well as coinciding conditions: non-steroidal anti-inflammatory drugs (NSAIDS), cyclooxygenase-2 (COX2) inhibitors, and prostacyclin analogs. [19, 20].

Aspirin, a common over-the-counter NSAID, was tested in clinical trials, advancing to phase III testing, when prior preclinical testing found and association with aspirin use and decreased NSCLC incidence [21]. Phase III trials, however, failed to meet established endpoint of reduced conversion from Barrett's metaplasia to adenocarcinoma [19, 22]. The phase III trial was conducted in a primary chemoprevention setting and all arms produced negative results [19].

Celecoxib, a COX2 inhibitor, was tested in a phase II clinical trial after a plethora of preclinical evidence implicated the COX2/prostaglandin E_2 (PGE2) pathway in lung carcinogenesis and indicated a potential opportunity for COX inhibitors in a lung cancer chemoprevention setting [23]. The primary intermediate endpoint assessed was the proliferative index marker Ki67, which was significantly decreased in accordance with reduction of lung nodules assessed through computed tomography (CT) scanning. However, not all patients experienced significant results with the drug, suggesting the need for further studies to elucidate a population of patients likely to receive the most benefit from this agent [23]. Furthermore, a subset of patients experienced adverse events related to toxicity, contraindicating safety which a major principle of chemoprevention agents [23]. Taken together, this data suggests progression towards viable lung cancer prevention options, but constitutes further investigation to find agents that meet all necessary benchmarks of an ideal chemoprevention agent.

Another recently investigated lung cancer prevention compound, iloprost, a synthetic prostacyclin analog that activates the prostaglandin pathway and peroxisome proliferator activated receptor gamma (PPARγ) pathway has shown some promising results in preclinical and early phase clinical testing. Prostacyclin is associated in normal lung tissue at high levels, whereas prostaglandin E2 (PGE2) is found to be at high levels in lung tumor cells [24]. Furthermore, elevating prostacyclin by genetic or pharmacological means results in lung

cancer prevention in murine models [23]. A phase II trial of oral iloprost was conducted to evaluate biopsy score change over a 6 month period of time [24]. Former smokers experienced a significant decrease of -0.39 compared to current smokers that experienced no difference in endobronchial dysplasia [24]. The lack of effect in the current smoker population reflects a common result in lung cancer chemoprevention studies, suggesting that smoking perpetuates pathways that cannot be negated by chemopreventive agents until active smoking ceases.

Retinoids make up the class of micronutrients falling under the umbrella of vitamin A derivatives. Retinoids have been well-studied and have published effects as chemopreventive agents [25]. However, there are also numerous instances in which it has negative or harmful effects [25]. In the context of lung cancer, a phase II clinical trial was conducted in a tertiary setting for patients with recurrent SCLC in which isotretinoin was used. In combination with interferon alpha (IFNα) and paclitaxel, the response in this study was 8.8% [25]. However, a phase III trial of isotretinoin for the prevention of lung cancer in current and former smokers was withdrawn due to increased mortality with the isotretinoin arm accounting for one third of the overall deaths in the study not attributed to lung cancer mortality [26]. Although retinoids may exhibit chemopreventive properties in lung cancer risk cohorts, it is clear that other compounds must be elucidated with improved safety profiles.

1.5 Sex Differences in Lung Cancer

Never smokers are defined as having smoked a total of 100 cigarettes or less in a lifetime as well as individuals who have been lifetime nonsmokers [7]. Prevalence of lung cancer in this cohort of individuals is about 15% of all lung cancer cases worldwide. When assessed by sex, 15% of worldwide lung cancer cases in men and 53% in women have no link to smoking history [7]. Although there is controversy regarding gender-specific susceptibility to the carcinogenicity of tobacco exposure, statistics remain clear delineating an increased female risk of mortality in nonsmoking lung cancer diagnoses compared to male risk [7]. Furthermore, women are more likely to develop both adenocarcinoma and small cell lung cancer while men are more likely to develop squamous cell carcinoma [13]. This large disparity raises questions on male versus female biological differences underlying lung cancer susceptibility and aggressiveness and strongly suggests a role of estrogen signaling in lung cancer [2].

1.6 Estrogen Receptor (ER) Structural Biology, Activation, and Functions

The ER is a ligand-inducible intracellular transcription factor belonging to the nuclear hormone receptor (NHR) family and can be characterized into 2 different forms, estrogen receptor alpha (ERα, also ESR1) and estrogen receptor beta (ERβ, also ESR2) located on chromosome 6 and 14, respectively [27, 28]. ERα is primarily distributed in breast, ovary, and endometrial tissue, and ERβ is more

prevalent with primary tissue distribution in bone, brain, colon, endothelium, kidney, lung, ovary, prostate, and testes [28]. Both isoforms have the same structure, containing a transcriptional activation site (A/B domain), a DNA binding domain (DBD), a hinge-region, and a ligand binding domain (E/F domain) [28]. ERα and ERβ have 55% homology to one another in the ligand binding domain, and as such, have differing affinities for estrone and estriol, respectively. Splice variants within the ligand and DNA binding domains have been previously reported, as well [28].

Activated ER can mitigate its effects in several ways. In a genomic, nuclear fashion, ER will homodimerize with its ligand and can alter expression of target genes through DNA-interaction with cofactors and corepressors at site-specific areas of the DNA termed estrogen response elements (EREs) upon translocating to the nucleus [27, 29]. It is thought that transcriptional activity is mediated through activity of 2 domains called activation function (AF1 and AF2) domains located in the N-terminal and ligand binding domains [27]. ERα and ERβ have both been reported to bind and confer transcriptional effects through the ERE as well as through binding with other transcription factors such as activator protein 1 (AP-1), stimulating protein 1 (Sp1), and NF-κB [27, 28, 29]. Additionally, ER can moderate signaling in a non-genomic manner, whereby 17β-estradiol (E2) binds ER and the ligand-receptor complex within the cell surface membrane can trans-activate kinase pathways that mediate proliferation and survival pathways such

as MAPK/ERK1, PI3K/Akt, and EGFR as well as transcriptional regulation of target genes [28, 29].

1.7 ERβ Signaling in Lung Cancer

As previously mentioned, ERα and ERβ have differing tissue distributions, and ERβ is the primary isoform located in the lung, whereas ERα has not been detected [28, 30]. ERβ murine knockout studies shed light on the biological function in the studies which includes alveoli formation and surfactant clearance. These mechanisms were found to be driven through transcriptional activation of ERβ target genes platelet-derived growth factor A (PDGF-A) and granulocyte-macrophage colony-stimulating factor (GM-CSF). These postnatal lung modifications are described as sex-driven dimorphic characteristics controlled by estrogens in the lungs [30]. This sex-driven dichotomy, also present in increased lung cancer susceptibility in women, is not fully understood, but believed to be linked to estrogen [30].

Further study into this postulation revealed epidemiologic evidence pointing to a worse prognosis and more advanced disease in pre-menopausal women with functioning endogenous sources than post-menopausal women, all of whom were never smokers [15, 31]. Older, post-menopausal women also beat out male counterparts in showing a survival advantage [15]. Another study also found that

more, assumed pre-menopausal, women under age 50 were diagnosed with lung cancer than men of the same age range [32].

To this end, a hormonal link to lung cancer has been extensively studied. One such retrospective study conducted between 1984 and 1999 found that women who had used hormone replacement therapy had a lower median age of diagnosis by 5 years and decreased survival time by 40 months than women who had never taken hormone replacement therapies (HRTs) [33]. Another study conducted by the Women's Health Initiative (WHI) reported a similar adverse effect on survival of women taking HRTs (estrogen plus progesterone) and a greater mortality risk to the HRT arm by 19% [15].

Although these sex differences in lung morphology and lung cancer exist, it is important to note that the lungs have been shown to be estrogen-dependent for normal morphology and estrogen-responsive in both males and females. ERβ knockout male and female mice experience alveolar collapse after 5 months of age, suggesting that functional estrogen receptor signaling is essential to both sexes. Furthermore, estrogen treatment caused reporter gene upregulation in both male and female mice ERE-luciferase reporter mice [34]. Additionally, human male tumor tissue contains similar expression amounts of ERβ to female tumor tissue, and human male-derived lung cancer cell lines are also estrogen-responsive [35]. Both male and female-derived lung tumors also contain CYP19 (aromatase) which is the rate-limiting enzyme necessary to convert androgen precursors into 17β-estradiol [35].

To further this understanding, studies on the functionality of the ER pathway in lungs utilizing a complete ER antagonist fulvestrant showed a blockade of tyrosine kinase signaling leading to decreased proliferation in lung tumor cell lines [34]. Estrogen has, likewise, gone on to show induction of proliferation in other studies using lung cancer cell lines, human cancer cell xenograft models, and murine lung cancer models [36, 37].

1.8 Antiestrogens and Lung Cancer Prevention

Selective estrogen receptor modulators (SERMs) such as tamoxifen and aromatase inhibitors (AIs) such as anastrazole have shown both safety and efficacy in large clinical trials to prevent breast cancer that is hormone-responsive. Tamoxifen in randomized trials conferred a decrease in both invasive and non-invasive breast cancer against the placebo groups by 50% [38]. As such, tamoxifen and raloxifen are now clinically prescribed for women at high-risk of breast cancer [39].

With a solid basis of data suggesting estrogen blockade can combat lung cancer initiation and progression, research explored the realm of antiestrogens for use in lung cancer models. A population-based study in Taiwan found that of 40,900 breast cancer patients taking antiestrogens (tamoxifen, raloxifen, toremifen, or AIs) as part of a therapy regimen experienced a significantly lower adjusted hazard ratio of 0.77 compared with nonusers [40].

Preclinical studies have gone on to evaluate the safety and efficacy of antiestrogens in lung cancer chemoprevention. Stabile et al. assessed chemopreventive abilities of aromatase inhibitor anastrazole alone and in combination with estrogen antagonist fulvestrant in an NNK-induced murine lung carcinogenesis model. The combination conferred a significant decrease in mean number of tumor with the anastrazole and the combination with the greatest decrease seen with combination treatment. Along this trend, Ki67 expression was significantly reduced in all treatment groups, again with the largest reduction seen in the combination. In a similar model, anastrazole and fulvestrant exhibited decreased mean tumor size as well as decreased Ki67, however, the model assessed tumor advancement once hyperplastic lesions were established [41]. Fulvestrant has also been investigated in clinical trials in combination with other therapies for the treatment of advanced stages of NSCLC, owing to its efficacy in reducing proliferation of abnormal or malignant cells [42-45].

Finally, gene expression analysis of patients with advanced airway dysplasia revealed upregulation of upstream regulators linked to the estrogen signaling pathway as well as estrogen-responsive genes. A few of these identified pathways include transcription factor TBX2 implicated in breast cancer signaling, vascular endothelial growth factor (VEGF), hepatocyte growth factor (HGF), all of which are known to be induced by estrogen. Furthermore, progesterone receptor (PR) was found to be negatively regulated which is consistent with literature citing a loss of the PR pathway correlating to more

aggressive disease as well as a previously identified coupling of ERβ high/PR low tumors conferring negative prognosis in NSCLC. This preclinical evidence linking estrogen signaling with airway dysplasia persistence and progression creates further opportunity to implement antiestrogens in chemoprevention models, both alone and in combination with other agents. As previously mentioned, iloprost phase II clinical trial data as well as preclinical data from prostacyclin over-expression mouse model studies point to the utility of prostacyclins as chemopreventive agents in reducing lung tumor formation and found this in large part to be due to their activation of the peroxisome proliferator activated receptor gamma (PPARγ) pathway [46]. Promising preclinical and clinical results testing the repurposing of antiestrogens as well as other known tumor blunting pathways for use in at-risk and progressing lung cancer cases constitute further research to hone in on ideal populations of individuals most likely to benefit through identification of biomarkers when histological features cannot provide this insight.

1.9 PPARγ Therapeutic Potential

Due to the dire state of lung cancer prognosis and survival rates, an imminent need for novel approaches to prevention and treatment drives research to investigate new targets. A natural progression towards investigation of agents capable of moderating smoldering inflammation leading to tumorigenesis has transpired after Hanahan and Weinberg established tumor-promoting

inflammation as a hallmark of cancer [47]. Among these agents are agonists of a potent anti-inflammatory and malignant growth inhibition pathway: the PPARγ pathway. PPARγ is a member of the nuclear hormone receptor superfamily and functions as a ligand-activated transcription factor most commonly known for driving transcription related to glucose homeostasis and adipocyte differentiation, thus its utility as a gold-standard target in anti-diabetic therapy [48]. Other known systemic roles outside of the utility of PPARγ in regulating metabolic processes include wound healing, inflammatory and immune modulation, angiogenesis, and augmentation of cellular processes including differentiation, proliferation and death [49, 50]. Discovery of these additional signaling effects has led to a plethora of preclinical research applying PPAR agonists in anti-cancer modalities.

1.10 PPARγ Structure, Function, and Signaling

PPARγ falls into a receptor family containing 3 receptor isoforms: PPARα, PPARβ/δ, and PPARγ. The three isoforms are reported to retain 60-80% homology between each other in both the DNA-binding and ligand-binding domains [51]. PPARα has specificity in tissues with high metabolic activity such as heart, liver, kidney, and skeletal muscle while PPARβ/δ has diverse expression in most tissues with the most expression seen in the liver, kidney, adipose tissue, intestinal tissue, and skeletal muscle [50]. PPARγ has been described as the most well-studied PPAR isoform and is most abundantly found in adipose tissue but has also been reported to be expressed in many other

tissues such as liver, kidney, intestinal tissue, immune cells, and the lung [51, 52]. PPARγ is further divided into two splice variants PPARγ1 and PPARγ2. Both isoforms have a similar amino acid sequence with PPARγ2 having 30 additional amino acids located at the N-terminal domain [53]. The structure of both PPARγ1 and PPARγ2 contain a transcriptional activation site (A/B domain), a DNA-binding domain (C domain), a hinge region (D domain), and a ligand-binding domain (E/F domain) [54].

Being a class of ligand-activated transcription factors, PPARs function by binding natural or synthetic ligands to agonize the receptor and allow release of co-repressors to facilitate binding of their counterpart, the retinoid-x receptor (RXR) to form a heterodimer. PPAR-RXR receptor heterodimerization then allows translocation to the nucleus to initiate mRNA transcriptional changes for PPAR target genes [51, 53]. This type of activation is PPARγ-dependent and confers the metabolic activity most-attributed to the pathway. PPARγ receptor-independent activity is also reported with PPARγ agonists in which ligands can induce changes in kinase signaling pathways such as PI3K/Akt and MAPK resulting in augmented expression of growth factors, oncogenes, and cell cycle proteins to confer inhibition of cancer cell proliferation [53].

There are several reported natural ligands to the PPARγ receptor. These compounds relate to the metabolic regulatory capabilities of the PPARγ-dependent processes and include certain fatty acids, eicosanoids, and some members of the family of low-density lipoproteins (LDLs). The most well-known

natural ligand reported to have the highest affinity to PPARγ of all the known naturally occurring ligands is 15-deoxy-Δ-12-14-prostaglandin J_2 (15d-PGJ_2) [49]. Although 15d-PGJ_2 is the endogenous ligand with most affinity for PPARγ, overall potency is low for naturally occurring ligands. As such, a class of synthetic PPARγ ligands known as thiazolidinediones (TZDs) were synthesized to have increased potency and specificity for the receptor and are commonly used in diabetic therapeutic regimens due to their ability to sensitize cells to insulin [55]. The synthetic ligands in the class of TZDs on the market currently include pioglitazone, rosiglitazone, and lobeglitazone (approved for use in South Korea), but there are other analogs that have published uses in preclinical studies including two other well-known members ciglitazone and troglitazone. These synthetic ligands have been widely studied and are used commonly in the clinic. One retrospective human cohort study of 87,678 patients from Veterans Affairs medical centers, found those taking TZDs for diabetic purposes in comparison with nonusers experienced a 33% reduction in lung cancer incidence [56]. Further preclinical investigation into PPARγ-independent mechanism of action relating to cell cycle, cellular proliferation, and inflammatory modulation in an anti-neoplastic context revealed its function in pathways that drive tumor suppression in several malignancies including lung cancer [48].

One such function identified as a downstream effect of PPARγ activation is terminal differentiation. Several NSCLC lineages have reported upregulation in pro-differentiation proteins such as surfactant protein A (SP-A) and gelsolin.

A549 cells, one such NSCLC line, have been shown to sustain extracellular signal-regulated kinase 1/2 (ERK1/2) activation as a result of PPARγ activation with an agonist [48]. In addition, studies have shown that activated PPARγ signaling in several human cancer cell lines induces cell cycle arrest, apoptosis, and in some cases, re-differentiation [57-60].

PPARγ has been extensively shown to regulate inflammation as an additional means of regulating the TME in cancer. One such study revealed that inhibition of PPARγ signaling in myeloid cells led to abnormal immune cell populations, expansion of myeloid-derived suppressor cell (MDSC) populations, reduced T-cell populations, and therefore, immunosuppression all contributing to tumorigenesis. Furthermore, a lack of PPARγ signaling depleted pro-inflammatory gene expression in MDSC populations [61].

Current findings summarize the effects of PPARγ activation on lung cancer to be cell context-dependent, resulting in a multitude of varying effects based on the cell type in question within the tumor microenvironment. Juxtaposing the aforementioned effects of PPARγ activation conferring an anti-tumor message in epithelial and other tumor microenvironment (TME) supporting cells, some current research exposes evidence linking PPARγ activation in certain myeloid cells with pro-tumorigenic functions. One such study found that systemically activating PPARγ in a syngeneic mouse model of lung cancer did not confer the expected tumor regression, but rather resulted in increased brain and liver metastases [62]. Upon further investigation, it was discovered that PPARγ

activation in tumor associated macrophages resulted in an increased Arginase-1+ population which is well-characterized to have pro-tumorigenic functions. Based on the results of this study, it is clear that understanding the dynamic between PPARγ activation and tumor-associated macrophage populations will prove essential in creating the most efficacious PPARγ-centric therapeutic modality.

However, conflicting evidence from a study using dominant negative PPARγ (dnPPARγ), a mutant PPARγ receptor capable of silencing activation of the wild-type receptor, indicates that an inhibition of PPARγ activity results in an overwhelming pro-inflammatory response with a cascade of negative effects including activation of myeloid-derived suppressor cell (MDSC) populations resulting in depletion of T-cell subsets, induction of proliferation and pro-survival pathways, and induction of metastasis [63].

Although mounting evidence underpinning the complex role of PPARγ activation in tumor progression leaves more questions than answers, it is clear that PPARγ is a key player in tipping the scale of the TME towards or against tumorigenesis. Furthermore, studies aimed at understanding the effects of combining thiazolidinediones with other anti-cancer modalities will not only advance knowledge of PPARγ mechanism of action in cancer, but also provide promising novel solutions to the growing need for newer, inventive therapy options.

1.11 PPARγ Clinical Significance in Lung Cancer

Due to the anti-neoplastic capabilities of agonizing the PPARγ pathway, preclinical support of its effects has begun to transition into clinical studies to elucidate its chemotherapeutic and chemopreventive potential in humans. Only a few clinical trials are reported using pioglitazone in the context of lung cancer therapy. One study, although it contained few participants, did cite reductions in post-treatment expression of Ki67, CycD1, and cell cycle protein p21. Furthermore, the study reported no serious adverse effects, suggesting that further studies be conducted with increased accrual to elucidate chemotherapeutic potential of TZDs in lung cancer [64]. Another study, conducted in a chemoprevention context using pioglitazone, aims to uncover potential utility of this agent in a safe and effective manner [65]. Further studies can help direct the use of this medication to benefit individuals at risk of developing lung cancer.

1.12 Pioglitazone Risk Factors

It is widely accepted that individuals with diabetes carry a higher risk of bladder cancer [66, 67, 68]. However, research varies on whether or not that risk can be positively associated with medications used to treat diabetes such as TZDs and angiotensin receptor blockers (ARBs). Several cohort studies have been performed in order to stratify this risk particularly pertaining to TZD use, and

yet, the results are widely varied. Both prevalent and incident-based statistics on pioglitazone use were analyzed in a Medicare cohort population during the years 2003-2011. There was a 16% risk associated with pioglitazone use in a prevalence context and no associated risk identified in the incidence cohort [66]. A meta-analysis collecting data dating to July 2013 of 5 randomized-controlled trials (RCTs) and 13 observational studies also identified an increased risk of bladder cancer with pioglitazone use with odds ratios of 2.51 and 1.21 in the RCT group and observational study group, respectively [69]. However, another meta-analysis conducted between 2000-2016 compiled data from epidemiologic, controlled, and randomized studies identifying risk ratios of pioglitazone use and bladder cancer occurrence and found no significant difference in hazard ratio (HR) between pioglitazone users and nonusers [67]. Several other studies conclude similar confounding results [70, 71]. Due to the inconsistency of results from these large studies, further stratification of factors such as age, sex, countries of study, cumulative dose, duration of dose, and other confounding medical factors that may potentiate the risk of bladder malignancy associated with TZD use is needed to properly distinguish increased risk populations.

1.13 PPARγ and ER Cross Talk

A paper published in 2014 by Chu et al. outlined a reciprocal regulation of PPARγ and both ERα and ERβ. It was found that overexpression of either receptor led to the repression of protein level and activity of the other, and

conversely, knockdown of either receptor with siRNAs led to an increase in expression of the opposite receptor. Treatment of the thyroid carcinoma cells with PPARγ agonist rosiglitazone reduced ERβ expression. In reciprocal fashion, ERβ agonist diarylpropiolnitrile (DPN) also reduced PPARγ expression. Furthermore, they observed that this novel interaction between PPARγ and ERβ were able to sensitize thyroid carcinoma cells to expression of pro-apoptotic molecules and reduced proliferative and migratory activity of the thyroid cancer cells [72].

Other studies have found links between the PPARγ and ER pathways, most of which are in reproductive or hormone-driven tissues. In an *in vitro* model of endometriosis, ciglitazone was found not only to reduce cell cycle proteins and increase apoptotic pathways, but also to decrease expression of aromatase and subsequent estrone production in the endometriotic cells, further supporting evidence of PPARγ/ER cross-talk [73].

A study in breast cancer MDA-MB-231 and MCF-7 cells found a similar bidirectional interaction between the two receptors. This was demonstrated, in part, through ER activation with expression vectors and measurement of subsequent peroxisome-proliferator response element (PPRE) reporter transcriptional activation with a Luciferase construct. ER activation conferred a decrease in reporter activity, and similarly, PPARγ activation increased reporter activity, and addition of ER expression vectors blunted this effect [74]. To this end, another paper published using MCF-7 and HeLa cells demonstrated for the

first time that a possible direct interaction between ERα and PPARγ exists. The study showed through coimmunoprecipitation that the two receptors are bound. Furthermore, they demonstrated that ERα can mediate its effects on the PPARγ signaling pathway by binding to the PPRE and suppressing transactivation [75]. Several other articles have shown a similar bidirectional interaction between PPARγ and ER; however, fewer have elucidated the role of ERβ, specifically, as opposed to ERα in this interaction and to-date, studies aimed at understanding this receptor interplay in lung cancer are lacking. Increased therapeutic benefit is possible with a heightened understanding of the communication between PPARγ and ERβ in lung cancer, allowing for inventive therapeutic combinations of new and existing agents.

1.14 Macrophages in Cancer

Macrophages provide necessary function in many normal physiological processes including mounting and resolving an immune response during infection, maintaining homeostatic balance in specific tissues, and wound healing following tissue damage. In addition to normal physiological functions, macrophages have also been implicated as initiators in tumorigenesis by sustaining inflammation associated with cancer risk and tumor initiation signals [76]. The infiltration of immune cells to the tumor microenvironment to promote tumor-specific inflammation is defined by Hanahan and Weinberg as one of the emerging hallmarks of cancer [77]. Of these immune cells, macrophages have

been identified as the main type of infiltrating leukocyte to the tumor bed to initiate tumor-promoting inflammation [78]. While these resident immune phagocytes can play normal, functional roles in organs such as the lungs, these infiltrating phagocytes are a noted player in tumor formation, progression, and metastasis [79]. This specific subset of macrophage has been given the term tumor-associated macrophages (TAMs) and their abundance in tissue is associated with poor prognosis in over 80% of published studies [80]. Like other subsets, TAMs are not fully understood, and studies have shown them to display both pro and anti-tumorigenic properties in a context-dependent manner [81]. A more complete understanding of TAM characterization in lung cancer will provide opportunity for therapeutic intervention in order to modulate macrophage support of tumorigenesis.

1.15 Clinical Relevance of TAMs in Lung Cancer

Macrophages are a highly plastic myeloid immune cell as a result of their innate function to respond to immune signals and facilitate appropriate supportive responses in various tissue types. Resident alveolar macrophages in the lungs mount an appropriate immune response upon air entering the lungs into favorable or detrimental downstream effects as a consequence of the mixed stimuli the airway transports. Furthermore, epithelial and other stromal influences can exacerbate macrophage-driven effects to cause enduring inflammation preceding a variety of pulmonary disease states. Macrophages recruited to

preneoplastic and malignant lesions within the lungs create opportunity to continue spurring on this tumor-promoting inflammation and communicate with tumors to facilitate a favorable environment for growth and metastasis [82]. Although TAMs in lung cancer and their participation in cancer initiation and progression have yet to be well understood, lung cancer-specific studies are being conducted in order to elucidate correlative links between different subsets of TAMs and prolonged survival. The literature reflects varying conclusions regarding TAM phenotype and prognosis that is context-dependent based on stage and location [82]. A study recently published in 2019 found a link between "M1-like" TAMs, also known as pro-inflammatory activated TAMs, and enhanced survival and prognosis [83]. Tissue samples from NSCLC samples have also revealed that adenocarcinoma tissue areas have more CD68 and CD163 – expressing macrophages than normal matched lung tissue [84]. A meta-analysis of lung cancer samples revealed that a higher rate of infiltrated TAMs correlated with worse overall survival (OS) and disease-free survival, and this association was likewise seen with the M2 population of TAMs, whereas the M1 population was associated with better survival [85].

1.16 Macrophage Activation States

Macrophages have been described to exert juxtaposing functionalities due to their ability to exert either pro-inflammatory or anti-inflammatory effects in response to external stimuli. For instance, M1 or pro-inflammatory macrophages

promote inflammation through release of pro-inflammatory cytokines as well as antigen presentation and are characterized as being IL-10 low, IL-12 high, inducible nitric oxide synthase (iNos) high, and tumor necrosis factor alpha (TNF-α) high [86]. M1 polarized macrophages through secretion of pro-inflammatory factors as well as reactive oxygen and nitrogen species confer immune responses to promote mounting immunity to destroy pathogens including tumors seen by the host immune system as foreign and detrimental to homeostasis [81]. Conversely, M2 or pro-tumorigenic macrophages facilitate the dampening of inflammation and wound-healing through release of anti-inflammatory and matrix remodeling cytokines and phagocytosis of debris. M2 macrophages are known to be characterized by Arginase1 (Arg1), IL-10, and mannose receptor c-type 1 (Mrc1) (also known as CD206) among others [81, 86].

Previous notions on macrophage functionality outlined the M1 and M2 dichotomy as black and white; however, extensive research on the functionality of these leukocytes supports a vast continuum of polarization states wherein these cells are plastic, subject to change fluidly with stimuli, and able to simultaneously express markers from more than one phenotypic category [87]. This plasticity is hypothesized to be highly complex *in vivo* due to the abundance of external varied stimuli that resident and recruited macrophages are subject to [88]. Moreover, recent research lacks a complete understanding of the vast immensity of macrophage phenotypes as a result of their plasticity [81].

Some literature suggests TAMs most closely resemble an alternatively activated M2 macrophage, exerting similar M2-like immunosuppressive functions related to promotion of cellular proliferation, angiogenesis, and resolution of inflammation [89, 90, 91]. This is thought to be due, at least in part, to a similar roster of cell-surface markers including CD163 and heat shock proteins [92]. However, there are other sources that have identified TAMs comprised of the traditional, M1/M2 dichotomy. Among many markers, a few identified to be potent and sensitive TAM markers are CD68, previously mentioned CD163, iNos, IL-1, VEGF, and Human Leukocyte Antigen – DR isotype (HLA-DR) [91]. These alternate subsets of TAMs work in opposing pro and anti-tumorigenic fashions to suppress or promote tumor growth, respectively [93].

1.17 Effect of Estrogen Signaling on Macrophage Functionality

Estrogen plays a pivotal role in macrophage functionality and involvement in tumorigenesis and tumor progression. It has been found to modulate inflammatory signaling of TAMs implicated in hormone-driven cancers. Estrogen induces signaling of the transforming growth factor receptor beta (TGF-β) pathway which has potent immunosuppressive functions as well as shuts off pro-inflammatory pathways IL-1 and TNF [94]. Furthermore, estrogen supplementation has shown to profoundly inhibit macrophage recruitment to areas of injury in a cardiovascular carotid artery disease *in vivo* model. The robust effect on chemotaxis was found to be mediated by monocyte

chemoattractant protein-1 (MCP1) also referred to as CCL2 [95]. Although research defining the role of estrogen and ER signaling on macrophage phenotype and functionality is scarce, there is evidence to support the role of ER signaling in alternative macrophage activation. ER knockout mice are resistant to IL-4-induced M2 differentiation, further supporting the evidence linking estrogen to an immunosuppressive microenvironment [95]. In addition to the direct effects on macrophage functionality and recruitment, estrogen was found to mediate T-cell inhibition through antigen-presenting macrophages [95]. As such, SERMs and other agents involved in ER signaling ablation are being investigated as points of intervention to control estrogen-driven immune modulation leading to tumorigenesis [94].

1.18 Effect of PPARγ Signaling on Macrophage Functionality

Owing to its dichotomy in pro and anti-tumorigenic effects, PPARγ activation although wholly identified as conveying anti-tumorigenic effects in a multitude of cells types, has also been implicated in tumor-promoting activities in certain stromal cells. PPARγ is widely expressed in stromal cells in the TME such as immune cell populations, endothelial cells, and fibroblasts [96]. Activation of PPARγ has been shown to vastly change the inflammatory landscape in a variety of disease states such as models of atherosclerosis and cancer. In the context of

cancer, TAMs have been implicated as a major population affected by this inflammatory shift with TZD administration. Several studies cite a shift towards TAMs with an anti-inflammatory, tumor-promoting phenotype with PPARγ activation [96, 97, 98]. Inflammatory pathways such as NF-κB are blunted, leading to downstream decreases in targets such as TNF, IL-1, and COX2 [99]. Shunting inflammatory responses away from pro-inflammatory pathways can lead TAMs to participate in pathways relating to angiogenesis, matrix remodeling, as well as other tumorigenic responses. As such, the cell context-dependent and time-sensitive manner in which PPARγ activation may affect the TME should be further investigated and thoroughly considered in order to maximize the benefit of PPARγ agonists with respect to chemotherapy and chemoprevention efforts.

2. Focus of Research

It is our overall hypothesis that activating the PPARγ pathway, an antineoplastic pathway in combination with inhibiting the pro-tumorigenic ER pathway is a more efficacious chemopreventive strategy than either approach individually in a chemoprevention model of NSCLC. We tested this hypothesis in two studies:

I. Determining interactions between the PPARγ signaling pathway and the estrogen signaling pathway *via in vitro* modeling of macrophages and lung carcinoma cells simulating the tumor microenvironment

II. Determining a potential enhanced effect between anti-estrogen fulvestrant and PPARγ agonist pioglitazone in reducing lung dysplasia and lung tumorigenesis in an animal model

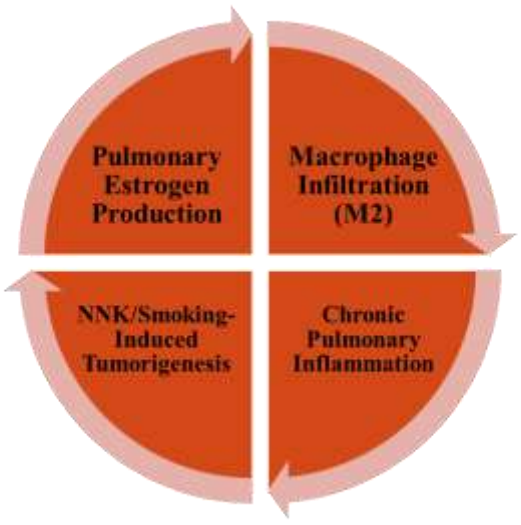

Model depicting the cycle of carcinogen induced adenocarcinoma, fueled by autocrine regulation of estrogen mediating smoldering inflammation via macrophages.

3. Materials and Methods

Chemical Reagents

Tobacco-specific NNK was purchased from TRC. Fulvestrant (ICI 182,780) was purchased from Tocris Bioscience, and pioglitazone was purchased from Thermo Fisher Scientific.

Cell Lines and Culture Conditions

THP-1 immortalized human leukemia monocytic cell line was acquired from the Schwertfeger lab (University of Minnesota) and cultured in RPMI 1640 medium (Gibco) supplemented with 10% heat-inactivated FBS, 1x penicillin/streptomycin (Thermo Fisher Scientific), and 1x GlutaMax (Life Technologies). A549 human immortalized NSCLC cell line was purchased from the American Type Culture Collection (ATCC) and was cultured in BME medium (Gibco) supplemented with 10% heat-inactivated FBS, 1x penicillin/streptomycin (Thermo Fisher Scientific), and 1x GlutaMax (Life Technologies). Cell lines were authenticated by short tandem repeat DNA profiling and used within 6 months of testing. Frozen cell stocks were passaged a maximum of 15 times, and cells were mycoplasma-free. Cells were grown to 80-90% confluence in full serum medium incubated at growth conditions of 37°C and 5% CO_2 prior to experimental setup.

Macrophage Individual Culture

THP-1 cells were seeded at 1.2E6 cells per well in a 6-well plate with 5 ng/mL PMA in full serum RPMI 1640 growth medium. After 24 hour attachment, cells were serum-starved overnight approximately 18 hours with phenol red-free RPMI 1640 medium supplemented with 1x penicillin/streptomycin and 1x GlutaMax. Cells were subsequently left untreated as resting M0 state, or differentiated into M2 phenotype by supplementing the medium with 10 ng/mL IL-4 (R&D Systems), 10 ng/mL IL-6 (R&D Systems), and 10 ng/mL IL-13 (R&D Systems), respectively, for 24 hours. After 24 hour incubation for phenotype differentiation, THP-1 cells were treated with dimethyl sulfoxide (DMSO) (Thermo Fisher), 500 nM pioglitazone, 5 μM fulvestrant, and combination (500 nM pioglitazone and 5 μM fulvestrant), all at 1 uL per 1 mL of growth medium of DMSO for 24 and 48 hours prior to quantitative real-time PCR (RT-qPCR) and enzyme-linked immunosorbent assay (ELISA) of conditioned media endpoint analyses, respectively.

Cancer Cell Individual Culture

A549 cells were seeded at 0.5E6 cells per well in a 6-well plate in full serum medium. After 24 hour attachment, cells were serum-starved overnight approximately 18 hours with phenol red-free MEM medium (Gibco) supplemented with 1x penicillin/streptomycin and 1x GlutaMax. Cells were

treated with DMSO, 500 nM pioglitazone, 5 μM fulvestrant, and combination (500 nM pioglitazone and 5 μM fulvestrant), all in 1 uL per 1 mL medium of DMSO for 48 hours prior to immunoblotting endpoint analysis.

Cancer Cell Conditioned Media Co-culture

A549 cells were seeded at 0.5E6 cells per well in a 6-well plate in full serum BME medium. After 24 hour attachment, cells were serum-starved overnight (approximately 18 hours) with phenol red-free MEM medium supplemented with 1x penicillin/streptomycin and 1x GlutaMax. Cells were treated with DMSO, 500 nM pioglitazone, 5 μM fulvestrant, and combination (500 nM pioglitazone and 5 μM fulvestrant), all in 1 uL per 1 mL medium of DMSO for 6 hours and medium was subsequently changed to fresh, serum free and incubated for 24 hours. Following 24 hour incubation, A549 conditioned media was placed on THP-1 cells seeded according to the macrophage individual culture protocol and given 24 hours to incubate prior to ELISA analysis of conditioned media.

Macrophage/Cancer Cell Transwell Co-culture

THP-1 cells were seeded at 1.2E6 cells per well in a 6-well plate with 5ng/mL PMA in full serum medium. After 24 hour attachment, cells were serum-starved overnight (approximately 18 hours) with phenol red-free 1:1 RPMI 1640:MEM medium supplemented with 1x penicillin/streptomycin and 1x

GlutaMax. Cells were subsequently left untreated as naïve M0 phenotype or differentiated into M2 phenotype by supplementing the medium with 10 ng/mL IL-4 (R&D Systems), 10 ng/mL IL-6 (R&D Systems), and 10 ng/mL IL-13 (R&D Systems), respectively, for 6 hours and medium was subsequently changed to fresh, serum free and incubated for 24 hours. Following 24 hour incubation, polyethylene terephthalate (PET) transwell membrane inserts (Falcon) seeded with 0.5E6 A549 cells per membrane for 24 hours and then for approximately 24 hours in serum-free 1:1 RPMI 1640:MEM medium were placed in wells with THP-1 seeded macrophages and replaced with fresh medium for 48 hours prior to ELISA analysis of conditioned media.

Isolation and Culture of Murine Bone Marrow-Derived Macrophages

After obtaining femurs and tibia from euthanized mice, bones were rinsed with ethanol followed by DMEM culture medium. Ends of bones were cut to expose the marrow and a 30mL syringe filled with DMEM culture medium was used to flush the marrow out of each bone into a 50mL conical tube. Bones were flushed from both cut ends to ensure maximum recovery of marrow. Once all bones were flushed, a single-cell suspension was made by drawing media containing the marrow back up into the syringe through the needle. Cells were centrifuged at 1200 rpm for 5 minutes at 4°C and supernatant was subsequently aspirated from the pellet. Pellet was resuspended in 3 mL ACK Lysis buffer (4.15 g NH_4Cl, 0.5 g $KHCO_3$, 0.1 mM EDTA) for 1 minute and quenched with 10 mL

DMEM10 medium (DMEM growth medium supplemented with 10% FBS, 1x sodium pyruvate, 1x penicillin/streptomycin, and 1x GlutaMax). Cells were again centrifuged at 1200 rpm for 5 minutes at 4°C. Pellet was resuspended in 31 mL DMEM10 medium and cell count was performed, and 1E7 cells per dish were plated in 15 cm plates with a final volume of 30 mL of DMEM10 medium supplemented with 1x penicillin/streptomycin. On day 4 of culture, 15 mL of the medium was replaced with fresh medium. Cells were confluent and ready to be plated for experiments on day 6.

Bone Marrow-Derived Macrophage Conditioned Media Co-culture

Bone marrow-derived macrophages (BMDMs) on day 6 are detached from culture plate with 0.25% Trypsin-EDTA (Gibco) for 5 minutes and quenched with culture medium, repeatedly pipetting the plate to ensure full detachment of cells. Cells were centrifuged at 1200 rpm for 5 minutes, and supernatant was aspirated. Cells were resuspended in medium, counted, and plated at a density of 1.3E6 cells per well in a 6-well dish and left as resting state or primed as M2 with 10 ng/mL IL-4, 10 ng/mL IL-6, and 10 ng/mL IL-13. Concurrently, 3.5E5 cells per well of FVBW-17 cancer cells were plated in separate wells. After 24 hours of attachment, complete growth medium was removed and replaced with serum-free DMEM and DMSO, pioglitazone, fulvestrant, and combination were added to BMDMs at previously specified doses. After 6 hour incubation of the drugs, medium was changed to fresh, serum-free and allowed to incubate for 24 hours.

After 24 hour incubation period, conditioned medium from BMDMs was placed on FVBW-17 wells. RNA was isolated from BMDM wells for future mRNA analysis and 0.5mL of conditioned media was reserved for ELISA analysis. After 24 hour incubation of BMDM conditioned media on the FVBW-17 cells, conditioned media was collected for ELISA analysis.

Bone Marrow-Derived Macrophage Transwell Co-culture

Following previously described BMDM culture protocol, detached from culture plate with 0.25% Trypsin-EDTA for 5 minutes and quenched with culture medium, repeatedly pipetting the plate to ensure full detachment of cells. Cells were centrifuged at 1200 rpm for 5 minutes, and supernatant was aspirated. Cells were resuspended in medium, counted, and plated at a density of 1.3E6 cells per well in a 6-well plate and left as resting state or primed as M2 with 10 ng/mL IL-4, 10 ng/mL IL-6, and 10 ng/mL IL-13. FVBW-17 cells were plated in separate plates in transwell inserts at a density of 3.5E5 cells per membrane. After BMDMs were primed overnight for 18 hours, complete growth medium was removed and replaced with serum-free DMEM and DMSO, pioglitazone, fulvestrant, and combination for 6 hours, prior to replacing with fresh, serum-free medium and adding membrane inserts containing FVBW-17 cells. Transwell incubation proceeded for 24 hours prior to conditioned media collection for ELISA analysis and RNA isolation from BMDM wells for future mRNA analysis.

Anchorage-Independent Colony Formation Assay

A549 NSCLC cells were detached from the plate using Trypsin-EDTA and seeded at a density of 1E4 cells per well in a 6-well plate in soft agar with full serum BME media to determine anchorage-independent growth. Sea Plaque Agarose (Lonza) was used to prepare 1.0% base agarose layer and a 0.75% upper agarose layer containing cells. After cell seeding in upper agarose layer, 1mL of full serum BME growth media supplemented with DMSO, 500 nM pioglitazone, 5 μM fulvestrant, and combination (500 nM pioglitazone and 5 μM fulvestrant), all in 1 uL per 1 mL media of DMSO prior to incubation. Medium was replaced every 2-3 days, and colony formation was monitored after 14 days of treatment. Prior to colony visualization, media was aspirated and wells were incubated with crystal violet in 10% formalin for 1.5 hours. Using a dissecting scope, colonies were photographed in a 6-well plate (with 4 quadrants/well) using ImageJ software analysis to automatically count colonies, using 100 pixels as a cutoff with no circularity requirements. Large colonies were defined as 3,000-infinity pixel units.

Protein Analysis

Immunoblotting

Following cell culture or lung isolation, cell or whole lung lysates were extracted and protein concentrations quantified using DC assay reagents (BioRad). Whole cell lysates (40 mg/sample) were electrophoresed on 7.5% SDS–polyacrylamide gels for 1.5 hours and transferred onto Trans-Blot polyvinylidene difluoride (PVDF) membranes (BioRad) for 1 hour at 100 volts on ice. The membranes were blocked using 5% nonfat dry milk and 0.1% Tween 20 in 1x phosphate-buffered saline (TBST) for 1 hour. Membranes were incubated in primary antibody (in 1% milk in 1x TBS-Tween) at 4°C overnight and washed 3 times with TBST at 15 minutes each followed by incubation with secondary host-specific IgG antibody for 1 hour at room temperature (RT). After secondary antibody incubation, membranes were washed an additional 3 times in TBST at 15 minutes each. Blots were developed using a super-enhanced chemiluminescence substrate according to the manufacturer's protocol (Thermo Fisher Scientific). Quantification of protein expression was assessed using ImageJ 1.X software (National Institute of Health, Bethesda, MD).

Primary Antibodies

Primary Antibody	**Host**	**Dilution**	**Manufacturer**

Aromatase	Rabbit	1:1000	Thermo Fisher
COX2	Rabbit	1:2000	Cell Signaling
Cyclin D1	Rabbit	1:1000	Cell Signaling
ERβ	Rabbit	1:1000	Thermo Fisher
PPARγ	Rabbit	1:1000	Abcam
NF-κB	Rabbit	1:2000	Cell Signaling
pAkt	Rabbit	1:1000	Cell Signaling
pMAPK	Rabbit	1:1000	Cell Signaling
GAPDH	Rabbit	1:1000	Cell Signaling

Quantitative Real-Time PCR analysis

Trizol (Invitrogen) was used to extract total RNA from cultured cells. One microgram of total RNA was reverse transcribed using a cDNA synthesis kit (Quanta Biosciences) using a T100 Thermal Cycler (BioRad). Real-time qPCR was performed using a SYBR Green Super Mix kit (Quanta) on a CFX connect Real-Time System (BioRad) according to manufacturer specifications. Gene-specific primers for target genes were used to assess mRNA levels normalized to GAPDH mRNA levels as an internal control, and the ratio of normalized mRNA to the control conditions was determined using the comparative DCT method for analysis. The primers used for real-time qPCR are as follows:

Primers

Target	Forward	Reverse
GAPDH	5’-GGA GCG AGA TCC CTC CAA AAT-3’	5’-GGC TGT TGT CAT ACT TCT CAT GG-3’
Aromatase	5’-ACC CTT CTG CGT CGT GTC A-3’	5’-TCT GTG GAA ATC CTG CGT CTT-3’
CD209	5’-AAT GGC TGG AAC GAC GAC AAA-3’	5’-CAG GAG GCT GCG GAC TTT TT-3’
IL-23	5’-ATT TTC ACA GGG GAG CCT TC-3’	5’-GAC TGA GGC TTG GAA TCT GC-3’
Mouse IL-10	5’-CTG GAC AAC ATA CTG CTA ACC G-3’	5’-GGG CAT CAC TTC TAC CAG GTA A-3’
Mouse GAPDH	5’-AAG GTC ATC CCA GAG CTG AA-3’	5’-CTG CTT CAC CAC CTT CTT GA-3’

Enzyme-Linked Immunosorbent Assay

ELISA analysis was performed using either BALF isolated as previously described or conditioned-media isolated from individual or co-culture cell cultures. Host-specific kits were adjusted based on the source of medium being analyzed. Ligands were measured using commercially available ELISA kits from R&D systems. Each sample was run in triplicate to ensure accuracy and readings were normalized for total protein in each sample.

In vivo NNK-Induced Lung Carcinogenesis Model

Timeline

All animal experiments were approved by Institutional Animal Care and Use guidelines. FVB/N mice were used for both intact and ovariectomized studies and were age and size matched. Mice were ovariectomized and delivered prior to study onset. Mice were given 3 mg of NNK intraperitoneally in sterile saline twice per week for a duration of 4 weeks, totaling 24 mg of NNK. Following carcinogen exposure, mice were given a 5 week rest period to simulate an ex-smoker population. Mice were then split into 4 treatment groups of DMSO in peanut oil vehicle (Thermo Fisher Scientific), 0.15% pioglitazone in medicated chow and DMSO in peanut oil vehicle twice per week, 30 mg/kg fulvestrant in peanut oil vehicle twice per week and control chow, and 0.15% pioglitazone in medicated chow plus 30 mg/kg fulvestrant in peanut oil twice per week. Peanut oil injections were given at a volume of 200 µL in the 14 week treatment groups for ovariectomized and intact models and for the 1 week intact treatment group. Vehicle oil volume was reduced to 100 µL for the 1,3, and 8 week ovariectomized treatment groups.

Endpoints

In 14 week-treated mice from both intact and ovariectomized studies, lungs were harvested and fixed in phosphate-buffered formalin, and subsequently transferred to 70% ethanol within 48 hours of formalin fixation.

Tumor burden of lungs was evaluated under a dissecting microscope for both tumor number and size. Tumors presented on the surface of the lung and were imaged and counted under a dissecting microscope. Images were then assessed for tumor size by measuring surface area using the LAS V4.12 Leica program. Lungs were further used for histological analysis *via* immunohistochemistry.

Bronchio-alveolar lavage fluid (BALF) was isolated from the lungs of 1, 3, and 8 week treated mice in both studies by flushing 1.5 mL of PBS through the bronchioles with a catheter and retracting all fluid to be saved for protein analysis and cells to be used for immunofluorescence. BALF was pooled by treatment group and saved on ice until all mice were euthanized. Samples were centrifuged at 1600 rpm for 5 minutes at 4°C and supernatant was saved for ELISA analysis at -80°C. Cell pellet was resuspended in PBS and cell count was performed. Cells were suspended at a final concentration of 1E5 cells per 300 µL PBS supplemented with 0.05% BSA. A Cytospin centrifuge was used to fix cells to slides at 1E5 cells per slide using a program set to run at 800 rpm for 3 minutes. Slides were fixed and dried overnight at RT and subsequently transferred to -80°C for long-term storage until use.

Lung Airway Histology and Immunohistochemistry

Following formalin inflation and ethanol incubation as previously described, whole lungs were separated into individual lobes, cleaned of excess

connective tissue, and loaded into immunohistochemical cassettes for paraffin processing and embedding. A series of ethanol, Citrisolv, and paraffin incubations were performed for a total run time of 16 hours and 39 minutes. Tissue was then transferred to a beaker of paraffin and pressurized in a vacuum chamber for 30 minutes and subsequently embedded into paraffin using the immunohistochemical cassette. Blocks cured at 4°C overnight prior to sectioning. A microtome was used to section blocks at a depth of 5 mm per section, and tissue was fixed onto glass slides overnight at 37°C.

For IHC staining, slides were deparaffinized and rehydrated using 3 successive washes of xylene followed by ethanol ranging from 100% to 70%. Antigen retrieval was performed in a microwave oven for 20 minutes in a sodium citrate-based unmasking solution at pH6 followed by peroxidase blocking in 3% hydrogen peroxide for 15 minutes. The sections were incubated in host-specific blocking buffer (Vector Laboratories) for 1 hour at RT. Sections were then incubated with protein-specific primary antibodies and peroxidase-conjugated host-specific secondary antibodies. Sections were developed with DAB and counterstained with hematoxylin. Bright field microscopy was performed using Leica DM 4000B LED microscope, and images were captured at 20X and 40X magnification using LASv4.7 software. IHC analysis was performed blinded with 15 images each from 5 mice per treatment group graded as low, moderate, or high. Staining was graded either as percent field or intensity-based. Percent-based was graded as negative (0% positive staining), low (1-30% positive

staining), moderate (30-60% positive staining), or high (60%-100% positive staining). Intensity-based quantification was determined after ascertaining the range of intensity of positive staining found in all tissues for each protein of interest.

Primary Antibodies

Primary Antibody	**Host**	**Dilution**	**Manufacturer**	**Catalog Number**
PPARγ	Rabbit	1:800	Cell Signaling	2435S
MMP9	Rabbit	1:1000	Abcam	ab38898
VEGF	Rabbit	1:200	Abcam	Ab52917
F4/80	Rat	1:100	BioRad	MCA497GA
Cyclin D1	Rabbit	1:100	Abcam	ab134175
pAkt	Rabbit	1:100	Cell Signaling	4060S
AREG	Rabbit	1:800	Invitrogen	PA5-27298

Flow Cytometry Analysis

Whole Lung Digestion

After mice were euthanized, lungs were suspended in RPMI 1640 medium supplemented with 10% FBS on ice. Lungs were subsequently incubated in 1x

collagenase (Sigma Aldrich) and 1x DNase I (Invitrogen) for 30 minutes in an incubator at 37°C with 5% CO_2, with periodic mixing of the digestion buffer. After incubation, lungs were transferred to a strainer filter and mechanically pushed through the filter using the blunt end of 3 mL syringe, with periodic flushing of the membrane with RPMI medium. Cell count was performed and 1E7 cells were separated into sample tubes and brought to equal volume with FACs buffer (PBS supplemented with 2% FBS and 5 mM EDTA). Cells were washed once and incubated with Fc blocking antibody at 1 uL per 1 million cells for 15 minutes on ice. Cells were washed again and subsequently stained with fluorescently labeled antibodies using EFluor 506 live/dead dye (eBioscience), CD45 (BD Bioscience), CD11b (Biolegend), F4/80 (Biolegend), and CD206 (Biolegend) for 30 minutes on ice in the dark. After incubation, cells were washed in FACs buffer and resuspended in FACs buffer supplemented with 0.5% paraformaldehyde (PFA) at a final volume of 0.5 mL. Fluorescently-labelled cells were analyzed and gated on an LSR Fortessa cell sorting machine, and data were further analyzed by FACsDiva.

Statistical Analysis

For statistical analyses, data were reported as mean ± SD or SEM. To assess significance between different treatment groups, a Student t test (two tailed) was used to determine significance with P values at least < 0.05 categorized as statistically significant. To analyze IHC scoring data, the Chi-

Squared test was used to compare the frequency of negative, low, moderate, and high scoring within and across treatment groups. Data represent biological triplicates with n=2 or n=3 per group per treatment group for all *in vitro* experiments.

4. Chapter I: Determining interactions between the PPARγ signaling pathway and the estrogen signaling pathway *via in vitro* modeling of macrophages and lung carcinoma cells simulating the tumor microenvironment.

4.1 Introduction

Owing to its aggressive nature and current limitations on early detection, lung cancer, although not the most prevalently diagnosed form of cancer in the United States, is the most lethal, killing more individuals annually than the two most frequently diagnosed cancers, breast and prostate combined [1, 2]. As such, efforts to identify chemoprevention options to curb these statistics as well as novel chemotherapeutic options to target current therapeutic limitations in lung cancer are vital to reversing the dire state of the disease. Current approaches in chemoprevention aim to delay or prevent onset of malignancy and reeducate the tumor microenvironment in such a way to facilitate this delay through manipulation of pathways outlined in Hanahan and Weinberg's widely accepted hallmarks of cancer [47].

ERβ cytoplasmic expression has been implicated as a negative prognostic indicator in lung cancer and has been shown to promote tumor growth and sustain tumorigenic inflammation, one such identified hallmark of cancer [47, 94, 100]. ERβ, specifically, is the primary isoform in the lungs and is expressed equally in both male and female lung cancers [35, 41]. Anti-estrogens have

already been implemented for primary and secondary breast cancer prevention, showing excellent safety profiles for long-term use [101].

PPARγ was identified as a potentially efficacious chemoprevention agent following a cohort study identifying a decrease in lung cancer incidence in patients taking TZDs as indicated for type 2 diabetes mellitus [56]. A barrage of preclinical data supporting its anti-neoplastic effects was also elucidated [57, 59, 61]. Furthermore, estrogen signaling was found to be upregulated in human lung dysplasias that positively regressed following a PPARγ agonism chemoprevention approach that were classified as persistent or aggressive at the onset of study [46]. Mouse models of lung cancer revealed that within the TME of these estrogen-sensitive lung cancers, an abundance of inflammatory cells positive for the estrogen synthesis enzyme aromatase as well as estradiol were identified, suggesting a local production and paracrine regulation of estrogen and ER signaling, supporting the exploration of anti-estrogens re-purposed for chemoprevention in lung cancer [41].

In this study, we tested the ability of a novel chemoprevention combination of PPARγ agonist pioglitazone and anti-estrogen fulvestrant to modify both the inflammatory environment *via* macrophages to decrease tumor-promoting pathways as well as the growth potential of cancer cells *in vitro.* Targeting two pathways known to be dually exploited in lung tumorigenesis could be a novel therapeutic niche to more effectively reeducate the TME against tumor-promoting effector signaling. To do this, we established a variety of co-culture models using

both human and murine macrophage and lung cancer cell lines to simulate cross-talk signaling occurring in the *in vivo* TME as a way to monitor the effect of pioglitazone and fulvestrant on macrophage functionality through inflammatory signaling pathways and cancer cell anchorage-independent growth.

4.2 Results

Receptors and Downstream Targets are Present in Cell Lines

We first established the presence of both ERβ and PPARγ receptors (Figure 1A) as well as several known downstream targets of both receptors in the human macrophage THP-1 cells (Figure 1B) and human NSCLC A549 cancer cells (Figure 1C). Cell lysates were analyzed *via* immunoblot analysis and probed for receptors and reported downstream targets. Both pioglitazone and fulvestrant single treatments upregulated expression of phosphorylated Akt and phosphorylated MAPK in THP-1 cells, both of which were alleviated with combination treatment (Figure 1B). Akt activation was not altered in A549 cells with treatments. Pioglitazone conferred a small decrease in MAPK activation which was not observed with combination (Figure 1C).

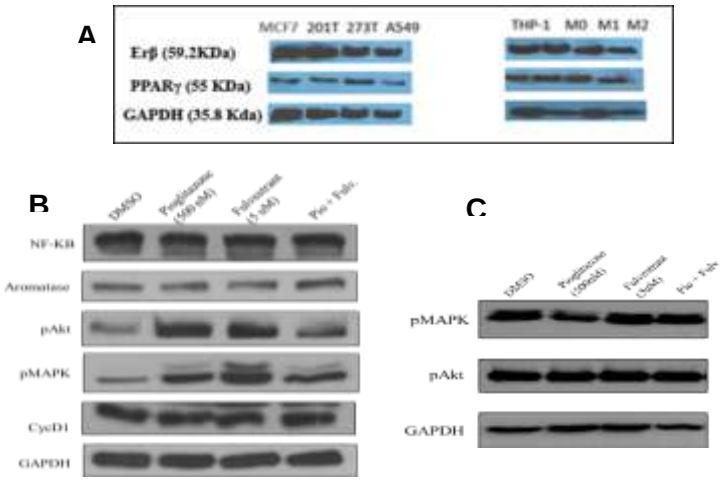

Figure 1. A. Immunoblot analysis of ERβ and PPARγ in both A549 NSCLC cells and THP-1 human macrophages. **B.** Immunoblot analysis of downstream ER and PPARγ protein targets in THP-1 macrophages after single and combination treatment for 24 hours. **C.** Immunoblot analysis of downstream ER and PPARγ protein targets in A549 NSCLC cells after single and combination treatment for 24 hours.

M2 Macrophages Compared with M0 Macrophages Display Increased Sensitivity to ER Blockade

To understand how M2-polarized TAM-like macrophages differentially regulate estrogen production, real-time qPCR of mRNA isolated from naïve, M0 THP-1 macrophages treated with PBS control and M2 THP-1 macrophages stimulated with IL4 and IL-13 confirmed by CD209 upregulation ($p<0.001$) revealed that M2 macrophages had approximately 2.5-fold significantly higher expression of aromatase, the rate-limiting enzyme that converts androgen precursors to estrogen, compared with the M0 counterpart (Figure 2A). This could suggest that M2 macrophages are more sensitive to estrogen signaling pathways as a feed-forward autocrine mechanism, as ER signaling has been reported to potentiate tumor-promoting immunosuppressive pathways in immune cells [94]. To test the functional effect of this upregulation in aromatase expression, M0 versus M2 macrophages were subject to an *in vitro* androgen precursor androstenedione (AD) and 17β-estradiol was measured in the supernatant *via* ELISA (Figure 2B). We observed a corresponding 2-fold increase in estradiol production that did not, however, reach statistical significance compared to M0 control.

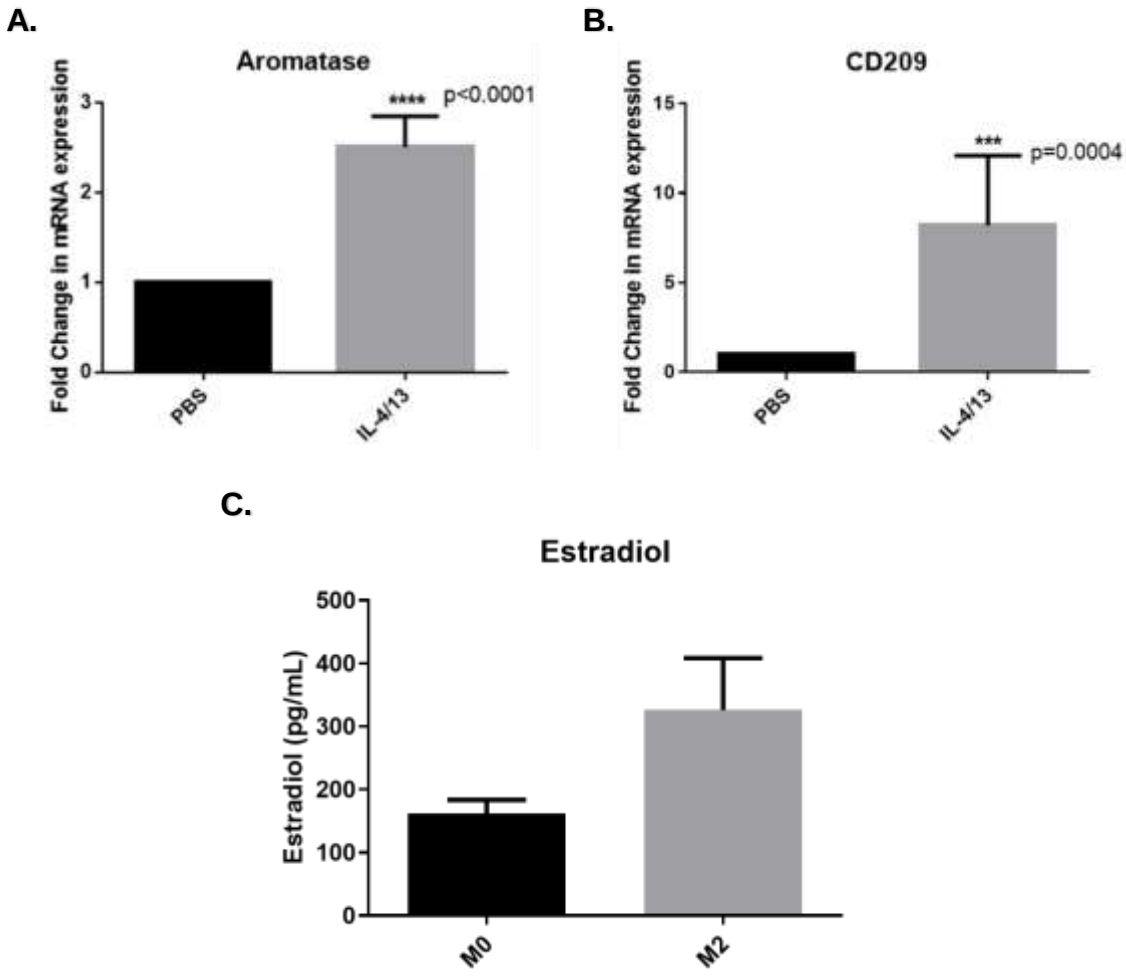

Figure 2. A. Real-time qPCR analysis of aromatase expression of THP-1 mRNA in resting state PBS control macrophages or in IL-4 and IL-13 (IL-4/13) M2 macrophages primed for 24 hours. **B.** Real-time qPCR analysis of CD209 expression of THP-1 mRNA in resting state PBS control macrophages or in IL-4 and IL-13 M2 macrophages primed for 24 hours. **C.** ELISA analysis of supernatant from resting state or M2-primed macrophages after 48 hours incubation with estrogen precursor androstenedione (AD) compared to control wells without precursor. Data are expressed as mean $\pm$ SEM.

Fulvestrant Causes a Paradoxical Upregulation of the ER Pathway in Macrophages

To determine the differential effect of drug treatments on estrogen regulation in M0 versus M2 macrophages, real-time qPCR of mRNA isolated from M0 or M2-stimulated THP-1 macrophages treated with DMSO control, 500 nM pioglitazone, 5 μM fulvestrant, or combination treatment (500 nM pioglitazone and 5 μM fulvestrant) showed that fulvestrant increased aromatase 2-fold ($p<0.05$) in M0 macrophages and nearly 6-fold ($p<0.0001$) in M2-stimulated macrophages (Figure 3A), suggesting that similarly to results in Figure 2A, M2 macrophages are more sensitive to pathways conferring anti-inflammatory effects such as the ER pathway, and that ER-blockade may further elevate this response. Combination treatment fully restored baseline aromatase expression in M0 macrophages and only partially rescued aromatase expression in the M2 polarized cells. To measure the functional effect of differential aromatase expression across treatments, cells were subject to androstenedione and estrogen was measured *via* ELISA analysis of the supernatant (Figure 3B). To functionally assess estrogen regulation in the M2-TAM population of macrophages in a TME-simulated culture, A549 NSLC cells were pre-cultured with DMSO control, 500 nM pioglitazone, 5 μM fulvestrant, or combination treatment (500 nM pioglitazone and 5 μM fulvestrant) and M2-polarized THP-1 macrophages were exposed to conditioned media from the drug-treated cancer cells in the presence of androstenedione and estradiol production by the

macrophages was measured *via* ELISA (Figure 3C). Fulvestrant treatment conferred a significant increase in estradiol production compared to DMSO control. Although this increase did not reach significance, combination treatment was able to ablate the paradoxical increase by more than 2-fold ($p<0.01$) bringing estrogen below DMSO baseline. Similarly to treating macrophages directly with the drugs in Figure 3A, fulvestrant, likewise, stimulated the cancer cells to upregulate the ER pathway in M2-macrophages through paracrine signaling mechanisms and addition of pioglitazone was sufficient to significantly block this effect.

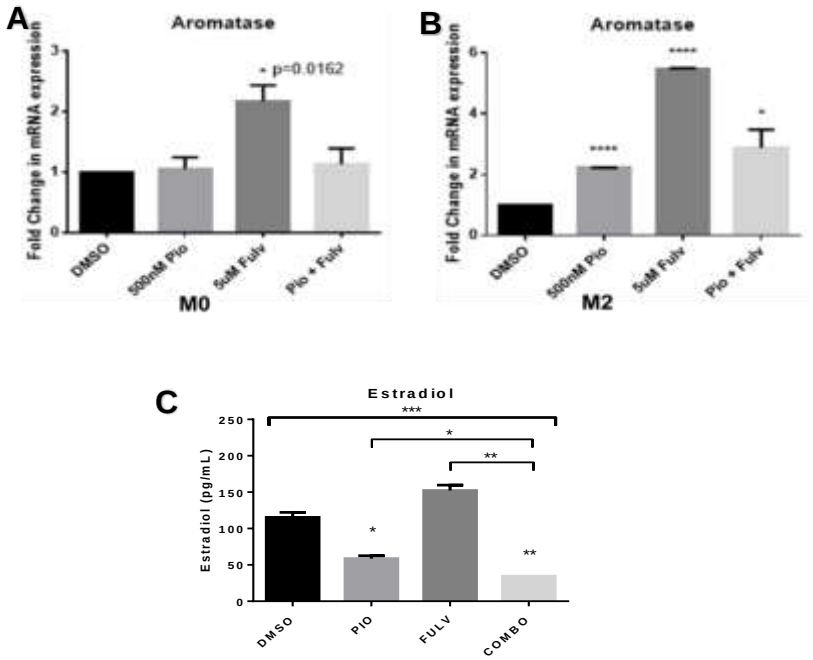

Figure 3. A. Real-time qPCR analysis of aromatase expression of THP-1 mRNA in resting state PBS control macrophages treated with DMSO control, single, or combination treatments for 24 hours. **B.** Real-time qPCR analysis of aromatase expression of THP-1 mRNA in IL-4 and IL-13 M2-primed macrophages treated with DMSO control, single, or combination treatments for 24 hours. **C.** ELISA analysis of estradiol in supernatant from M2-primed macrophages that were challenged with conditioned media for 24 hours from A549 cells that were pre-treated with DMSO, single, or combination treatments for 6 hours. Data are expressed as mean $\pm$ SEM.

Pioglitazone and Fulvestrant Combination Treatment Shifts Macrophages Away from a Tumor-Promoting Phenotype in Human Macrophage Cells

We then investigated the ability of pioglitazone and fulvestrant, both alone and in combination, to reeducate macrophages away from a TAM phenotype. To do this, we ran real-time qPCR of mRNA isolated from naïve, M0 or M2-stimulated THP-1 macrophages treated with DMSO control, 500 nM pioglitazone, 5 μM fulvestrant, or combination treatment (500 nM pioglitazone and 5 μM fulvestrant) to assess classic M1 markers iNOS and IL-23, alternative M2 marker CD209, and well-defined TAM markers CCL2 and MMP9. Naïve macrophages were educated by both single treatment and maximally by the combination to express higher levels of iNOS and IL-23 (Figure 4A). Furthermore, M0 macrophages had lower expression of TAM markers CCL2 and MMP9, linked with macrophage chemotaxis propensity and matrix remodeling capability when treated with the combination (Figure 4C). Finally, in pre-educated M2 macrophages, combination was able to regress expression of M2 marker CD209 below DMSO control baseline expression, suggesting that the combination has the potential to revert already-established tumorigenic macrophages back to an inert state. (Figure 4B).

To more accurately confirm this potential regression of a TAM phenotype in a functional assay and elucidate the ability of the drugs to manipulate macrophage functionality in a paracrine fashion through cancer cells, we challenged the macrophages to the same TME-simulated culture as described in

Figure 3D where the A549 cells were cultured in the presence of the drugs and the cancer cell-conditioned media was then used to challenge M2-stimulated macrophages. We measured cytokines that have been previously reported to be secreted by TAMs to promote tumorigenesis. Pioglitazone, individually, does not alter VEGF levels, but fulvestrant single treatment is able to reduce secreted VEGF levels significantly ($p<0.01$) (Figure 5A). Combination showed the greatest decrease, surpassing the reduction seen with fulvestrant single treatment ($p<0.001$). This suggests that pioglitazone may confer its primary effect on VEGF synergistically through an estrogen-mediated pathway in macrophages to illicit maximal regulation of this well-defined mediator of angiogenesis. We also measured levels of IL-1β, a known inducer of COX2/PGE2 signaling which has also been reported to be negatively implicated in cancers [23]. Conversely to VEGF secretion, pioglitazone, alone, was sufficient to illicit maximal down-modulation of IL-1β levels as a single treatment ($p<0.01$), suggesting that pioglitazone may work primarily to augment inflammatory pathways in the macrophages rather than pathways implicated in other tumorigenic activity (Figure 5B). Fulvestrant single treatment was able to reduce IL-1β, as well ($p<0.05$), although not to the degree that pioglitazone single treatment did. Furthermore, combination treatment maintained similarly reduced IL-1β secretion to pioglitazone single treatment ($p<0.01$), illustrating that combination does not have an additive effect on IL-1β secretion as it does on other targets.

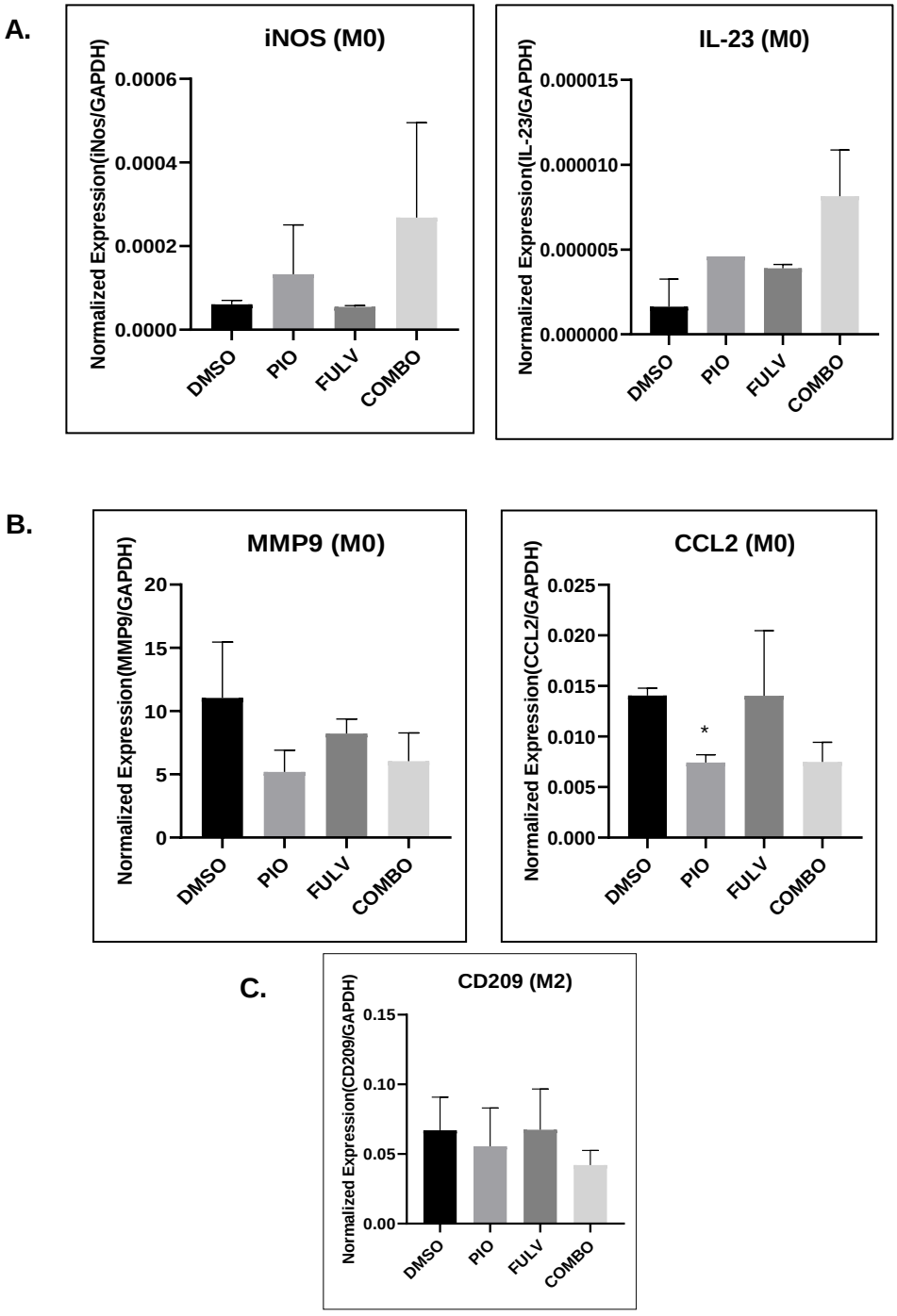

Figure 4. A-B. Real-time qPCR analysis of expression of M1 markers iNOS and IL-23 and TAM markers MMP9 and CCL2 in THP-1 mRNA in resting state PBS control macrophages treated with DMSO, single, or combination treatments for 24 hours. **C.** Real-time qPCR analysis of M2 marker CD209 expression in THP-1 mRNA in M2-primed macrophages treated with DMSO, single, or combination treatments for 24 hours. Data are expressed as mean ± SEM.

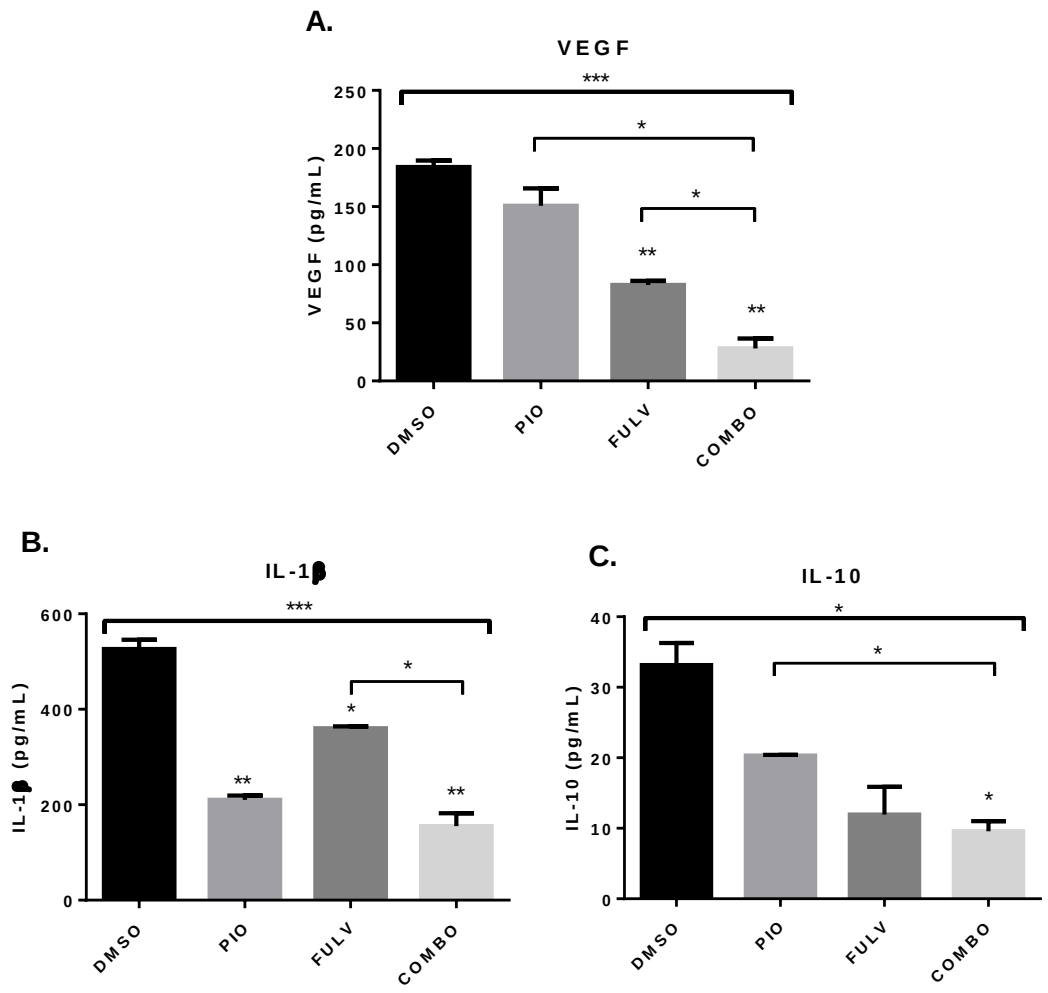

Figure 5. A-C. ELISA analyses of VEGF, IL-1β, and IL-10 in supernatant from M2-primed macrophages that were challenged with conditioned media for 24 hours from A549 cells that were pre-treated with DMSO, single, or combination treatments for 6 hours. Data are expressed as mean + SEM.

Pioglitazone and Fulvestrant Combination Treatment Shifts Macrophages Away from a Tumor-Promoting Phenotype in Primary Murine Macrophages

We next aimed to investigate if the ability of single or combination treatments to reinstruct macrophages would translate to primary cells of murine origin. Primary murine macrophages were differentiated from bone-marrow-derived monocytes and used in a resting state or primed as M2. After treating the macrophages with single or combination treatments, conditioned media from the macrophages was used to challenge FVBW-17 immortalized murine adenocarcinoma cells. We analyzed gene expression of the macrophages after subsequent drug treatments *via* real-time qPCR and analyzed secreted IL-1β expression by the cancer cells to determine the ability of pioglitazone and fulvestrant to modify macrophage function (Figure 6A-D) and subsequently, alter tumorigenic IL-1β cytokine production by the cancer cells (Figure 6E-F).

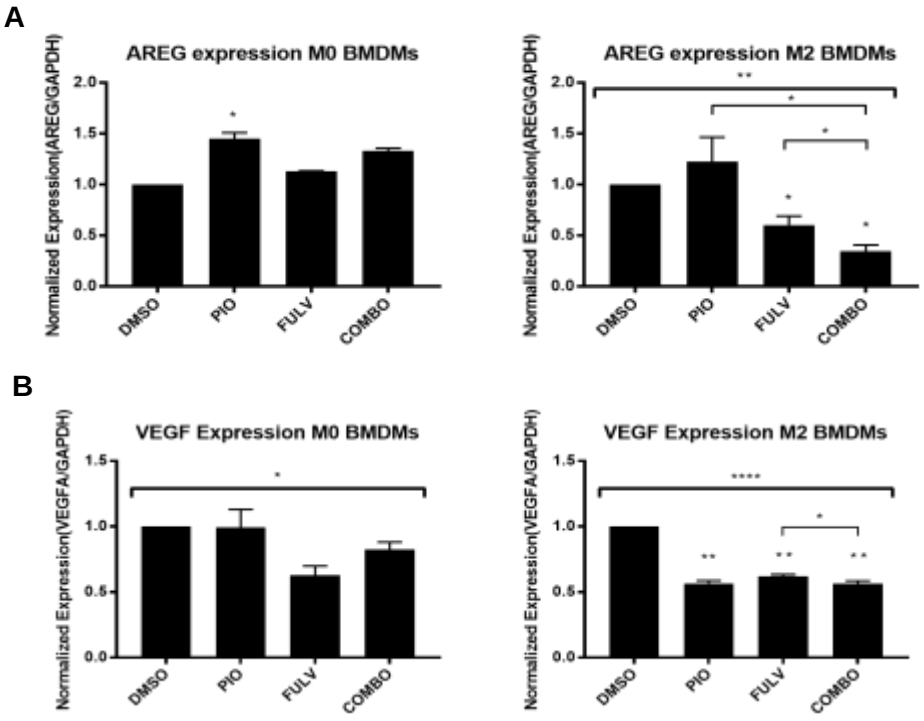

C.

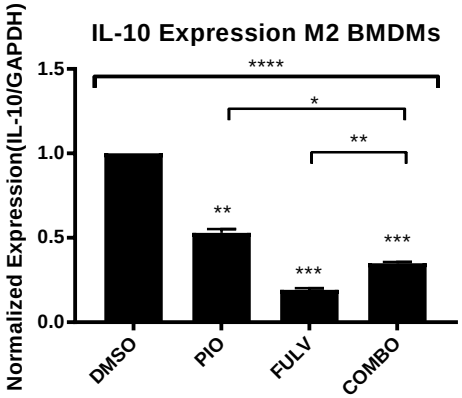
IL-10 Expression M2 BMDMs
Normalized Expression(IL-10/GAPDH)
1.5
1.0
0.5
0.0
****
*
**
**
***
***
DMSO
PIO
FULV
COMBO

D.

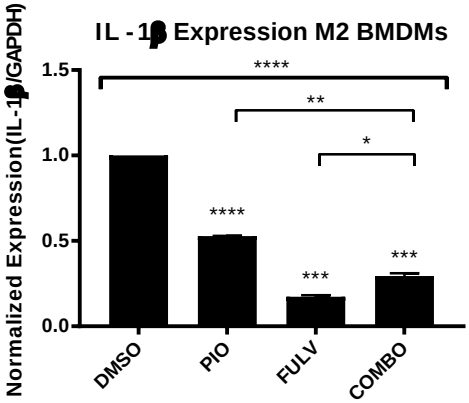
IL -1β Expression M2 BMDMs
Normalized Expression(IL-1β/GAPDH)
1.5
1.0
0.5
0.0
****
**
*
****
***
***
DMSO
PIO
FULV
COMBO

E.

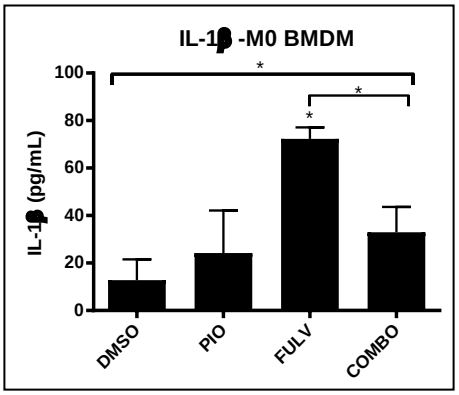
IL-1β -M0 BMDM
IL-1β (pg/mL)
100
80
60
40
20
0
*
*
*
DMSO
PIO
FULV
COMBO

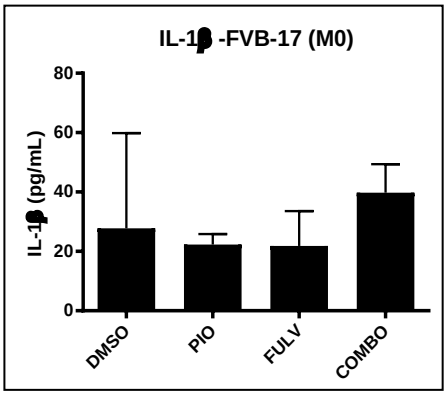
IL-1β -FVB-17 (M0)
IL-1β (pg/mL)
80
60
40
20
0
DMSO
PIO
FULV
COMBO

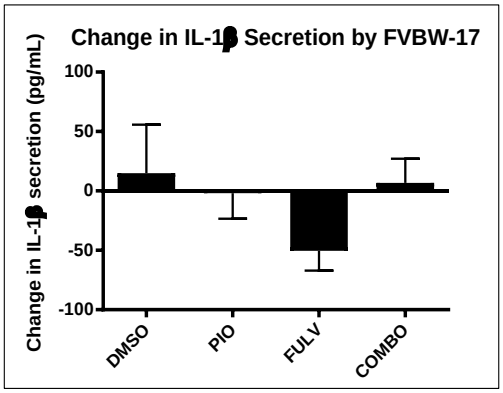
Change in IL-1β Secretion by FVBW-17
Change in IL-1β secretion (pg/mL)
100
50
0
-50
-100
DMSO
PIO
FULV
COMBO

F.

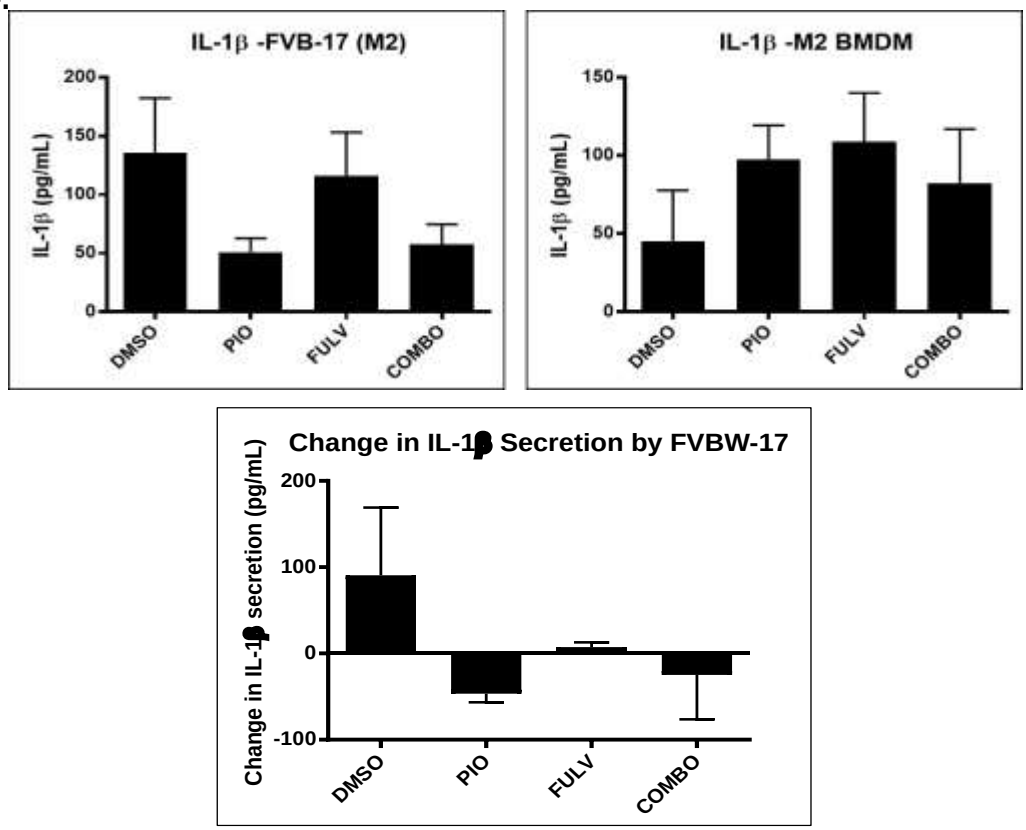

Figure 6. A. Real-time qPCR analysis of AREG expression of mRNA isolated from murine bone marrow-derived macrophages in resting state PBS control or in IL-4, IL-6, and IL-13 M2 macrophages primed for 24 hours treated with DMSO control, single, or combination treatments for an additional 24 hours. **B.** Real-time qPCR analysis of VEGF expression of mRNA isolated from murine bone marrow-derived macrophages in resting state PBS control or in IL-4, IL-6, and IL-13 M2 macrophages primed for 6 hours treated with DMSO control, single, or combination treatments in a transwell model with FVBW-17 cells for an additional 24 hours. **C-D.** Real-time qPCR analysis of IL-10 and IL-1β expression of mRNA isolated from murine bone marrow-derived macrophages (BMDMs) in IL-4, IL-6, and IL-13 M2 macrophages primed for 24 hours then treated with DMSO control, single, or combination treatments for an additional 24 hours. **E-F.** ELISA analysis of secreted IL-1β in response to drug treatments of resting state or M2-primed BMDMs, murine adenocarcinoma FVBW-17 cells, and the change in IL-1β secretion of FVBW-17 cells in response to challenge of conditioned-media (CM) from drug-treated BMDMs. All cells were incubated for 24 hours with drug treatments or CM. Data are expressed as mean ± SEM.

Pioglitazone and Fulvestrant Combination Treatment Alleviates Compensatory Signaling through EGFR and IL-1β

During our assessment of single versus combination treatments on pathways linked to inflammation and proliferation, we identified EGFR and IL-1β as two mechanisms by which pioglitazone and fulvestrant single treatments may attempt to overcome downstream effects of PPARγ and ER modulation. In order to assess the ability of combination treatment to rescue compensatory activation of these pathways, we analyzed EGFR ligand Amphiregulin (AREG) *via* ELISA in both a cancer cell conditioned media co-culture (Figure 7A) and transwell co-culture (Figure 7B) models as previously described. A549 cancer cells under influence of fulvestrant, stimulated an increase in AREG production by M2-primed THP-1 macrophages, which was significantly reduced by pioglitazone and fulvestrant combination treatment compared with DMSO baseline and with fulvestrant single treatment. This effect may be due to education of macrophages by the cancer cells to invigorate ER non-genomic signaling to cross-activate EGFR signaling as a means to compensate for loss of ER genomic signaling (Figure 7A). A similar trend was seen in conditioned media combining secreted protein from A549 and THP-1 macrophages, although in this model, combination treatment is only sufficient to revert AREG production back to the co-culture DMSO baseline. The baseline production of AREG in the DMSO control in Figure 7A illustrates the propensity for A549 cancer cells to stimulate EGFR signaling when compared with AREG secretion in the THP-1 individual culture DMSO

control in Figure 7B. This suggests that paracrine signaling between macrophages and cancer cells elevates this compensatory pathway.

In Figure 7C, we analyzed secreted IL-1β *via* ELISA in the same transwell co-culture model described in 7B but with M2-primed macrophages. Similarly, fulvestrant elicited an upregulation of IL-1β secretion in THP-1 cells cultured alone; however, when the macrophages were combined with the cancer cells in the transwell system, pioglitazone single treatment exhibited the compensatory upregulation, whereas fulvestrant single treatment was able to significantly reduce IL-1β secretion, suggesting differential regulation of IL-1β in macrophages versus cancer cells or that paracrine interaction is necessary for fulvestrant to mediate its effects on the IL-1β pathway.

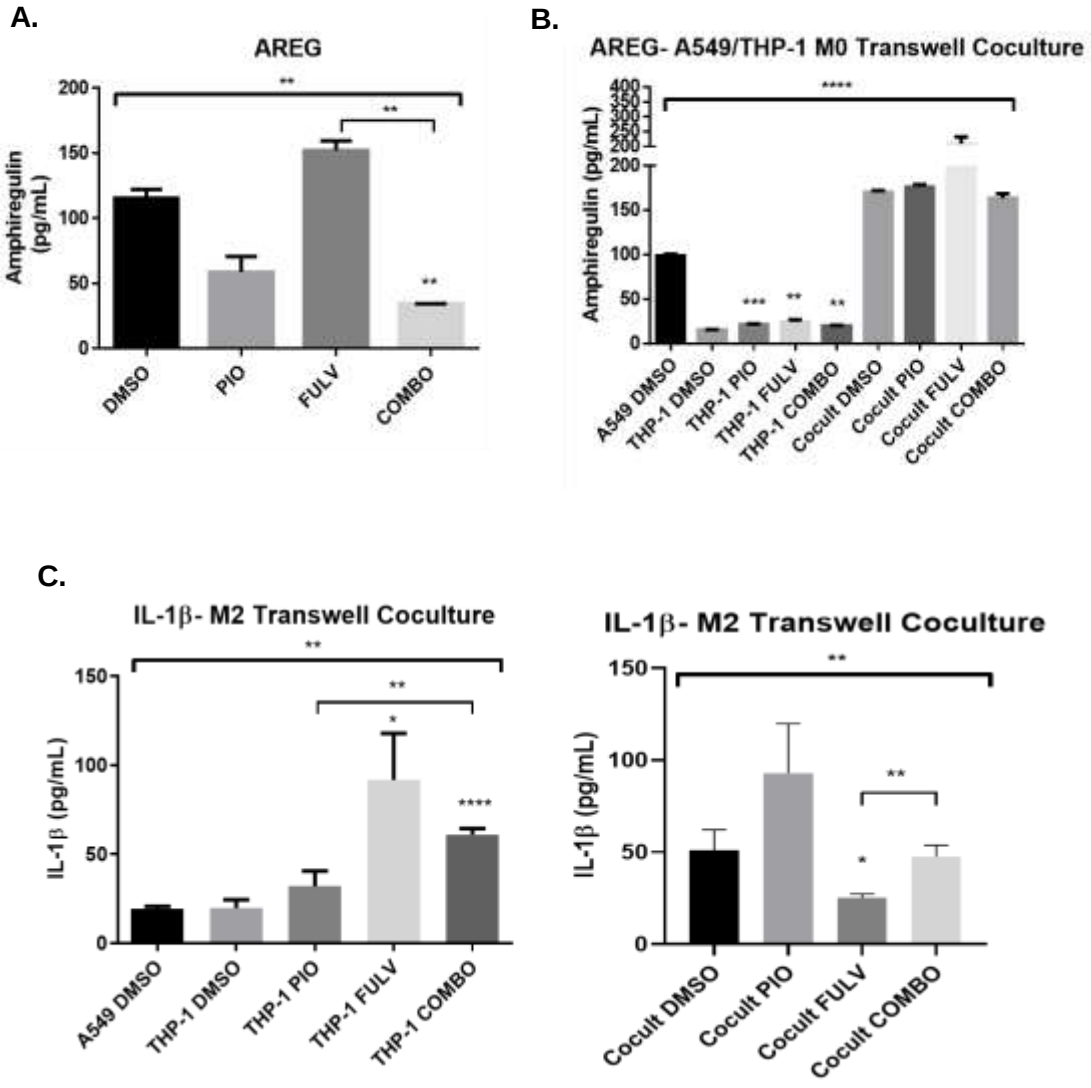

Figure 7. A. ELISA analysis of AREG in supernatant from M2-primed macrophages that were challenged with conditioned media for 24 hours from A549 cells that were pre-treated with DMSO, single, or combination treatments for 6 hours. **B.** ELISA analysis of AREG in supernatant from resting state THP-1 individual cultures challenged with drug treatments and transwell co-cultures of resting state THP-1 and A549 cells challenged with drug treatments for 48 hours prior to analysis. **C.** ELISA analysis of Il-1β in supernatant from M2-primed THP-1 individual cultures challenged with drug treatments and transwell co-cultures of M2-primed THP-1 and A549 cells challenged with drug treatments for 48 hours prior to analysis. Data are expressed as mean + SEM.

Combination Treatment Suppresses Colony Formation of A549 Cells in the Absence and Presence of THP-1 Macrophages

To assess the capability of single and combination treatment in reducing anchorage-independent colony formation of lung cancer cells, we cultured the A549 cells in agar alone (Figure 8A) or at a 1:1 ratio with the resting state THP-1 macrophages (Figure 8B) in a soft agar plate. After DMSO, single, or combination treatment for a duration of 14 days, colonies were imaged and counted with ImageJ software. In the cancer cell individual culture, colonies were assessed in size categories gated by pixel units as small (1,000-2,000 pixel units), medium (2,000-3,000 pixel units), or large (3,000+ pixel units). In the cancer cell co-culture with macrophages, colonies presented in fewer quantity and resided below the 1,000-2,000 pixel unit gate previously mentioned, and as such, were quantified without size restrictions above a threshold of 184 pixel units in order to eliminate background debris and single cells. In the cancer cell individual culture, fulvestrant alone or in combination with pioglitazone confers a 4-fold significant reduction in the quantity of large colonies formed (Figure 8A). In the cancer cell co-culture with macrophages, fulvestrant single treatment as well as combination treatment confer a significant 50% overall reduction in colony formation of all sizes (Figure 8B).

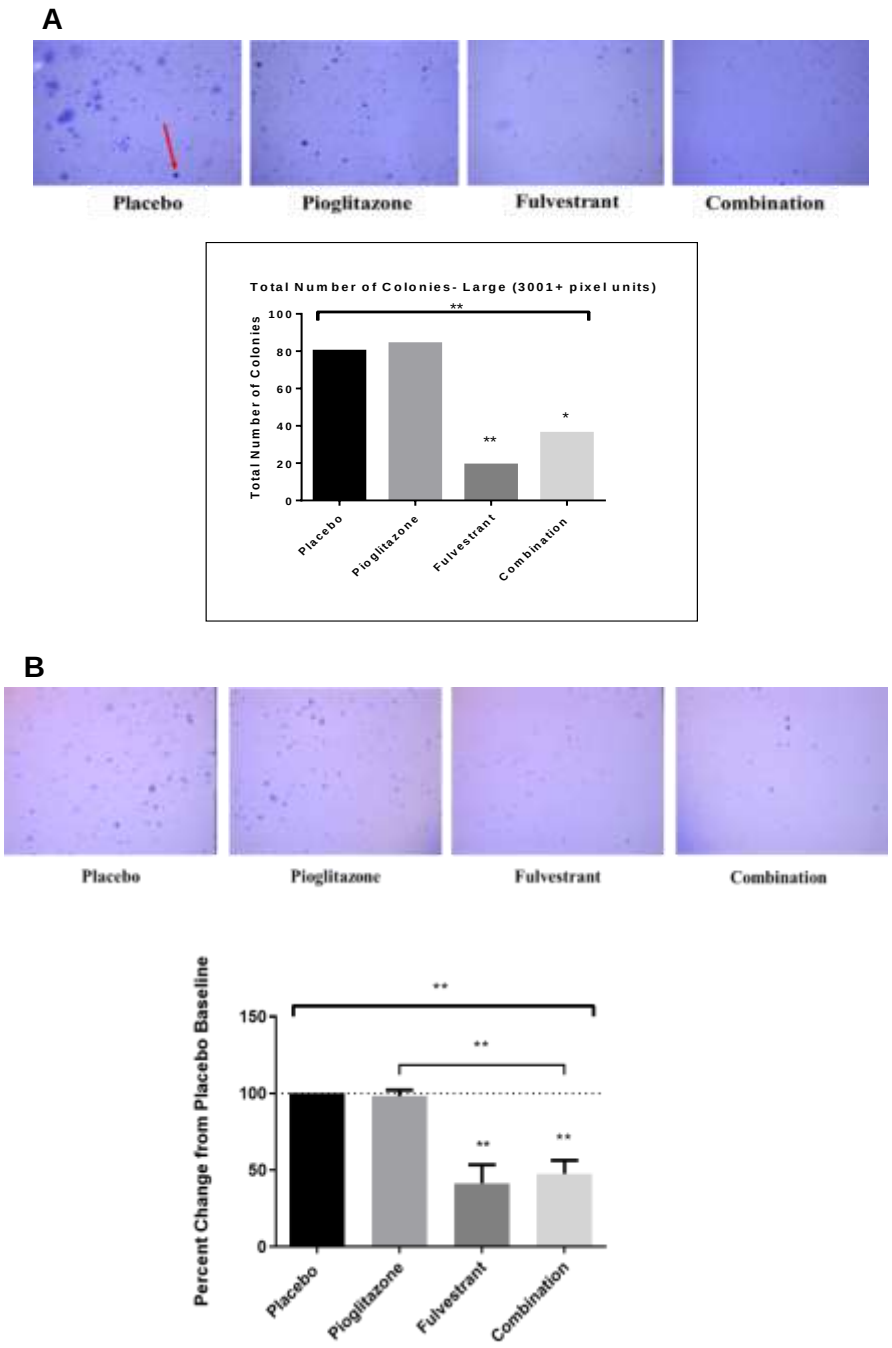

Figure 8. A. Representative images of colony formation of A549 cells cultured in soft agar across treatment groups (red arrow indicates a colony) and graphical representation of total number of large colonies (3,000+ pixel units) formed in DMSO control, single, or combination treatments. **B.** Representative images of colony formation of A549 cells cultured in a 1:1 ratio with THP-1 macrophages in soft agar across treatment groups and graphical representation of total number of colonies formed in each group above 184 pixel threshold. Data are expressed as mean $\pm$ SEM.

4.3 Discussion

One identified mechanism of action for the anti-tumor effects of pioglitazone and fulvestrant in our postmenopausal lung cancer model is through the inhibition of stromal-derived aromatase and subsequent local estrogen production. *In vitro* analysis of macrophages shows a strong regulation of macrophage-driven estrogen production with combination, but not single treatments. Furthermore, this effect is magnified in an M2 macrophage population. Giles and colleagues were the first to describe aromatase expression as a particular feature of the M2, tumor-promoting macrophage phenotype within a breast cancer model [102]. To our knowledge, this is the first time these findings extend to the context of lung cancer and demonstrate that pioglitazone and fulvestrant are able to augment this upregulation to reduce the M2-driven estrogen feed-forward loop within the lung TME.

Our findings suggesting overcompensation of the ER pathway proceeding fulvestrant administration represents a recurring theme of resistance in single therapy approaches [103-106]. In an estrogen-dependent breast cancer model, Macedo and colleagues demonstrated a similar effect, whereby an intratumoral aromatase xenograft model displayed resistance to fulvestrant due to ER hypersensitivity conferred through increased ERα expression and aromatase activity [107]. This model was able to demonstrate the utility of fulvestrant in a combination approach to achieve enhanced reduction of xenograft tumor volume with aromatase inhibitor anastrazole. The ability to rescue fulvestrant-induced

estrogen hypersensitivity with the addition of pioglitazone presents a unique opportunity to purpose a known anti-tumorigenic agent in preclinical lung cancer models to rescue this hormone-dependent resistance mechanism in order to transition this combination application to be relevant in other hormone-driven models such as lung cancer.

Elucidating agents capable of educating the lung TME against the promotion of tumorigenic activities can be especially challenging, as some approaches in the repertoire of explored chemopreventive targets simply skew the dichotic switch from M2 to M1 phenotypic functionality. Potential pitfalls to these approaches lie in the reprogramming macrophages to a classically “M1” or pro-inflammatory primed state which is widely accepted to decrease tumorigenic stromal support; however, emerging evidence has shown that this approach may be oversimplified, as it can overlook certain pathways that are typically classified as pro-inflammatory, but actually have downstream activity that can promote tumor growth such as IL-1β [108]. Understanding the complexity of TAMs including their ability to manipulate both “M1” and “M2” signaling to facilitate pro-tumorigenic activity is an important emerging concept in crafting agents capable of educating macrophages and other adaptive immune components to holistically promote anti-tumorigenic activity. Our novel chemoprevention approach combining pioglitazone and fulvestrant in macrophage and lung cancer TME models has shown efficacy in modulating both M1 and M2 cytokines to promote an overall anti-tumorigenic outcome. Maximum modulation of VEGF, IL-1β, IL-10,

AREG, and estradiol was achieved, signifying an important step forward in acknowledging and effectively modulating the heterogeneity of TAM signaling rather than the standard M1/M2 bipolar dichotomy. To our knowledge, this is the first data elucidating the inflammatory regulation of pioglitazone and fulvestrant in a combination approach and represents a promising foundation for future pre-clinical study of this drug combination in lung cancer chemoprevention.

5. Chapter II: Determining a potential enhanced effect between anti-estrogen fulvestrant and PPARγ agonist pioglitazone in reducing lung dysplasia and lung tumorigenesis in an animal model.

5.1 Introduction

Efforts in chemoprevention of lung cancer are surging forward as a consequence of the high rate of diagnosis and dismal rate of survival. Despite ongoing advances in chemoprevention for other types of cancer, lung cancer is, to date, still lacking any FDA-approved options [16]. Sought after hallmarks of an ideal chemopreventive agent include a well-defined high-risk population in need of such therapy and utilizes compounds that are both efficacious to delay the onset of malignancy and have favorable safety profiles [16]. Smoldering inflammation, an emerging feature of malignant progression identified by Hanahan and Weinberg, has quickly become a target for chemoprevention efforts [47]. Several agents ascertained for lung cancer chemoprevention have surpassed preclinical testing, entered into early phase clinical trials, and advanced into phase III testing, only to be met without great success [19].

Often, patients that present in high-risk cohorts have comorbidities such as COPD, PAH, and diabetes mellitus that present their own set of risk factors and have the potential to contribute to the risk of lung cancer. Several agents have been explored to address these comorbid risks such as NSAIDS, COX2 inhibitors, and prostacyclin analogs. [19, 20]. Within the NSAID category, aspirin held high promise for NSCLC chemoprevention after preclinical testing identified

a potential benefit [21]. However, phase III clinical trials failed to meet established endpoints or produced negative results [19]. Another inflammatory mediator identified as a potential beneficial agent in lung cancer prevention, celecoxib, works to block COX2. The agent, like aspirin, exhibited promise in preclinical models but failed to produce significant benefit in the majority of patients, and a subset of patients presented with toxicity, suggesting the need for further refinement of the cohort that can show clinical benefit without systemic toxicities [23].

The PPARγ pathway represents another unique pathway being investigated in lung cancer prevention, and preclinical evidence implicates PPARγ in both anti-neoplastic as well as anti-inflammatory modalities [48, 51, 53]. The PPARγ agonist iloprost showed clinical benefit in reducing lung dysplasia in former smokers when tested in a phase II clinical trial. Former smokers experienced a significant decrease in endobronchial histology by -0.39 units compared to current smokers who experienced no difference in dysplasia [24]. In addition to clinical benefit seen by activating PPARγ, another major discovery from this study was the activated estrogen signaling gene signature present in dysplasias that were classified to be persistent/progressive [24]. Estrogen signaling has already been implicated as a driver of lung cancer, and antiestrogens have been implicated in murine models of lung cancer [41-45]. The selective estrogen receptor degrader fulvestrant has also been investigated in clinical trials in combination with other therapies for the treatment of advanced stages of

NSCLC, owing to its efficacy in reducing proliferation of abnormal or malignant cells [42-45]. Furthermore, in the context of chemoprevention, SERMs such as tamoxifen and aromatase inhibitors (AIs) such as anastrazole have shown both safety and efficacy in large clinical trials to prevent breast cancer that is hormone-responsive [38, 39]. Owing to this emerging data, combining a PPARγ agonist pioglitazone and an antiestrogen fulvestrant can provide a therapeutic niche to pinpoint two pathways known to be implicated in the onset of malignancy in lung cancer and may provide a novel approach to more efficaciously delay this progression to malignancy.

5.2 Results

Receptors and a Representative Downstream Target are Present in the *In Vivo* Mouse Model

We first established the presence of both ERβ and PPARγ receptors (Figure 9A) as well as COX2, a known downstream target of both receptors in whole lung tissue lysates isolated from the FVB/N mouse model with NNK exposure with MCF-7 breast cancer cells as a positive control. Study setup and timeline are shown in Figure 9B.

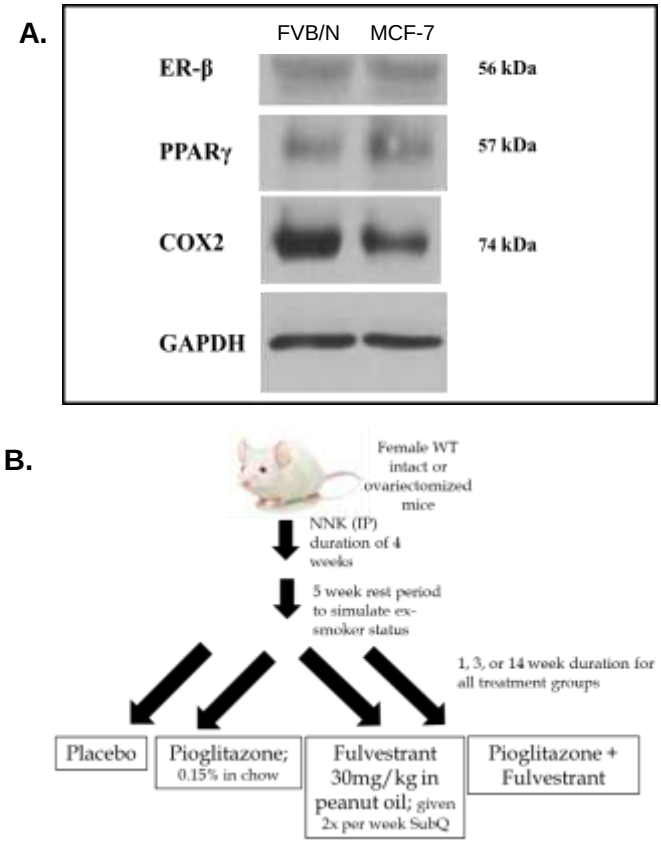

Figure 9. A. Immunoblot analysis of whole lung protein lysates from NNK-exposed FVB/N female mice and MCF-7 cell control. **B.** Murine study setup and timeline of NNK and drug exposure.

Combination Treatment Significantly Reduces Tumor Burden in NNK-Exposed Intact Female Mice

In order to define the efficacy of pioglitazone and fulvestrant, both singly and in combination, in a pre-menopausal model of lung cancer, we initiated adenocarcinoma formation with NNK in FVB/N mice and treated with placebo (DMSO control), single, or combination treatment for 14 weeks. After harvesting the lungs and assessing both tumor incidence and tumor size burden, defined as the sum of the surface area of all tumors in each mouse individually or across entire treatment group, we found that combination had reduced mean tumor incidence by 4.2 and reduced median tumor size by 0.6 mm^2 (Figure 10A). Combination, but not single treatments, achieved significance in reduction of tumor size burden by 36% fewer tumors compared to placebo ($p<0.01$) (Figure 10A) and a 2-fold reduction in average tumor size burden per mouse compared to placebo (Figure 10B). Average individual tumor size was found to be significantly smaller by 0.6 mm^2 in combination treatment compared to placebo ($p<0.05$) depicted graphically (Figure 10C). Furthermore, assessment of individual tumor sizes observed across treatment groups were significantly different in combination treatment compared with pioglitazone single treatment ($p<0.05$) and fulvestrant single treatment ($p<0.05$) (Figure 10D). Finally, tumor incidence was found to be significantly less in pioglitazone single treatment ($p<0.01$) and combination treatment ($p<0.001$), both compared with placebo (Figure10E).

A.

Treatment Group	Placebo	Pioglitazone	Fulvestrant	Combination
Number of Animals	10	11	10	11
Number of Tumors				
Total Number of Tumors	117	96	122	82
Mean # Tumors per Animal (SD)	11.70 (1.83)	8.73 (2.69)	12.20 (4.61)	7.46 (2.62)
Median (min, max) # Tumors per Animal	12.5 (9, 14)	10 (4, 13)	14 (4, 19)	7 (3, 12)
Tumor Size (mm^2)				
Mean Size (SD)	3.10 (2.75)	2.88 (2.26)	2.81 (2.18)	2.28 (2.20)
Median Size (min, max)	2.34 (0.1, 14.4)	2.19 (0.2, 10.5)	2.24 (0.1, 11.2)	1.74 (0.3, 13.9)
Percent Reduction in Tumor Size (p value)	N/A	23.8 (0.5303)	5.6 (0.3591)	48.4 (0.0265)

B.

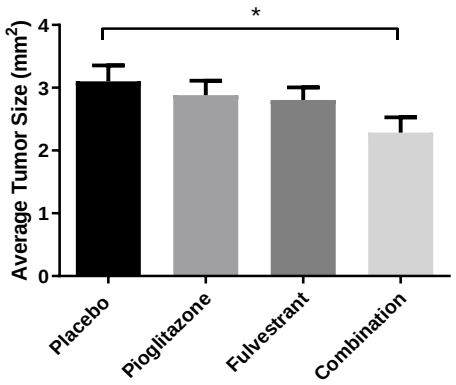

C.

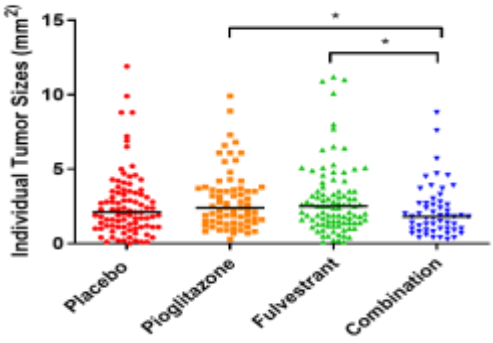

D.

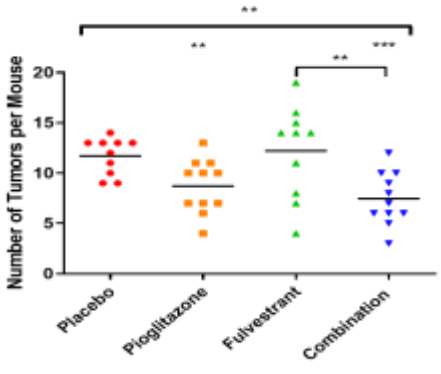

Figure 10. A. Table depicting 14-week intact treatment group study and major statistical results. **B.** Graph depicting group average tumor size per mouse (mm^2). **C.** Graph depicting individual tumor sizes per mouse (mm^2). **D.** Graph depicting tumor incidence per mouse across treatment groups. Data are represented as mean ± SEM.

Whole Lung Lysate Protein Analysis from 1 and 14 week-Treated Lungs Indicates Individual Variation between Mice

In order to assess the effect of pioglitazone and fulvestrant on downstream targets within the lung tissue, lungs from two mice harvested after 1 week of treatment and 14 weeks of treatment were made into protein lysates and immunoblotting was performed to probe for several downstream targets of PPARγ and ER signaling. Variable expression of targets can be seen between treatment groups after 1 week of treatment (Figure 11A). There was not a clear trend seen towards modification of targets as we would have expected, but this could suggest that treatment effects may take longer than one week to alter protein expression in the lungs. After 14 weeks of treatment, COX2 and Cyclin D1 were down-modulated in the lung tissue of both representative mice from combination treatment, supporting our hypothesis that both pathways are downstream and subject to augmentation by both pathways (Figure 11B). We did not, however, observe a change in phosphorylated Akt as we expected (Figure 11B).

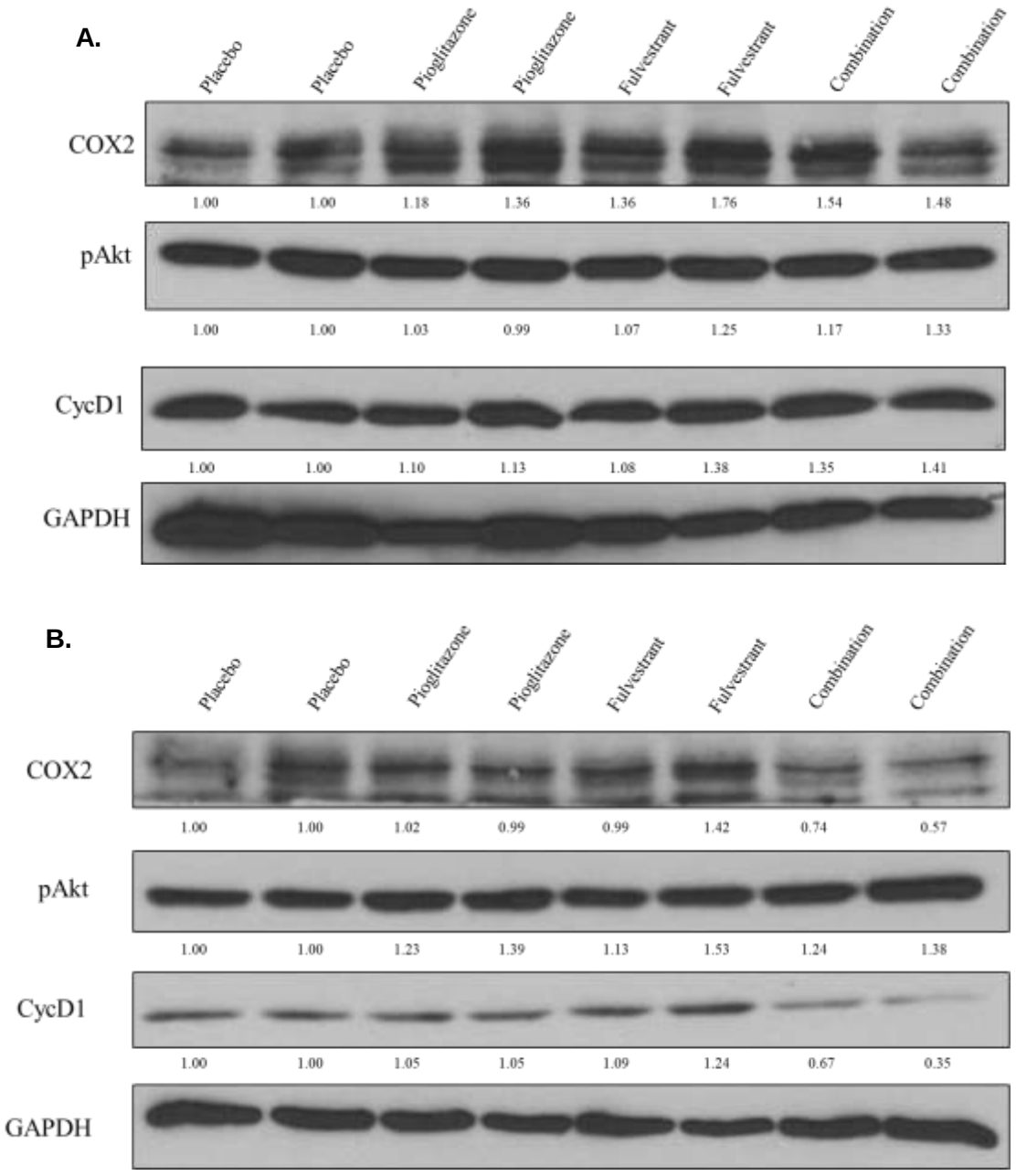

Figure 11. A. Immunoblot analysis of whole lung protein lysates from 2 representative NNK-exposed FVB/N female mice treated for 1 week in each group. **B.** Immunoblot analysis of whole lung protein lysates from 2 representative NNK-exposed FVB/N female mice treated for 14 weeks in each group. Quantification of protein expression was assessed using ImageJ 1.X software and changes are expressed below each lane.

Combination Treatment Alleviates Compensatory Estradiol Production in Single Treatment Groups in BALF of Intact Female Mice

We next assessed estradiol production in the BALF of 1, 3, and 14 week-treated mice to determine if similar compensatory regulation of estrogen production with fulvestrant treatment was seen *in vivo* as it was *in vitro*. We observed an upregulation of estradiol production in both single treatment groups and the largest upregulation with combination treatment in the BALF of 3 week-treated mice (Figure 12B). This could suggest that an early response to both single and combination treatments, which are working to block local lung estrogen signaling, potentially caused by a compensatory increase in aromatase, leading to more estrogen secretion as a means to overcome ER blockade. After just 1 week of treatment, estradiol levels are not significantly different in any treatment group compared with placebo (Figure 12A). However, compared with BALF from placebo-treated mice, BALF from a group of mice not exposed to NNK show over 2-fold significantly less pulmonary estradiol, supporting evidence linking estradiol to inflammatory pathways preceding tumorigenesis (Figure 12A). In contrast, estradiol levels are equivalent by week 14 across all groups (Figure 12C). This suggests that the increase in estradiol over time seen in placebo represents a tumor-driven autocrine source of estrogen to continue to drive tumor progression at a late-stage time point.

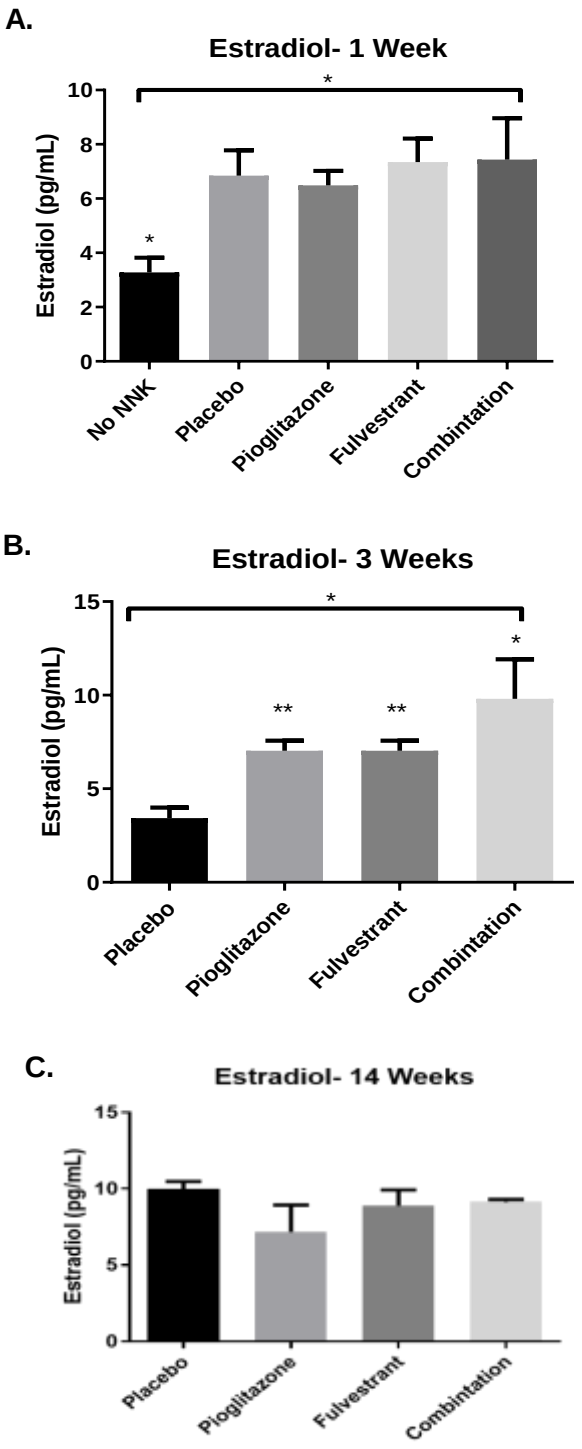

Figure 12. A. ELISA analysis of estradiol production in the BALF of intact, female FVB/N mice subject to 1 week of treatment. **B.** ELISA analysis of estradiol production in the BALF of intact, female FVB/N mice subject to 14 weeks of treatment. Data are expressed as mean ± SEM.

Single and Combination Treatments Significantly Reduce Tumor Burden in NNK-Exposed Ovariectomized Female Mice

Based on results showing a lack of efficacy on tumor size burden in single treatment groups and compensatory regulation of estradiol production in the BALF from the intact NNK mouse model, we hypothesized that the combination may display increased efficacy in a model without a reproductive source of estrogen. In order to assess the efficacy of pioglitazone and fulvestrant single and combined treatment on a post-menopausal model of lung cancer, we used the same experimental setup as shown in Figure 9B with female mice that were ovariectomized (OVX). After 14 weeks of treatment, tumor size and incidence were assessed similarly to the intact model (Figure 13A). Pioglitazone single treatment yielded a 28% reduction in overall group tumor size (p=0.9867) compared with placebo, fulvestrant yielded a reduction of 13% (p=0.2402) compared with placebo, and combination conferred a decrease of 51% (p=0.2601) when compared with placebo (Figure 13A). Median tumor number per animal was 2-fold lower in the combination treatment group compared with placebo (Figures 13A and 13E). Representative lung lobes from each treatment group in Figure 13B illustrate the main effect on reduction in tumor size seen in this study, and results representing average tumor size observed per mouse, all individual tumor sizes observed, and tumor incidence per mouse are reflected (Figures 13C and 13D).

A.

Treatment Group	Placebo	Pioglitazone	Fulvestrant	Combination
Number of Animals	21	22	21	20
Number of Tumors				
Total Number of Tumors	162	124	165	95
Mean # Tumors per Animal (SD)	7.71 (4.00)	5.64 (3.14)	7.86 (4.11)	4.75 (3.26)
Median (min, max) # Tumors per Animal	8 (1, 19)	5 (1, 11)	7 (3, 19)	4 (1, 16)
Tumor Size (mm^2)				
Mean Size (SD)	4.42 (6.83)	4.41 (4.23)	3.72 (3.34)	3.60 (2.70)
Median Size (min, max)	2.71 (1.5, 72.5)	2.92 (1.5, 34.6)	2.66 (1.5, 30.1)	2.54 (1.5, 16.7)
Percent Reduction in Tumor Size (p value)	N/A	28.1 (0.9867)	13.7 (0.2402)	51.5 (0.2601)

B

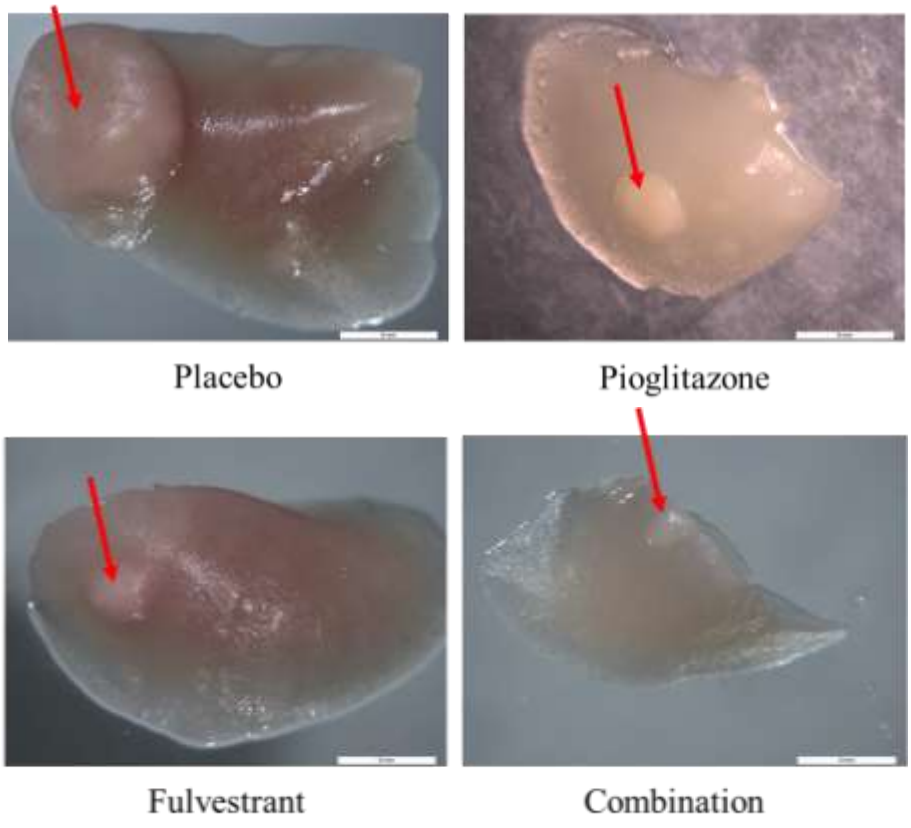

C.

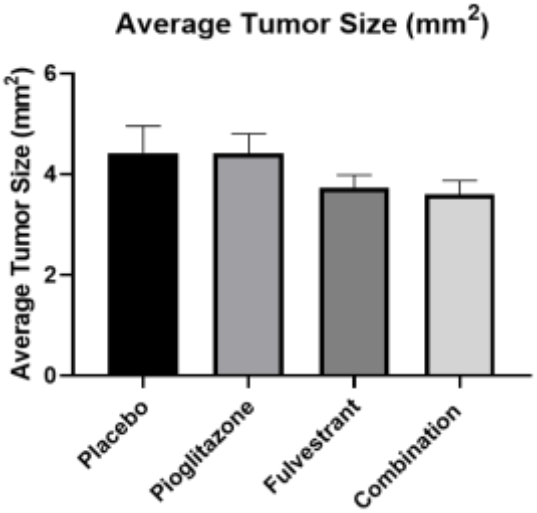

D.

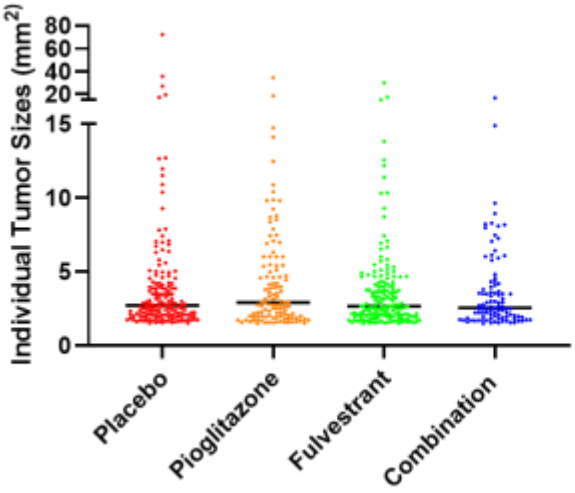

E.

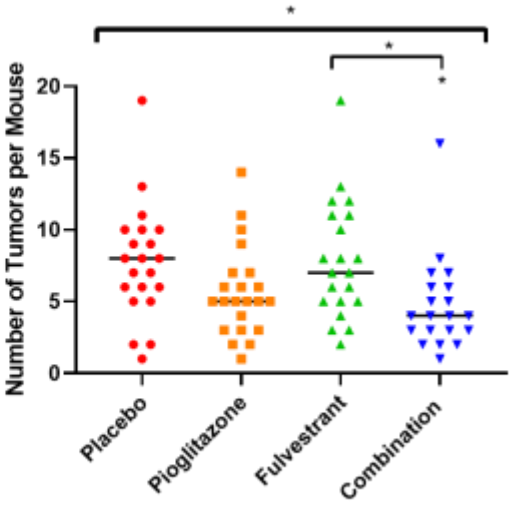

Figure 13. A. Table representing major tumor burden results from 14 week-treated ovariectomized female mice. **B.** Representative images of lung lobes containing tumors from 14 week-treated ovariectomized female mice. **C.** Graph depicting group average tumor size per mouse (mm^2). **D.** Graph depicting individual tumor sizes per mouse (mm^2). **E.** Graph depicting tumor incidence per mouse across treatment groups. Data are represented as mean $\pm$ SEM.

Combination Treatment Alleviates Compensatory Estradiol Production in Pioglitazone Single Treatment Group in BALF of Ovarectomized Female Mice

To assess whether compensatory estradiol regulation occurs when exogenous reproductive estrogen is removed from the system, we performed ELISA analysis on BALF from the 3 week-treated ovariectomized mice. In this model, we observed a significant decrease in estradiol in the fulvestrant-treated group, suggesting that ovariectomy was sufficient to prevent fulvestrant from increasing local estrogen production in the lungs (Figure 14) when compared with ELISA analysis of estradiol in BALF from the intact model (above). This result suggests that the effect of fulvestrant is dependent on an intact pituitary-ovary reproductive axis, whereas the effect of pioglitazone likely affects the local tissue sources of estrogen irrespective of reproductive status. If PPARγ activation could potentially affect ER activity, which could lead to a slight increase in subsidiary estradiol levels if estradiol is incapable of binding the receptor.

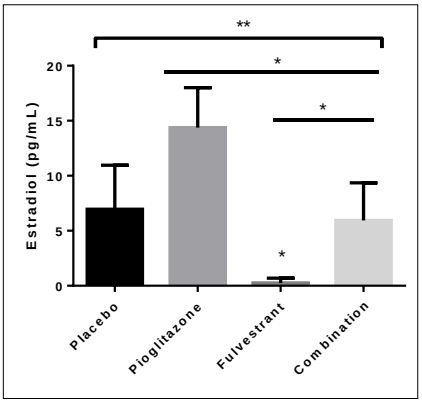

Figure 14. ELISA analysis of estradiol production in the BALF of OVX, female FVB/N mice subject to 3 weeks of treatment. Data are expressed as mean ± SEM.

Combination Treatment Significantly Down-Modulates Production of Secreted Factors in the BALF Involved in Mitigating a Pro-Tumorigenic Tumor Microenvironment

In order to assess the modulation of the pulmonary immune landscape across treatment groups, we analyzed secreted cytokines in BALF from 3-week treated mice in the OVX study *via* ELISA analyses. Pioglitazone treatment alone resulted in a significant decrease in EGF secretion ($p<0.001$). Both single and combination treatments were able to suppress EGF levels by 50%, although combination did not create added benefit (Figure 15C). IL-10 levels were maximally regulated by both fulvestrant ($p<0.05$) and combination treatment, and IL-1β levels reflected a similar trend (Figure 15A and 15B). Likewise, levels of AREG were maximally regulated by fulvestrant ($p<0.0001$) and combination was able to compensate for the increase seen in pioglitazone single treatment ($p<0.0001$) (Figure 15D). CCL2, a known regulator of macrophage chemotaxis, was also maximally down-regulated with fulvestrant single treatment ($p<0.01$) and combination treatment ($p<0.001$) (Figure 15E).

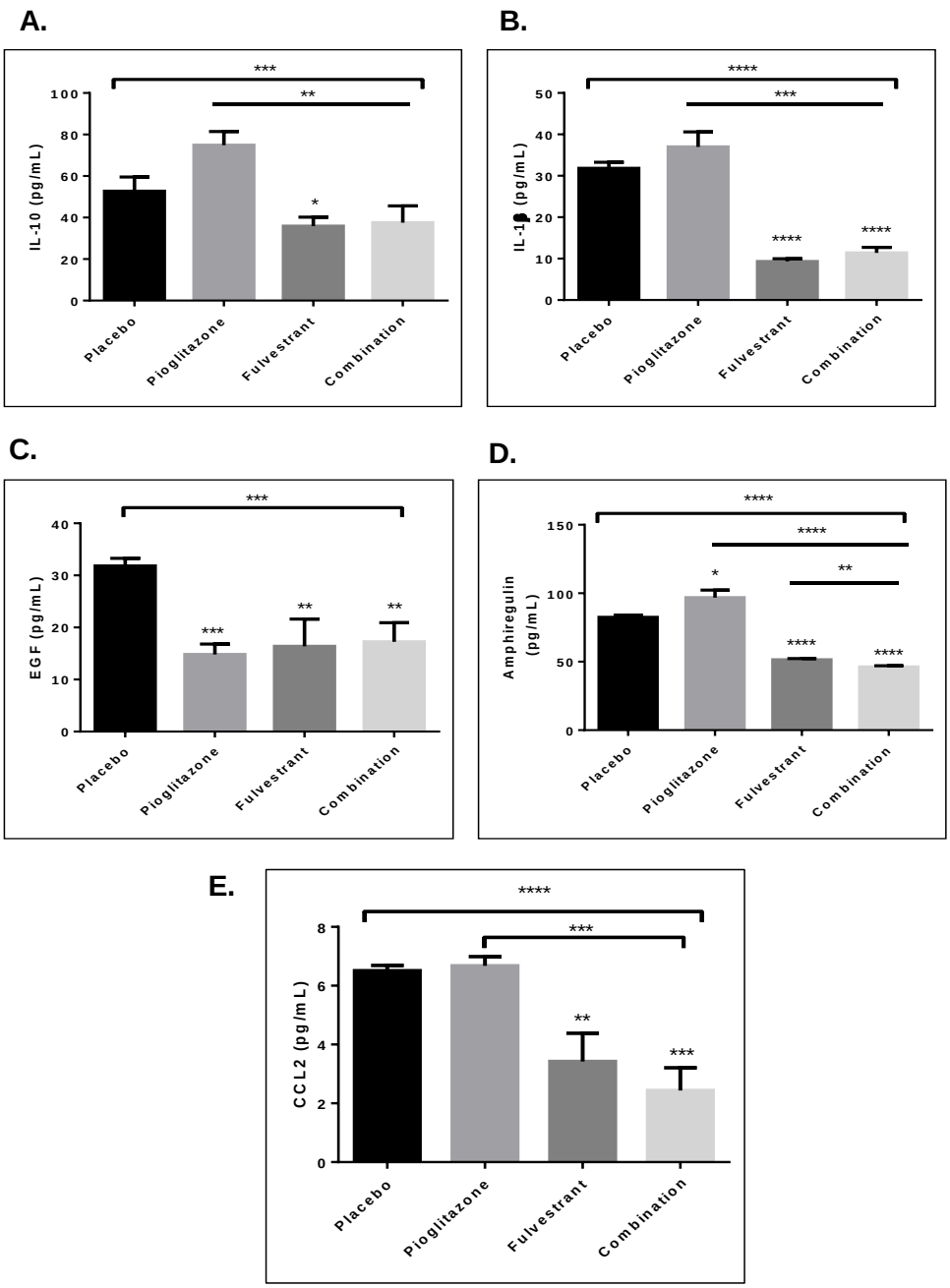

Figure 15. A. ELISA analysis of IL-10 production in the BALF of OVX, female FVB/N mice subject to 3 weeks of treatment. **B.** ELISA analysis of IL-1β production in the BALF of OVX, female FVB/N mice subject to 3 weeks of treatment. **C.** ELISA analysis of EGF production in the BALF of OVX, female FVB/N mice subject to 3 weeks of treatment. **D.** ELISA analysis of AREG production in the BALF of OVX, female FVB/N mice subject to 3 weeks of treatment. **E.** ELISA analysis of CCL2 production in the BALF of OVX, female FVB/N mice subject to 3 weeks of treatment. Data are expressed as mean ± SEM.

Single and Combination Treatments Significantly Reduce Macrophage Burden in the Lungs of Ovariectomized Female Mice Treated for 8 Weeks and 14 Weeks

As a secondary means of evaluating the inflammatory effect of pioglitazone and fulvestrant in the lungs, we analyzed the macrophage population within the lung tissue of 8 and 14 week-treated OVX mice. After 8 weeks of treatment, we analyzed a single-cell suspension isolated from whole lung digestion of 4 mice per group *via* flow cytometry, and we observed that the primary $CD45^+$ immune cell type present in the lungs were $CD45^+/CD11b^+/F4/80^+$ macrophages depicted as population P6 within the dot plots. (Figures 16A-E). Furthermore, both single and combination treatments significantly reduce this macrophage population by 5% from the total immune cell population (Figure 16E). We also analyzed the effect of single and combination treatments on the $CD45^+/CD11b^+/F4/80^+/CD206^+$ macrophage population depicted as population P7 within the dot plots (Figures 16A-D and F). Here, we observed that both pioglitazone and fulvestrant single treatments increased the percent of M2 macrophages observed in the lungs after 8 weeks of treatment. Combination treatment alleviated the single-treatment effect on M2 macrophage burden back to placebo baseline (Figure 16F). Based on literature suggesting a role for pioglitazone in promoting M2 macrophage activation, we expected a potential single treatment effect on this population of M2 cells. Our hypothesis that the combination can alleviate negative effects on the promotion of M2

macrophage activation was supported, as we observed a decrease in $CD206^+$ M2 macrophages with combination treatment (Figures 16D and F).

We observed a large macrophage presence in the placebo group and a steady decline across treatments (Figure 17B). In order to assess potential differences in response to treatment within each treatment group, we split treatment groups into responder and non-responder populations, which consisted of mice with the smallest and largest tumor incidence and size burden, respectively. We hypothesized that a potential factor in a lacking response to treatments involved sustained macrophage presence in the TME. We found this hypothesis to be supported; each corresponding responder treatment group had a lower macrophage density than its non-responder counterpart (Figure 17B). Moreover, combination treatment groups, overall, displayed the lowest macrophage density compared with placebo or single treatments, suggesting roles of pioglitazone and fulvestrant in chemotaxis blockade of macrophages or corresponding chemokines, one of which could be CCL2 as previously identified (Figure 15E).

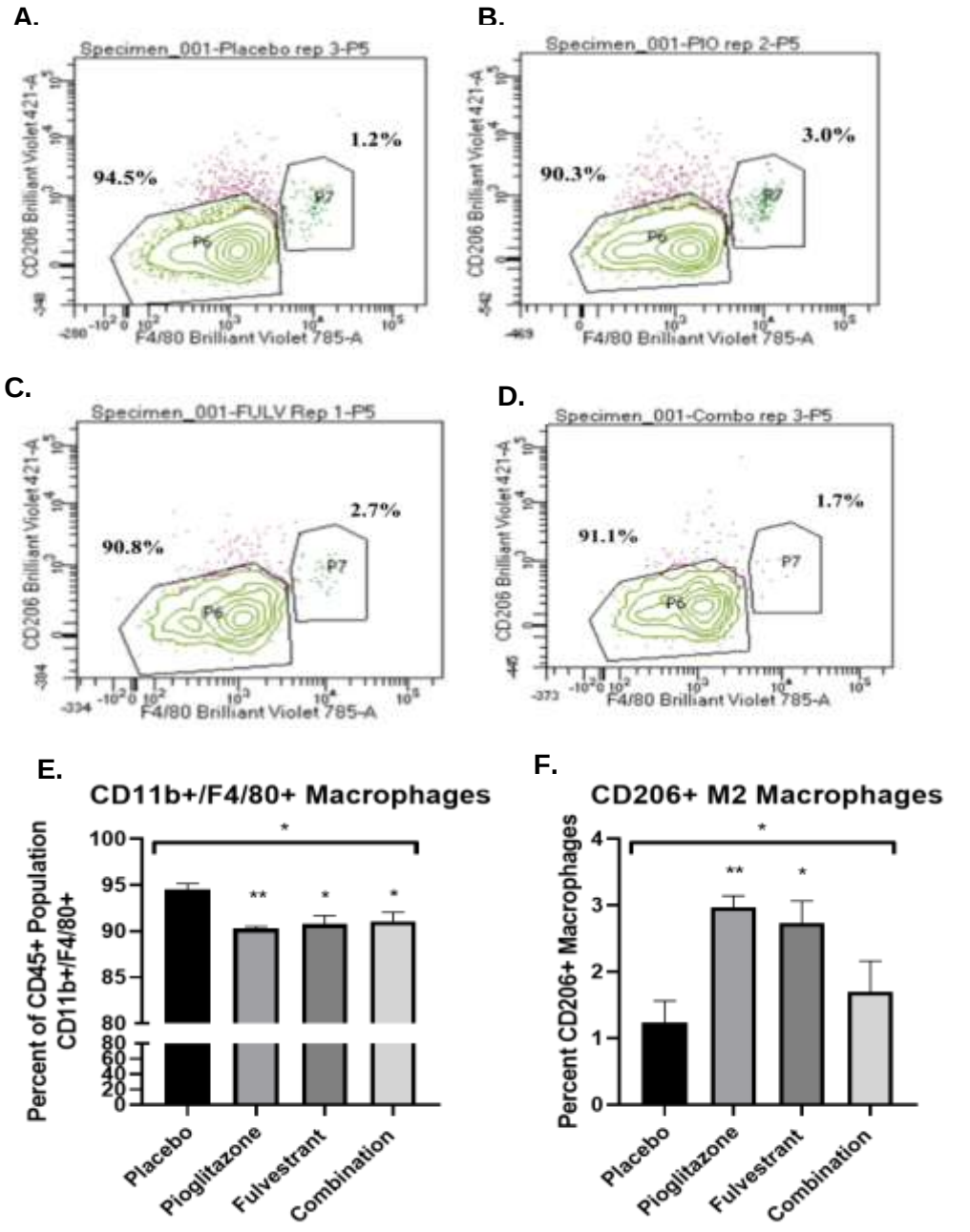

Figure 16. A-D. Dot plots representing percent events of CD45+ parent population positive for CD11b, F4/80, and CD206 macrophage markers in OVX mice subject to 8 weeks of treatment in *A.* Placebo *B.* Pioglitazone *C.* Fulvestrant *D.* Combination treatment groups. **E.** Graphical representation of the percent of CD45+ cells that are CD11b+/F4/80+ macrophages quantified across n=4 mice in each treatment group. **F.** Graphical representation of the percent of CD45+ cells that are CD11b+/F4/80+/CD206+ M2 macrophages quantified across n=4 mice in each treatment group. Data are represented as mean ± SEM.

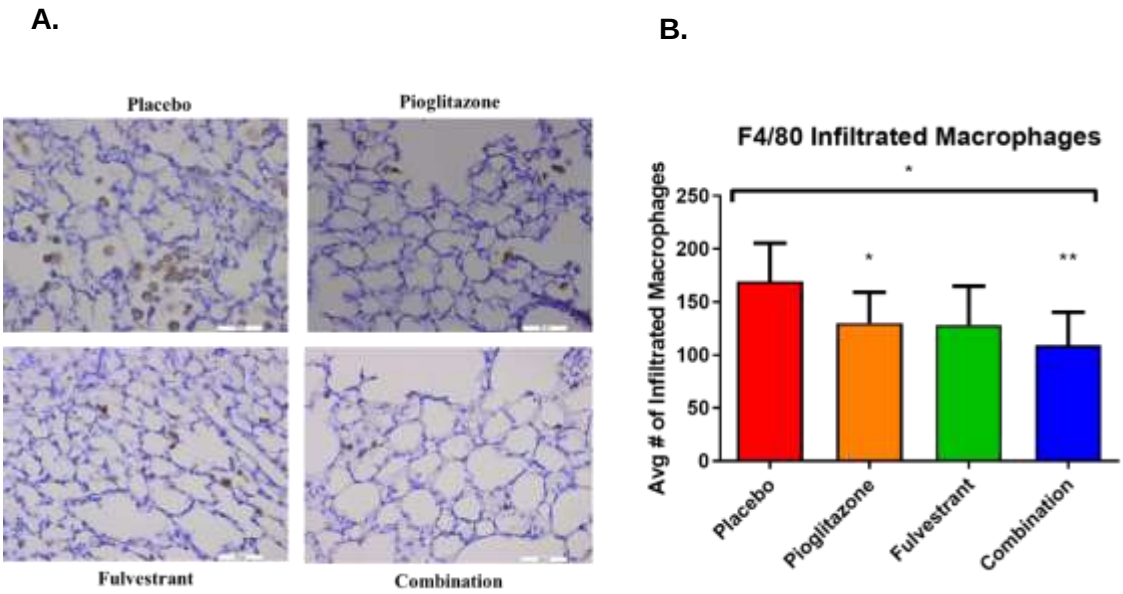

Figure 17. A. Representative images of F4/80 positive macrophages via immunohistochemistry of lung sections taken from NNK-exposed 14 week-treated OVX mice. **B.** Graphical representation of the total number of macrophages quantified across n=5 mice in each treatment group.

Combination and Single Treatments Modify PPARγ and Downstream Targets of PPARγ and ER Pathways in Lungs of 14 Week-Treated Ovariectomized Female Mice

In order to assess ER and PPARγ downstream signaling *in vivo*, we performed immunohistochemical analysis of a variety of targets both in preneoplastic lesions and tumor tissue from lungs of 14 week-treated mice in the OVX model. We wanted to analyze if maximal modulation of downstream signaling could be seen in early stage tumorigenesis as well as late stage. Protein targets analyzed were PPARγ (Figure 18), pAkt (Figure 19), Cyclin D1 (Figure 20), VEGF (Figure 21), AREG (Figures 22-23), and MMP9 (Figures 24-25).

PPARγ expression was measured in preneoplastic airways in responder and non-responder populations as previously described. As expected, we found that pioglitazone responder mice exhibited a significant induction of PPARγ compared with placebo ($p<0.0001$) (Figure 18). We saw an induction only in moderate staining in the pioglitazone non-responder cohort and a reduction of high staining when compared with placebo ($p<0.0001$). Pioglitazone responder and non-responder populations were significantly different from one another ($p<0.0001$), suggesting that regulation of PPARγ levels could be a contributing factor in response to treatment. Both fulvestrant responder ($p<0.01$) and non-responder ($p<0.0001$) cohorts displayed a small induction of moderate, but not high PPARγ expression, suggesting that ER inhibition may have the ability to

alter PPARγ, although not to the extent of PPARγ agonism. A similar significant increase in moderate expression was seen in both combination treatment populations ($p<0.01$ and $p<0.05$).

Next, to assess anti-neoplastic activity of both treatments, we analyzed Akt survival signaling, a projected target of both PPARγ and ER signaling (Figure 19). Neither single treatments nor combination treatment resulted in a significant reduction in Akt signaling within preneoplasias as we had expected. We hypothesized that combination would yield enhanced benefit in this pathway, but IHC of pAkt expression, although not statistically significant, appears to shift slightly towards increased high expression.

In order to assess the effect of pioglitazone and fulvestrant on a projected target of cell cycle regulation, we analyzed Cyclin D1 expression in tumor tissue to see if treatment effects are delineated in late-stage tumorigenesis versus early-stage neoplasia transformation (Figure 20). All treatment groups, regardless of response, did show an induction of negative and low expression, suggesting that pioglitazone and fulvestrant can induce pathways linked to cell cycle arrest. Furthermore, both single treatments and combination treatment were able to significantly reduce high expression of CycD1. Although we expected to see a shift towards lower expression pattern with combination treatment compared with single treatments, we observed an induction in high expression in the responder cohort of the combination treatment group, but we did not observe this effect in the non-responder cohort.

We next wanted to compare tissue VEGF levels, both in preneoplastic airways (Figure 21) and in tumor tissue (Figure 22) after 14 weeks of treatment to VEGF regulation seen in the BALF from the 3 week early time point of study. In preneoplastic airways, VEGF expression was not significantly different between any treatment group and placebo, nor were there significant differences between responder and non-responder populations (Figure 21). However, VEGF expression in both response populations to pioglitazone single treatment displayed a decrease in moderate and high VEGF expression in tumor tissue ($p<0.05$ for both). Fulvestrant single treatment did not significantly alter VEGF expression. Combination treatment in the responder population, however, strongly induced VEGF moderate and high expression in tumors ($p<0.01$), and this response was reversed in the non-responder cohort ($p<0.01$), displaying an increased presence of low VEGF expression in tumor and a decrease in the abundance of moderate and high expression that was significantly different from the responder cohort ($p<0.0001$) (Figure 22). There was no low expression observed in this population, suggesting another potential rescue mechanism from anti-tumorigenic mechanisms likely amplified with combination treatment.

Based on previous data showing AREG-induced EGFR compensation with fulvestrant treatment, we wanted to confirm AREG expression in preneoplastic airways (Figure 23) as well as presence of AREG expression in the immune cell population of the lungs after 14 weeks of treatment (Figure 24). Similarly to previous data, AREG was shown to be induced in both single

treatment groups; however, unlike AREG secreted protein expression in the BALF after 3 weeks of treatment, combination treatment showed the largest induction of AREG expression by 14 weeks in the preneoplastic airways. This could suggest a stronger compensatory activation in response to anti-neoplastic effects of the combination seen after 14 weeks of treatment. This compensatory response appears to be sequestered to the epithelium, as the AREG-positive immune cell population decreases with both single and combination treatments (Figure 24).

Finally, in order to assess effects of pioglitazone and fulvestrant on invasive and metastatic potential of forming lesions, we measured MMP9 expression of tumor tissue as well as MMP9-positive immune cell density after exposure to single and combination treatments for 14 weeks (Figures 25-26). Pioglitazone and fulvestrant single treatments confer a propensity of tumor tissue towards increased negative and low MMP9 expression, suggesting the ability of both treatments to affect the aggressiveness of the phenotype. However, combination treatment induces higher expression of MMP9, suggesting another potential compensatory mechanism to escape anti-tumorigenic treatment effects. A similar shift towards MMP9-high expression is seen in the tumor-infiltrated immune cell landscape (Figure 26) suggesting that pioglitazone and fulvestrant can affect matrix degradation and mobility of cancer cells through both direct and indirect mechanisms.

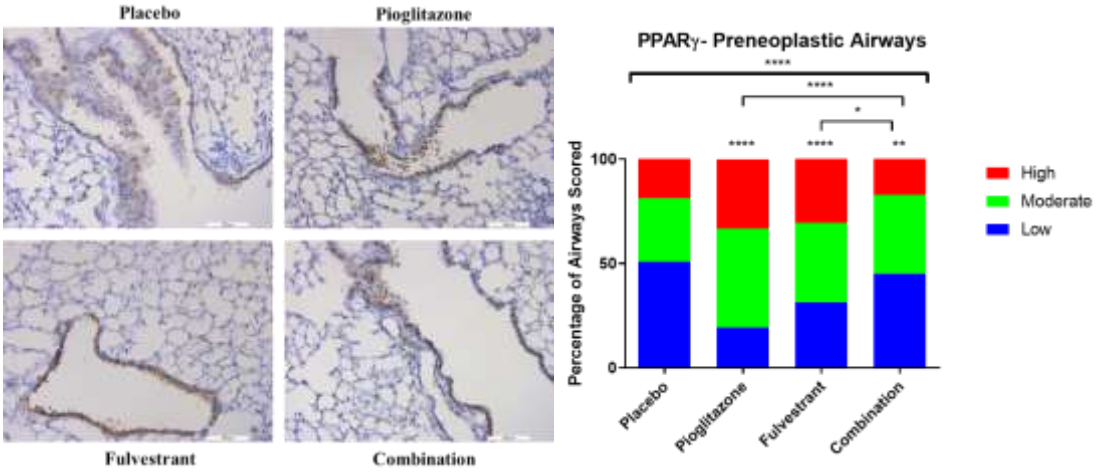

Figure 18. Immunohistochemical analysis of PPARγ expression in the preneoplastic airways of 14 week-treated OVX mice. Expression was quantified as intensity-based expression in fields with negative, low, moderate, and high intensity of positive staining.

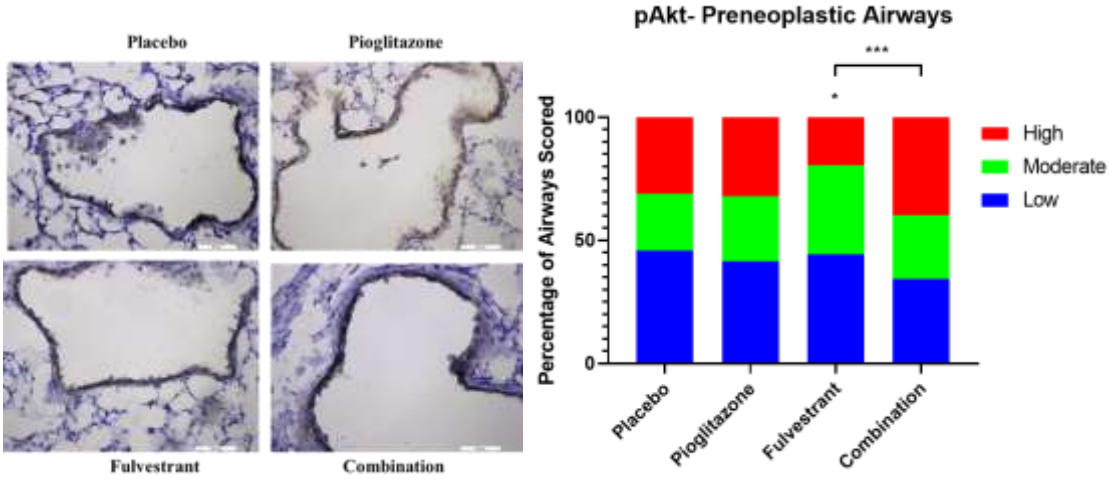

Figure 19. Immunohistochemical analysis of pAkt expression in the preneoplastic airways of 14 week-treated OVX mice. Expression was quantified as percentage of positive staining in preneoplastic airways with low (0-30%), moderate (30-60%), and high (60-100%).

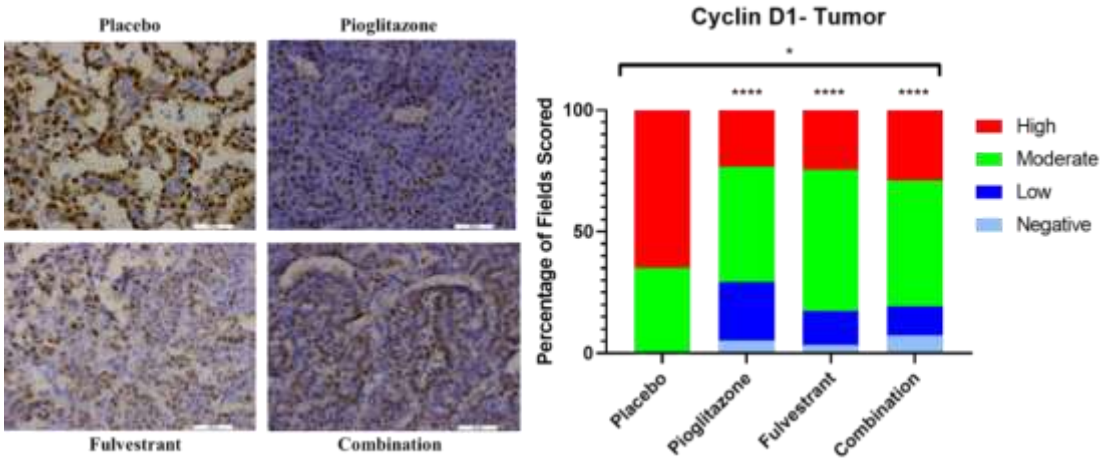

Figure 20. Immunohistochemical analysis of Cyclin D1 expression in the tumors of 14 week-treated OVX mice. Expression was quantified as intensity-based expression in fields with negative, low, moderate, and high intensity of positive staining.

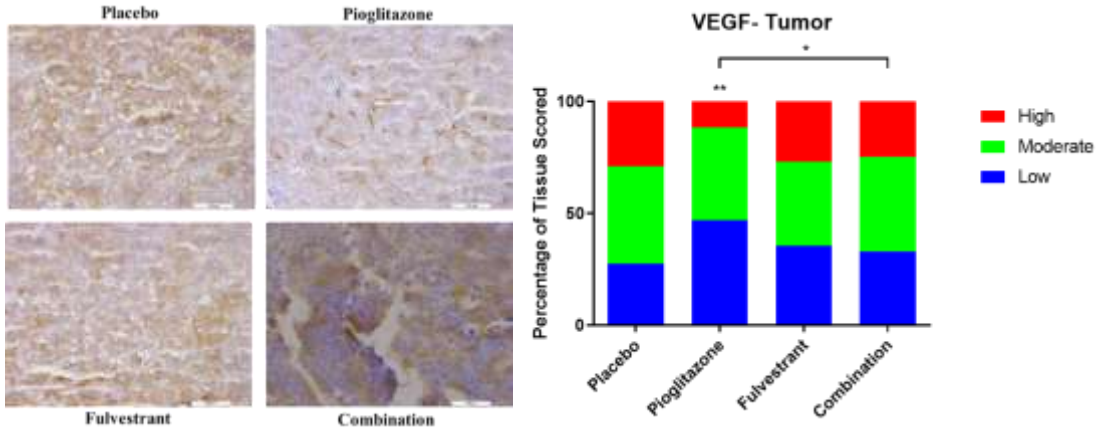

Figure 21. Immunohistochemical analysis of VEGF expression in the tumors of 14 week-treated OVX mice. Expression was quantified as percentage of positive staining in fields with low (0-20%), moderate (20-50%), and high (50-100%).

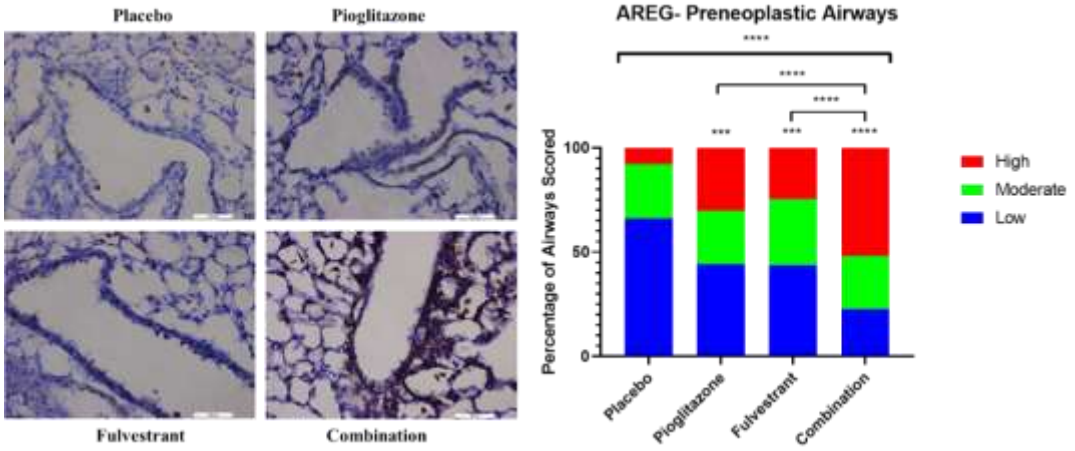

Figure 22. Immunohistochemical analysis of AREG expression in the preneoplastic airways of 14 week-treated OVX mice. Expression was quantified as percentage of positive staining in preneoplastic airways with low (0-30%), moderate (30-60%), and high (60-100%).

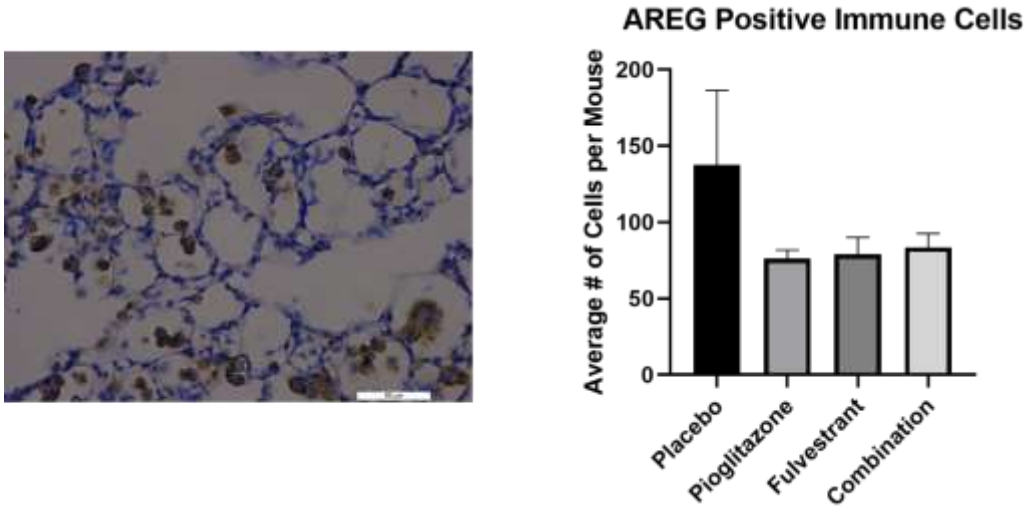

Figure 23. Graphical representation of the total number of immune cells staining positive for AREG quantified in random fields across n=5 mice in each treatment group.

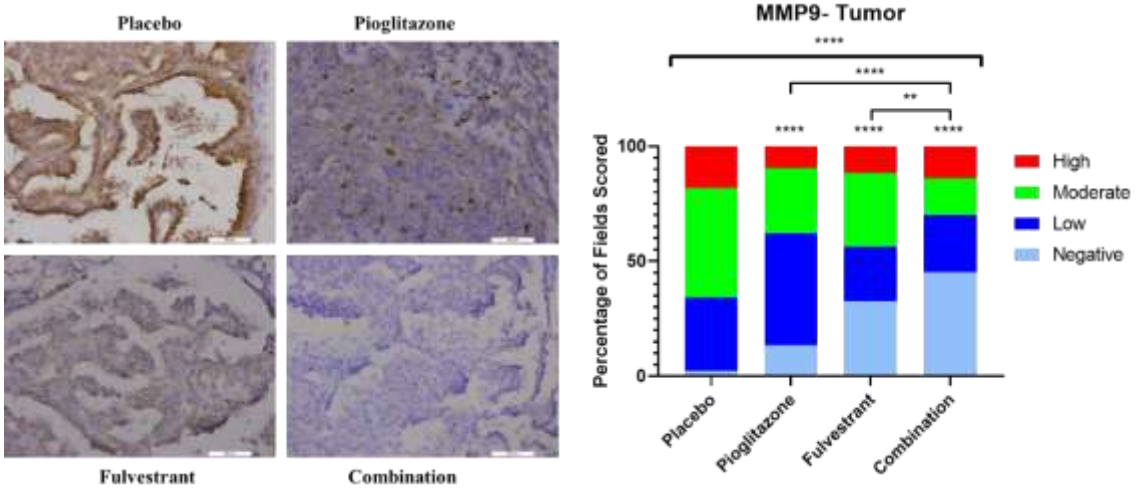

Figure 24. Immunohistochemical analysis of MMP9 expression in the tumors of 14 week-treated OVX mice. Expression was quantified as intensity-based expression in fields with negative, low, moderate, and high intensity of positive staining.

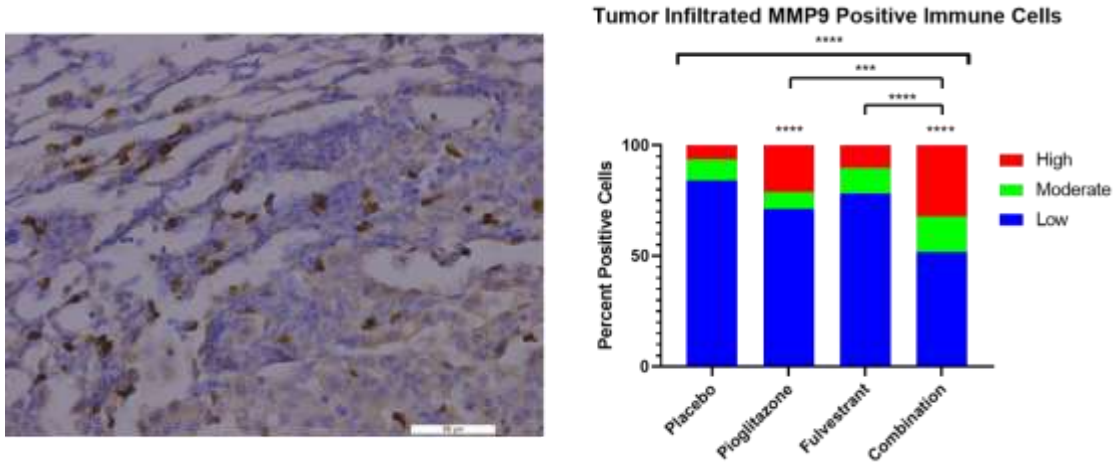

Figure 25. Immunohistochemical analysis of tumor-infiltrated immune cells positive for MMP9 in the tumors of 14 week-treated OVX mice. Expression was quantified as number of positive staining cells in fields with low (0-10 cells), moderate (11-20 cells), and high (>20 cells).

5.3 Discussion

An NNK-induced adenocarcinoma model of lung cancer in intact female mice represents an inclusive model of a population of at-risk individuals synonymous with pre-menopausal women with a history of smoking at an increased risk of developing lung cancer. Assessment of tumor burden from intact mice subject to 14 weeks of pioglitazone or fulvestrant single treatment did show a therapeutic benefit; however, single treatments did not reach statistical significance. Combination treatment resulted in a 44% decrease in tumor incidence compared with placebo and a 26% reduction in mean tumor size. Based on previously published results on pioglitazone and fulvestrant single treatment effects on lung tumor formation, we expected to achieve significant single treatment benefit as well as an added benefit with combination treatment. Previous studies using pioglitazone reported a significant decrease in tumor incidence in a benzo-α-pyrene model of lung cancer in A/J mice [109]. Another adenocarcinoma model utilizing pioglitazone found that it mitigated a maximum 64% decrease in tumor load in a p53 wild-type vinyl carbamate-induced adenocarcinoma mouse model [110]. Furthermore, a previous study from our lab using fulvestrant in the ovariectomized NNK-induced adenocarcinoma model shown in this study cited a 44% decrease in tumor incidence and a 47% decrease in median tumor size burden [41]. Thus, this combination treatment model was expected to produce significance in single treatments and increased benefit in combination treatment with respect to tumor incidence and burden.

Pioglitazone has been reported to be most efficacious when given in the earliest stages of adenoma formation. It is possible that the potency to which NNK can induce adenoma formation in FVB/N NNK-susceptible mice allowed a more rapid adenoma formation than other carcinogen-induced models, and the timeline in which treatments began limited single treatment efficacy. Moreover, understanding that a major mechanism of action of fulvestrant relies on the competitive displacement of estradiol from the ER, it is plausible that circulating estradiol made by an intact reproductive system may displace kinetics that affect the ability of fulvestrant to effectively out-compete estradiol for the receptor. Therefore, it is possible that the lack of efficacy in fulvestrant single treatment may be, in part, due to an intact reproductive system, suggesting that this treatment modality may be most efficacious in a post-menopausal model of lung cancer. We can confirm that estrogen production was not adequately regulated in the intact model at any of the assessed endpoints in the BALF isolated from the lungs. As such, we opted to transition to an ovariectomized model for further testing.

The ovariectomized model was sufficient to mitigate a 50% decrease in tumor incidence with combination treatment compared with placebo, a 51% decrease in overall group tumor size with combination treatment, and a 13% and 28% reduction in fulvestrant and pioglitazone single treatments, respectively. Estradiol assessment in BALF isolated from lungs after 3 weeks of treatment confirms that estrogen regulation is more efficaciously managed in the OVX

model when compared with that of the intact model. The increase in inhibition of tumor formation supports the earlier hypothesis that fulvestrant can more effectively compete for the ER. However, the observed reduction in tumor burden from both single and combination treatments was still not as sizable as the expected effect. It is possible that compensatory activation and overcompensation of target pathways downstream of both PPARγ and ER may be responsible for dampening the expected effect on tumor incidence and size burden.

Assessment of the early inflammatory response to pioglitazone and fulvestrant reveals a steady, decreased regulation of inflammatory and compensatory mediators of PPARγ and ER signaling with combination treatment such as IL-10, IL-1β, VEGF, and AREG. Furthermore, late-stage assessment of macrophage burden in the lungs after 14 weeks of treatment in the OVX model supports a role for the combination in modulating the inflammatory landscape away from a tumor-promoting TME. A strong, significant down-regulation of macrophage burden suggests than in addition to the roles of pioglitazone and fulvestrant in mediating inflammatory responses, they likely regulate presence of inflammatory cells through chemotaxis mechanisms like CCL2, as well.

However, late-stage assessment of similar TAM-like, pro-tumorigenic pathways points to steep compensation in combination treated mice. This suggests that combination can most effectively regulate these pathways, and as a result, proteins implicated in pathway signaling are being upregulated to

compensate for the loss. This effect was seen in several proteins involved in mitigating a pro-tumorigenic environment such as Akt, AREG, and MMP9 in tumor-infiltrated immune cells. As a result, due to the “rescue” phenotype seen in combination-treated mice after 14 weeks, it is reasonable to hypothesize that modulating other pathways in addition to PPARγ and ER can create added benefit in reducing lung tumor formation above that observed in this model in carcinogen-exposure models.

6. Discussion

PPARγ and ERβ are known individually to be mediators of lung tumorigenesis and progression with downstream signaling pathways such as MAPK, Akt, Cyclin D1, and COX2/PGE2. Key roles for PPARγ in mediating tumorigenesis through survival, apoptosis, and terminal differentiation are well-defined and have been previously validated in cell culture and mouse models of lung cancer [58-61]. Likewise, ERβ plays a key role in regulating tumorigenesis, with known targets in proliferative and immunosuppressive pathways [34, 35, 37, 94, 100]. A phase II clinical trial of iloprost, a PPARγ activator, revealed a link between PPARγ-responsive dysplasias that were phenotypically classified as aggressive which regressed with treatment and an activated ER signature, suggesting the potential for combined chemopreventive therapeutic benefit [46]. Additionally, both PPARγ and ERβ have been reported to interact in other models such as breast and thyroid cancer [72, 74, 75]. These targets, individually, are well-defined and present as prime targets for chemopreventive intervention. Prior chemoprevention agents that have targeted similar proliferative and inflammatory pathways had limited success in clinical trials either due to failure to meet established primary or secondary outcomes and confer therapeutic benefit, a poorly-defined biomarkers to predict a defined population likely to receive therapeutic benefit, or toxicity issues. An emerging hallmark of new-age chemoprevention strategies target at-risk populations for lung cancer that have comorbidities such as COPD and diabetes mellitus. Agents capable of

addressing comorbid risks for lung cancer initiation as well as underlying cellular mechanisms of tumorigenesis have the potential to increase therapeutic benefit. We have examined a novel therapeutic combination pioglitazone and fulvestrant that target the PPARγ and ER pathways. Pioglitazone is FDA-approved to treat type 2 diabetes mellitus as well as confers anti-neoplastic benefit in lung cancer models. Both pioglitazone and fulvestrant have established safety and efficacy profiles. The combination has not, to our knowledge, been studied in model systems of lung cancer.

Here, we demonstrate that pioglitazone and fulvestrant have a robust chemopreventive effect on a mouse model of smoking-induced lung cancer. Treatment with the combination *in vivo* mitigated the growth of tumors by 40% compared with placebo. We predict that this effect on cell growth and proliferation slows or delays the growth of tumors based on *in vitro* analysis of treatments on anchorage-independent colony formation. Combination treatment mitigated a 55% decrease in anchorage-independent colony formation compared with placebo in culture alone and by 50% in large colony formation compared with placebo in co-culture with macrophages. We observed the slow growth of colonies over time in cell-culture rather than regression of established colony size with treatment, suggesting that pathways that mitigate the rate of growth such as cell cycle proteins like Cyclin D1 likely confer some of the therapeutic benefit seen with the combination.

We also hypothesized that the combination would mitigate immunosuppressive smoldering inflammation more effectively than either single treatment. A potential pitfall of agents that modulate the immune response of tumor and stromal cells emerges when agents implicated in chemopreventive intervention skew the dichotic switch away from M2-functional cytokines, chemokines, and growth factors and push M1-specific responses, some of which are involved in tumorigenic activity such as IL-1β [108]. Previously published studies cited therapeutic benefit of ER blockade in freeing immune-stimulatory pathways such as TNF and IL-1 that are blocked in the presence of functional estradiol signaling pathways as well as dampening estrogen-stimulated M2 macrophage activation [94, 95]. Several studies cited a potentially deleterious effect of pioglitazone-drive macrophage TAM-like activation and functionality [96-98]. We predicted that adding fulvestrant to pioglitazone could mediate this effect, as a published study in cardiovascular disease identified the need for a fully-functional ER signaling pathway to mitigate a full M2 response [95]. This study was able to validate this observation in the context of lung cancer TME model. Here, we showed that the combination more-effectively mitigated TAM-functionality than single treatments both in the BALF of an NNK-induced lung carcinogenesis model as well as in co-culture modeling of the lung TME with human immortalized and murine primary macrophage and lung cancer cell lines. We have been able to demonstrate that the combination can maximally regulate pathways known to promote tumor initiation and progression including IL-1β, IL-10, EGF, VEGF, AREG, MMP9, CCL2, and ER. We predict that one method of

rendering this inhibitory effect on smoldering inflammation is through the reduction in macrophage density with combination treatment. We hypothesize that decreased macrophage presence in the TME is likely through TME-mediated chemotaxis both in a paracrine fashion through cancer cells and other stromal components and autocrine fashion by the macrophages themselves based on decreased CCL2 expression both in macrophages and BALF from NNK-exposed mice receiving treatments. Taken together, we predict that pioglitazone and fulvestrant combined, unlike approaches taken in previously-tested chemopreventive strategies, can manipulate both classic M1 and M2 cytokines as well as proliferative and angiogenic pathways associated with tumor initiation and sustainment. This model signifies an important step forward in acknowledging and effectively modulating the heterogeneity of TAM signaling to precisely address the complexity of TAM regulation of the TME to more holistically promote anti-tumorigenic therapeutic benefit.

We further hypothesized that the lungs are able to synthesize a local source of estrogen which can drive lung cancer formation and progression in an autocrine fashion based on models of the TME in breast cancer, TAM phenotyping in lung cancer, and preliminary data from previously published studies on mouse models of estrogen signaling in NNK-induced adenocarcinoma through assessment of ER pathway-compounds in TME immune cells. We identified autocrine production of estrogen in the *in vitro* models elucidating macrophage functionality. We also found estradiol production in BALF from NNK-

exposed mice in the *in vivo* intact and ovariectomized studies. The presence of estradiol in the lung lavage from ovariectomized mice confirms a local source of estrogen production in the absence of a reproductive source of estrogen. Furthermore, we identified an increased sensitivity of M2, TAM-like macrophages to ER blockade compared with resting-state macrophages, suggesting that this pathway is key in mediating necessary TAM functions within that phenotype. Finally, we identified a hormone-dependent resistance mechanism similarly described in previous models of anti-estrogen use in other models of cancer, whereby estrogen-blockage causes an antiestrogen-induced estrogen hypersensitivity [103-106]. To our knowledge, this phenomenon has not yet been described in models of lung cancer. Furthermore, we show here that the addition of pioglitazone is sufficient to alleviate this compensatory regulation of estradiol production, creating a novel therapeutic benefit of this combination not previously described.

We identified two other potential resistance-mechanisms to ERβ blockade and PPARγ activation. Single treatment of pioglitazone or fulvestrant in *in vitro* TME models with macrophages and NSCLC cells as well as BALF from *in vivo* studies showed a compensatory up-regulation of both the EGFR pathway through AREG and pro-tumorigenic and pro-angiogenic IL-1β. We predict these pathways are being turned on to rescue loss of positive proliferative signals and angiogenic signals by fulvestrant and pioglitazone. Combination treatment effectively ablates these compensatory increases both *in vitro* and *in vivo*,

representing a novel benefit of the combining both agents to more effectively mitigate rescue pathways.

Despite ablation of rescue pathways seen *in vitro* and in early-stage tumorigenesis *in vivo*, we identified a potent rescue effect seen in preneoplastic airways and tumors during late-stage tumorigenesis after a 14-week treatment duration. Expression of Cyclin D1, a known downstream target of both PPARγ and ER, was reduced in both single treatments and with the combination compared with placebo tumors. However, the combination treatment group that displayed greatest response to treatment conferring the lowest overall tumor burden presented with more high tumor-expression of Cyclin D1 compared with single treatments or combination-treated mice less responsive to treatments. This suggests that proliferation and cell cycle is being decreased in these tumors, and as a result, Cyclin D1 is being upregulated to push to re-activate cell cycle progression. A similar phenomenon was observed in tumor-secreted VEGF, another target of both pathways suggesting enhanced regulation of angiogenesis by the combination. This effect was especially apparent in mice that were most responsive to combination treatment presenting with the lowest tumor incidence and size burden. We also observed this influence on AREG expression seen in preneoplastic airways as well as tumor-secreted MMP9 and tumor-infiltrating immune cells that were MMP9-positive, suggesting that this potent rescue-phenotype is not limited to one downstream pathway, but is likely invigorated in pathways involved in both tumor-cell proliferation and the TME inflammatory

landscape downstream of PPARγ and ER and merits further study to elucidate treatment resistance mechanisms and biomarkers predictive of response to treatments. Taken together, our findings, to date, support the utility of combined pioglitazone and fulvestrant to mediate growth capacity of tumor cells and inflammatory mediation of the pulmonary TME to confer an overall chemopreventive benefit in a smoking-induced carcinogenesis model. These findings represent a promising foundation for future pre-clinical study of this drug combination in chemoprevention of lung cancer.

7. REFERENCES

1. National Cancer Institute. Cancer Stat Facts: Lung and Bronchus Cancer. https://seer.cancer.gov/statfacts/html/lungb.html (accessed 2019 February 23).
2. Ridge CA, McErlean AM, Ginsberg MS. Epidemiology of lung cancer. Semin Intervent Radiol 2013;30:93-8.
3. Siegel RL, Miller KD, Jemal A. Cancer statistics, 2018. CA Cancer J. Clin. 2018;68:7–30. doi: 10.3322/caac.21442.
4. The Health Consequences of Smoking—50 Years of Progress: A Report of the Surgeon General. National Center for Chronic Disease Prevention and Health Promotion (US) Office on Smoking and Health. Atlanta (GA): Centers for Disease Control and Prevention (US); 2014. https://www.ncbi.nlm.nih.gov/books/NBK294310/
5. American Cancer Society. Lung Cancer Risks for Non-Smokers. https://www.cancer.org/latest-news/why-lung-cancer-strikes-nonsmokers.html (accessed 2019 February 23).
6. American Cancer Society. Lung Cancer Risk Factors. https://www.cancer.org/cancer/lung-cancer/prevention-and-early-detection/risk-factors.html (accessed 2019 February 23).
7. Dela Cruz CS, Tanoue LT, Matthay RA. Lung cancer: epidemiology, etiology, and prevention. Clin Chest Med. 2011;32(4):605–644.
8. Rivera GA, Wakelee H. Lung cancer in never smokers. Oxygen Transport Tissue XXXIII. 2016;893(10):43–57.
9. Zheng M. Classification and pathology of lung cancer. Surg Oncol Clin N Am. 2016;25(3):447–468. doi: 10.1016/j.soc.2016.02.003.
10. Pikor LA, Ramnarine VR, Lam S, et al. Genetic alterations defining NSCLC subtypes and their therapeutic implications. Lung Cancer 2013;82:179-89.
11. Vijayalakshmi R, Krishnamurthy A. Targetable “driver” mutations in non small cell lung cancer. Indian. J Surg Oncol. 2011;2:178–188.
12. Akopyan G., et al. (2006). Understanding tobacco smoke carcinogen NNK and lung tumorigenesis. Int. J. Oncol., 29, 745–752.
13. Ge GZ, Xu TR, Chen C. Tobacco carcinogen NNK-induced lung cancer animal models and associated carcinogenic mechanisms. Acta biochimica et biophysica Sinica. 2015;47:477–487.
14. Xue J, Yang S, Seng S. Mechanisms of cancer induction by tobacco-specific NNK and NNN. Cancers (Basel) 2014;6(2):1138–56.
15. Siegfried JM, Hershberger PA, Stabile LP. Estrogen receptor signaling in lung cancer. Semin Oncol. 2009;36:524–31.
16. Keith R, Miller Y. Lung cancer chemoprevention: current status and future prospects. Nat Rev Clin Oncol. 2013;10:334–43.

17. Fu M, Travier N, Martín-Sánchez JC, et al. Identifying high-risk individuals for lung cancer screening: Going beyond NLST criteria. PLoS One. 2018 Apr 5;13(4):e0195441.
18. American Cancer Society. Benefits of Quitting Smoking Over Time. https://www.cancer.org/healthy/stay-away-from-tobacco/benefits-of-quitting-smoking-over-time.html (accessed 2019 Feb 27).
19. Keith R, Miller Y. Lung cancer chemoprevention: current status and future prospects. Nat Rev Clin Oncol. 2013;10:334–43.
20. National Institute of Health, ClinicalTrials.gov. Pioglitazone for Lung Cancer Chemoprevention. https://clinicaltrials.gov/ct2/show/NCT00780234 (Accessed 2019 Feb 26)
21. Van Dyke AL, Cote ML, Prysak G, Claeys GB, Wenzlaff AS, Schwartz AG. Regular adult aspirin use decreases the risk of non-small cell lung cancer among women. Cancer Epidem Biomark Prev. 2008;17(1):148–157.
22. National Institute of Health, ClinicalTrials.gov. A Phase III, Randomized, Study of Aspirin and Esomeprazole Chemoprevention in Barrett's Metaplasia (AspECT). https://clinicaltrials.gov/ct2/show/NCT00357682?cond=aspirin+chemoprevention&rank=4 (Accessed 2019 Feb 27)
23. Mao JT, Roth MD, Fishbein MC, Aberle DR, Zhang ZF, Rao JY, Tashkin DP, Goodglick L, Holmes EC, Cameron RB, Dubinett SM, Elashoff R, Szabo E, Elashoff D. Lung cancer chemoprevention with celecoxib in former smokers. Cancer Prev Res (Phila) 2011;4:984–93.
24. Keith RL, Blatchford PJ, Kittelson J, et al. Oral iloprost improves endobronchial dysplasia in former smokers. Cancer Prev Res (Phila) 2011;4:793–802.
25. Bunaciu RP, Yen A. Retinoid Chemoprevention: Who Can Benefit? Curr Pharmacol Rep. 2015;1:391–400.
26. Lee J.J., Feng L., Reshef D.S., Sabichi A.L., Williams B., Rinsurongkawong W. Mortality in the randomized, controlled lung intergroup trial of isotretinoin. Cancer Prev Res (Phila) 2010;3(6):738–744.
27. Kumar R, Zakharov MN, Khan SH, Miki R, Jang H, Toraldo G, Singh R, Bhasin S, Jasuja R. The dynamic structure of the estrogen receptor. J Amino Acids. 2011;2011:812540.
28. Hsu L., Chu N., Kao S. Estrogen, Estrogen Receptor and Lung Cancer. Int. J. Mol. Sci. 2017;18:1713
29. Marino M, Galluzzo P, Ascenzi P. Estrogen signaling multiple pathways to impact gene transcription. Current Genomics. 2006;7(8):497–508.
30. Patrone C., Cassel T.N., Pettersson K., Piao Y.S., Cheng G., Ciana P., Maggi A., Warner M., Gustafsson J.A., Nord M. Regulation of postnatal

lung development and homeostasis by estrogen receptor beta. Mol. Cell. Biol. 2003;23:8542–8552.
31. Hsu L.H., Liu K.J., Tsai M.F., Wu C.R., Feng A.C., Chu N.M., Kao S.H. Estrogen adversely affects the prognosis of patients with lung adenocarcinoma. Cancer Sci. 2015;106:51–59.
32. Fu JB, Severson RK, Kalemkerian GP. Lung cancer in women: analysis of the national Surveillance, Epidemiology, and End Results database. Chest. 2005;127:768–77.
33. Ganti A.K., et al: Hormone replacement therapy is associated with decreased survival in women with lung cancer. J. Clin. Oncol. 2006; 24: pp. 59-63
34. Siegfried JM, Stabile LP, Estrongenic steroid hormones in lung cancer. Semin Oncol. (2014) 41:5–16.
35. Siegfried JM. Smoking out reproductive hormone actions in lung cancer. Mol Cancer Res 2014;12:24-31.
36. Patrone C, et al. Regulation of postnatal lung development and homeostasis by estrogen receptor beta. Mol. Cell. Biol. 2003;23:8542–52.
37. Burns TF, Stabile LP. Targeting the estrogen pathway for the treatment and prevention of lung cancer. Lung Cancer Manag. 2014;3:43–52.
38. Al-Amri. Prevention of Breast Cancer. J Family Community Med. 2005 May-Aug; 12(2): 71–74.
39. National Institute of Health: National Cancer Institute Division for Cancer Prevention. FDA Approves Raloxifene for Breast Cancer Prevention. https://prevention.cancer.gov/news-and-events/news/fda-approves-raloxifene. (Accessed 2019 Feb 28)
40. Chu SC, Hsieh CJ, Wang TF, et al. Antiestrogen use in breast cancer patients reduces the risk of subsequent lung cancer: a population-based study. Cancer Epidemiol 2017;48:22–8.
41. Stabile LP, Rothstein ME, Cunningham DE, Land SR, Dacic S, Keohavong P, et al. Prevention of tobacco carcinogen-induced lung cancer in female mice using antiestrogens. Carcinogenesis (2012) 33:2181–9.
42. National Institute of Health, ClinicalTrials.gov. Erlotinib With or Without Fulvestrant in Treating Patients With Stage IIIB or Stage IV Non-Small Cell Lung Cancer. https://clinicaltrials.gov/ct2/show/NCT00100854?cond=fulvestrant+lung+cancer&rank=1. (Accessed 2019 Feb 28)
43. National Institute of Health, ClinicalTrials.gov. Fulvestrant and Anastrozole as Consolidation Therapy in Postmenopausal Women With Advanced Non-small Cell Lung Cancer.

https://clinicaltrials.gov/ct2/show/NCT00932152?cond=fulvestrant+lung+cancer&rank=2. (Accessed 2019 Feb 28)
44. National Institute of Health, ClinicalTrials.gov. Study Evaluating the Addition of Fulvestrant to Erlotinib in Stage IIIB/IV Non-Small Cell Lung Cancer. https://clinicaltrials.gov/ct2/show/NCT00592007?cond=fulvestrant+lung+cancer&rank=3. (Accessed 2019 Feb 28)
45. National Institute of Health, ClinicalTrials.gov. Lung Cancer in Women Treated With Anti-oestrogens and Inhibitors of EGFR (LADIE). https://clinicaltrials.gov/ct2/show/NCT01556191?cond=fulvestrant+lung+cancer&rank=5. (Accessed 2019 Feb 28)
46. Keith RL, Blatchford PJ, Kittelson J, et al. Oral iloprost improves endobronchial dysplasia in former smokers. Cancer Prev Res (Phila) 2011;4:793–802.
47. Hanahan D, Weinberg RA. Hallmarks of cancer: the next generation. Cell (2011) 144:646–74.
48. Reddy AT, Lakshmi SP, Reddy RC: PPARgamma as a novel therapeutic target in lung cancer. PPAR Res 2016;2016:8972570
49. Simpson-Haidaris PJ, Pollock SJ, Ramon S, Guo N, Woeller CF, Feldon SE, Phipps RP. Anticancer role of PPARgamma agonists in hematological malignancies found in the vasculature, marrow and eyes. PPAR Res. 2010;2010:814609.
50. Berry EB, Eykholt R, Helliwell RJ, Gilmour RS, Mitchell MD, Marvin KW. Peroxisome proliferator-activated receptor isoform expression changes in human gestational tissues with labor at term. Mol Pharmacol. 2003;64:1586–1590.
51. Han S., Roman J. Peroxisome proliferator-activated receptor γ: A novel target for cancer therapeutics? Anti-Cancer Drugs. 2007;18(3):237–244.
52. Grygiel-Górniak B. Peroxisome proliferator-activated receptors and their ligands: nutritional and clinical implications—a review. Nutrition Journal. 2014;13, article 17 doi: 10.1186/1475-2891-13-17.
53. Theocharis S., Kanelli H., Politi E., et al. Expression of peroxisome proliferator activated receptor-gamma in non-small cell lung carcinoma: correlation with histological type and grade. Lung Cancer. 2002;36(3):249–255.
54. Wei J., Bhattacharyya S., Jain M., Varga J. Regulation of matrix remodeling by peroxisome proliferator-activated receptor-γ: A novel link between metabolism and fibrogenesis. Open Rheumatol. J. 2012;6:103–115.
55. Lehmann JM, Moore LB, Smith-Oliver TA, Wilkison WO, Willson TM, Kliewer SA. An antidiabetic thiazolidinedione is a high affinity ligand for

peroxisome proliferator-activated receptor γ (PPARγ). Journal of Biological Chemistry. 1995;270(22):12953–12956.
56. Govindarajan R, Ratnasinghe L, Simmons DL, Siegel ER, Midathada MV, Kim L, Kim PJ, Owens RJ, Lang NP. Thiazolidinediones and the risk of lung, prostate, colon cancer in patients with diabetes. J Clin Oncol. 2007;25:1476–1481.
57. Kopelovich, L.; Fay, J.R.; Glazer, R.I.; Crowell, J.A. Peroxisome proliferator-activated receptor modulators as potential chemopreventive agents. Mol. Cancer Ther., 2002, 1(5), 357-363.
58. Koeffler, H.P. Peroxisome proliferator-activated receptor gamma and cancers. Clin. Cancer Res., 2003, 9(1), 1-9.
59. Grommes, C.; Landreth, G.E.; Heneka, M.T. Antineoplastic effects of peroxisome proliferator-activated receptor gamma agonists. Lancet Oncol., 2004, 5(7), 419-429.
60. Jiang, M.; Shappell, S.B.; Hayward, S.W. Approaches to understanding the importance and clinical implications of peroxisome proliferator-activated receptor gamma (PPARgamma) signaling in prostate cancer. J. Cell. Biochem., 2004, 91(3), 513-527.
61. Weng, J.R.; Chen, C.Y.; Pinzone, J.J.; Ringel, M.D.; Chen, C.S. Beyond peroxisome proliferator-activated receptor gamma signaling: the multi-facets of the antitumor effect of thiazolidinediones. Endocr. Relat. Cancer, 2006, 13(2), 401-413.
62. Li H, Sorenson AL, Poczobutt J, Amin J, Joyal T, Sullivan T, Crossno JT, Weiser-Evans MC, Nemenoff RA. Activation of PPARgamma in myeloid cells promotes lung cancer progression and metastasis. PLoS One. 2011;6:e28133. doi:10.1371/journal.pone.0028133.
63. Zhao T., Du H., Blum J. S., and Yan C. (2016) Critical role of PPARγ in myeloid-derived suppressor cell-stimulated cancer cell proliferation and metastasis. Oncotarget 7, 1529–1543
64. National Institute of Health, ClinicalTrials.gov. Pioglitazone Hydrochloride in Treating Patients With Stage IA-IIIA Non-small Cell Lung Cancer. https://clinicaltrials.gov/ct2/show/NCT01342770?cond=pioglitazone+lung+cancer&rank=3. (Accessed 2019 March 15).
65. National Institute of Health, ClinicalTrials.gov. Pioglitazone for Lung Cancer Chemoprevention. https://clinicaltrials.gov/ct2/show/NCT00780234?cond=pioglitazone+lung+cancer&rank=1. (Accessed 2019 March 15).
66. Mackenzie T. A., Zaha R., Smith J., Karagas M. R., Morden N. E. Diabetes pharmacotherapies and bladder cancer: a medicare epidemiologic study. Diabetes Therapy. 2016;7(1):61–73.

67. Filipova E, Uzunova K, Kalinov K, Vekov T. Pioglitazone and the Risk of Bladder Cancer: A Meta-Analysis. Diabetes Therapy. 2017;8:705–726.
68. Xu Y, Huo R, Chen X, et al. Diabetes mellitus and the risk of bladder cancer: a PRISMA-compliant meta-analysis of cohort studies. Medicine (Baltimore) 2017;96:e8588.
69. Turner RM, Kwok CS, Chen-Turner C, Maduakor CA, Singh S, Loke YK. Thiazolidinediones and associated risk of bladder cancer: a systematic review and meta-analysis. Br J Clin Pharmacol. 2014;78:258–273.
70. Lewis J. D., Ferrara A., Peng T., et al. Risk of bladder cancer among diabetic patients treated with pioglitazone: interim report of a longitudinal cohort study. Diabetes Care. 2011;34(4):916–922.
71. Hsiao FY, Hsieh PH, Huang WF, Tsai YW, Gau CS. Risk of bladder cancer in diabetic patients treated with rosiglitazone or pioglitazone: a nested case–control study. Drug Safety. 2013;36:643–649.
72. Chu R, et al. The cross-talk between estrogen receptor and peroxisome proliferator-activated receptor gamma in thyroid cancer. Cancer. 2014;120:142–153.
73. Lebovic DI, Kavoussi SK, Lee J, Banu SK, Arosh JA. PPARγ activation inhibits growth, survival of human endometriotic cells by suppressing estrogen biosynthesis and PGE2 signaling. Endocrinology. 2013;154:4803–4813.
74. Wang X, Kilgore MW (2002) Signal cross-talk between estrogen receptor alpha and beta and the peroxisome proliferator-activated receptor gamma 1 in MDA-MB-231and MCF-7 breast cancer cells. Mol Cell Endocrinol 194:123–133.
75. Bonofiglio D, Gabriele S, Aquila S, Catalano S, Gentile M, Middea E, Giordano F, Ando S. Estrogen receptor alpha binds to peroxisome proliferator-activated receptor response element and negatively interferes with peroxisome proliferator-activated receptor gamma signaling in breast cancer cells. Clin Cancer Res. 2005;11:6139–6147.
76. Wynn TA, Chawla A, Pollard JW (2013) Macrophage biology in development, homeostasis and disease. Nature 496(7446): 445–455.
77. Hanahan D., Weinberg R. A. Hallmarks of cancer: the next generation. Cell. 2011;144(5):646–674.
78. Dranoff G. Tumour immunology: immune recognition and tumor protection. Curr Opin Immunol. 2002;14:161–164.
79. Panni, R.Z.; Linehan, D.C.; DeNardo, D.G. Targeting tumor-infiltrating macrophages to combat cancer. Immunotherapy 2013, 5, 1075–1087.
80. Aras S, Zaidi MR. TAMeless traitors: macrophages in cancer progression and metastasis. Br J Cancer (2017) 117(11):1583–91.

81. A Sica, P Larghi, A Mancino, L Rubino, C Porta, MG Totaro, et al. Macrophage polarization in tumour progression. Semin Cancer Biol, 18 (5) (2008), pp. 349-355.
82. Guilbaud E, Gautier EL, Yvan-Charvet L. Macrophage Origin, Metabolic Reprogramming and IL-1 Signaling: Promises and Pitfalls in Lung Cancer. Cancers 2019, 11(3), 298.
83. Rakaee M, Busund LR, Jamaly S, et al. Prognostic Value of Macrophage Phenotypes in Resectable Non-Small Cell Lung Cancer Assessed by Multiplex Immunohistochemistry. Neoplasia. 2019 Mar; 21(3):282-293.
84. Almatroodi S. A., McDonald C. F., Darby I. A., Pouniotis D. S. Cancer Microenviron. 2016;9:1–11.
85. Wu P, Wu D, Zhao L, Huang L, Chen G, Shen G, et al. Inverse role of distinct subsets and distribution of macrophage in lung cancer prognosis: a meta-analysis. Oncotarget 2016;7:40451–60.
86. Liu YC, Zou XB, Chai YF, Yao YM. Macrophage polarization in inflammatory diseases. Int J Biol Sci(2014) 10(5):520–9.
87. Fan X, Zhang H, Cheng Y, Jiang X, Zhu J, Jin T (2016) Double roles of macrophages in human neuroimmune diseases and their animal models. Mediators Inflamm 2016: 8489251.
88. Laoui D, Movahedi K, Van Overmeire E, Van den Bossche J, Schouppe E, Mommer C, et al. Tumor-associated macrophages in breast cancer: distinct subsets, distinct functions. Int J Dev Biol (2011) 55:861–7.
89. Sica A, Saccani A, Mantovani A (2002) Tumor-associated macrophages: a molecular perspective. Int Immunopharmacol 2(8): 1045–1054.
90. Mantovani A, Sozzani S, Locati M, Allavena P, Sica A. Macrophage polarization: tumor-associated macrophages as a paradigm for polarized M2 mononuclear phagocytes. Trends Immunol. 2002;23:549–555.
91. Bio-Rad. Macrophage Polarization: Mini-review. https://www.bio-rad-antibodies.com/macrophage-polarization-minireview.html. (Accessed 2019 March 27).
92. Zhang M, He Y, Sun X, Li Q, Wang W, Zhao A, Di W. A high M1/M2 ratio of tumor-associated macrophages is associated with extended survival in ovarian cancer patients. Journal of Ovarian Research. 2014;7:19.
93. Yuan A, Hsiao YJ, Chen HY, et al. Opposite Effects of M1 and M2 Macrophage Subtypes on Lung Cancer Progression. Sci Rep. 2015;5:14273.
94. Harkonen PL, Vaananen HK. Monocyte-macrophage system as a target for estrogen and selective estrogen receptor modulators. Ann N Y Acad Sci. (2006) 1089:218–27.

95. C. Bolego, A. Cignarella, B. Staels, G. Chinetti-Gbaguidi. Macrophage function and polarization in cardiovascular disease: a role of estrogen signaling? Arterioscler. Thromb. Vasc. Biol., 33 (2013), pp. 1127-1134
96. Li H, Weiser-Evans MCM, Nemenoff R. Anti- and protumorigenic effects of PPARγ; in lung cancer progression: a double-edged sword. PPAR Res. 2012;2012.
97. Li H, Sorenson AL, Poczobutt J, Amin J, Joyal T, Sullivan T, Crossno JT, Weiser-Evans MC, Nemenoff RA. Activation of PPARgamma in myeloid cells promotes lung cancer progression and metastasis. PLoS One. 2011;6:e28133.
98. Bouhlel M. A., Derudas B., Rigamonti E., et al. PPARγ activation primes human monocytes into alternative M2 macrophages with anti-inflammatory properties. Cell Metabolism. 2007;6(2):137–143.
99. Vella V., Nicolosi M.L., Giuliano S., Bellomo M., Belfiore A., Malaguarnera R. PPAR-gamma agonists as antineoplastic agents in cancers with dysregulated IGF axis. Front. Endocrinol. 2017;8:31.
100. Stabile LP, Dacic S, Land SR, Lenzner DE, Dhir R, Acquafondata M, et al. Combined analysis of estrogen receptor beta-1 and progesterone receptor expression identifies lung cancer patients with poor outcome. Clin Cancer Res. (2011) 17:154–64.
101. Al-Amri, AM. Prevention of breast cancer. J Family Community Med. 2005;12(2): 71–74.
102. Giles ED, Jindal S, Wellberg EA, et al. Metformin inhibits stromal aromatase expression and tumor progression in a rodent model of postmenopausal breast cancer. Breast Cancer Res. 2018; 20: 50.
103. Nicholson RI, Gee JM. Estrogen and growth factor cross-talk and endocrine insensitivity and acquired resistance in breast cancer. Br J Cancer 2000; 82: 501–13.
104. Chen S, Masri S, Wang X, Phung S, Yuan YC, Wu X. What do we know about the mechanisms of aromatase inhibitor resistance? J Steroid Biochem Mol Biol 2006; 102: 232–40.
105. Leary A, Dowsett M. Combination therapy with aromatase inhibitors: the next era of breast cancer treatment? Br J Cancer 2006; 95: 661–6.
106. Wang JP, Conaway M, Masamura S, Li S, Santen RJ. Activation of the MAPK pathway enhances sensitivity of MCF-7 breast cancer cells to the mitogenic effect of estradiol. Endocrinology 2002; 143: 3221–9.
107. Macedo LF, Sabnis GJ, Goloubeva OG, Brodie A. Combination of anastrozole with fulvestrant in the intratumoral aromatase xenograft model. Cancer Res 2008; 68: 3516–22.
108. Brady NJ, Chuntova P, Schwertfeger KL. Macrophages: Regulators of the Inflammatory Microenvironment during Mammary Gland

Development and Breast Cancer. Mediators Inflamm. 2016;2016:4549676.
109. Wang Y, James M, Wen W, Lu Y, Szabo E, Lubet RA, et al. Chemopreventive effects of pioglitazone on chemically induced lung carcinogenesis in mice. Mol Cancer Ther. 2010;9:3074–82.
110. Seabloom DE, Galbraith AR, Haynes AM et al Fixed‐dose combinations of pioglitazone and metformin for lung cancer prevention. Cancer Prev Res (Phila) 2017; 10: 116‐23.